Dynamics of Quantum Information of the Central Spin Problem

by

Mohamad Niknam

A thesis
presented to the University of Waterloo
in fulfillment of the
thesis requirement for the degree of
Doctor of Philosophy
in
Physics

Waterloo, Ontario, Canada, 2018

© Mohamad Niknam 2018

Examining Committee Membership

The following served on the Examining Committee for this thesis. The decision of the Examining Committee is by majority vote.

External Examiner	Lu Jeu Sham Professor Emeritus
Supervisor	David Cory Professor
Committee Member	Jan Kycia Professor
Committee Member	Joseph Emerson Associate Professor
Internal-external Member	Jonathan Baugh Associate Professor

I hereby declare that I am the sole author of this thesis. This is a true copy of the thesis, including any required final revisions, as accepted by my examiners.

I understand that my thesis may be made electronically available to the public.

Abstract

Environmental effects on the evolution of a spin system in the context of the central spin problem, have been studied for more than 60 years. With the growing complexity of quantum information processors there is a new need to better understand and control the interactions of qubits with their environment. Decoherence is an apparent loss of quantum coherence of the central spin, which is the result of the coherent evolution of the central spin and its spin environment. This evolution may be understood as the consequence of local field fluctuations induced by heteronuclear dipolar interaction between the central spin and the environment spins and homonuclear dipolar interaction of spins in the environment. A complete theoretical description for the evolution of the central spin does not exist and numerical solutions are restricted to small spin environments.

Another way of looking at the central spin problem is to study the correlations between the central spin and the environment spins. In this method the evolution of the central spin is described with the dynamics of multi-spin correlations resulting from interactions of the central spin and the environment spins. Using Multiple Quantum Nuclear Magnetic Resonance (MQ NMR) techniques, we have designed experiments for the direct detection of multi-spin correlations between the central spin and environment spins. These experiments are used to observe the progress in production of correlations between the central spin and the environment. They reveal the multi-spin dynamics that underlies the decoherence process.

The central spin is initially uncorrelated with the environment and quantum information resides exclusively on it. After the interaction with the environment spins quantum information is shared in the form of correlated operators between the central spin and the environment. Using our experiments this flow of quantum information from the central spin to the environment and the quantum information content of the environment, can be quantified. Further, these experiments are used to gauge the sensitivity of correlation to perturbation in the environment, by observing the mixing dynamics of the multi-spin correlations. The Out-of-Time Correlation metric is used for the sensitivity measurements. We find that the dynamics of correlations in our system is better explained by the extent of information flow to the environment rather than the evolution time.

Acknowledgements

First I would like to express my deepest gratitude to my advisor, Dr. David Cory for giving me the opportunity to work in the Cory group. His insight and enthusiasm as a teacher has been encouraging me every day and I am grateful for his mentorship.

I am deeply grateful to my committee members Dr. Kycia, Dr. Emerson and Dr. Baugh for their guidance and helpful discussions and Dr. Lu Sham who accepted to participate in my defence. I also would like to thank Dr. Lea Santos and Dr. Sekhar Ramanathan for showing interest in my research and making useful suggestions.

It is a pleasure to thank all the members of Cory group whom I have learned a lot from. In particular I am thankful for friendship and help of Dr. Osama Moussa, Ivar Taminiau, Dr. Patryk Gumann, Dr. Kevin Krsulich, Dr. Sarah Sheldon, Holger Haas, Ian Hinks, Dr. Troy Borneman, Dr. Joachim Nsofini and Jiahui Chen. Thanks are also due to Dr. George Nicholas who helped with proofreading this thesis.

It is an honor for me to acknowledge the support and the help of many scientists who encouraged me in pursuing a career in physics in particular Dr. Nader Ghahramani, Dr. John Ellis, Dr. Hartwig Peemoeller, Dr. Hossein Dehghani and Dr. Payam Bagheri.

I wish to extend my gratitude for my parents whom have been a source of encouragement and patience for me.

Most importantly this was not possible without the boundless support and love of my best friend and partner, Negar, who inspires me every day.

Dedication

To Negar

For her Love, her understanding and her patience.

Because she always inspired me.

Table of Contents

List of Figures

List of Tables

Chapter 1

Introduction

As the field of quantum information advances and a variety of physical implementations of qubits are realized, there is a need to better understand and control the interactions of qubits with their environment. Such interactions may have two undesired outcomes: they may cause decoherence or a loss of quantum information on the qubit subsystem which limits the fidelity of quantum information processes. In addition, if we consider a larger Hilbert space, which includes the environment spins, these interactions may allow a flow of quantum information from the qubit to the environment spins and then back to the qubit. This flow of quantum information back to the qubit will interfere and corrupt the quantum information stored on the qubit.

Environmental effects on the evolution of a spin system in the context of the central spin problem, has been studied for more than 60 years [3, 4, 5]. In its simplest form, the central spin structure consists of a single spin that contains the desired quantum information and interacts with a spin environment. The spin environment may also be self-interacting. Today's relevance of the central spin problem to quantum information devices is that the fidelity of quantum processes and the integrity of quantum information on a qubit is influenced by the qubit's interaction with the environment. Useful quantum processing demands extraordinary control of the qubits and decoherence (loss of quantum coherence of the central spin [6, 7, 8, 9]) is a limiting factor for quantum information processing [10]. To achieve fault tolerant quantum information processing, Quantum Error Correction (QEC) algorithms are used. QEC codes can be successful when the fidelity of quantum gates

are high, the environment noise have Markovian characteristics and it is local (there is a length scale beyond which no additional error occurs), and there is no memory in the bath. Existence of a long-range quantum memory in the environment can remarkably change the structure of quantum noise and interfere with the quantum information processing. These questions on the dynamics of quantum information and quantum noise in the environment, can be addressed in the context of the central spin problem by examining the correlations between the system and the environment.

Decoherence phenomenon has been studied in many physical setups including spin systems, superconductive qubits, nitrogen-vacancy, quantum dots and ion traps [2, 11, 12, 13, 14, 15, 16, 17]. Spin systems are a particularly convenient experimental platform since we have good control over both the central spin and the environment. Solid state NMR offers many techniques to control the Hamiltonian terms in a multi-spin system. The system-environment Hamiltonian and environment self-interaction terms can be individually turned on or off, be scaled or be inverted [18, 19, 20, 21, 22, 23, 24, 25]. This flexibility makes solid state NMR a good test bed for investigating the central spin problem.

A common and useful description of the central spin problem is to recast it in terms of the effective local field that the central spin experiences due to the states of all of the environmental spins [26]. The dipolar coupling describes the interaction between two spins depending on their relative positions and their magnetic moment vector $\mu = \frac{1}{2}\gamma\hbar\sigma$:

$$\mathcal{H}_{Dij} = \frac{\gamma_i\gamma_j\hbar^2}{4r_{ij}^3}\{\sigma_i \cdot \sigma_j - 3\frac{(\sigma_i \cdot r_{ij})(\sigma_j \cdot r_{ij})}{r_{ij}^2}\} \tag{1.1}$$

where r_{ij} is the vector connecting the two spin i and j, γ is the gyromagnetic ratio and σ_i are the Pauli operators. This can be written as :

$$\mathcal{H}_{Dij} = \mu_i \cdot \mathbf{H}_{ij} = -\gamma_i\hbar\frac{1}{2}\sigma_i \cdot \mathbf{H}_{ij} \tag{1.2}$$

here $\mathbf{H}_{ij}$ indicates the magnetic field induced by the spin j at the location of the spin i. The local field produced by a nuclear spin in a solid with distance of the order of Angstroms between spins, can be up to a few Gauss [27]. In a large external magnetic field the $\mathbf{H}_{ij}$ has a static component along the field direction and a rotating part perpendicular to the static field, resulting from the Larmor precession of spin j. Since in this case the central spin and environment spins have different Larmor frequencies the effect of the rotating

component of the local field is negligible and the collective effect of the environment spins on the central spin can be evaluated by adding the static component of local field induced by each spin in the environment. Consequently, variations of the static component of the local field induced by the environment spins for different elements of spin ensemble cause a spread in the Larmor frequencies of the central spin and broaden its spectral line shape. Changes in the local field induced by fluctuations of neighboring spins have been used to explain the spectral line shape of the central spin [28, 29, 30].

One way of analyzing the central spin problem is to investigate the correlations between the central spin and the environment spins which results from their interaction. As an example consider a qubit initialized in the $\rho_{(0)}^{qubit} = \frac{\sigma_{\mathrm{X}}}{2}$ state with the system-environment interaction described by $\mathcal{H}_{zz} = \sum_i \omega_i \sigma_{\mathrm{Z}}^{qubit} \otimes \sigma_{\mathrm{Z}}^{env_i}$, where σ_{X}, σ_{Y} and σ_{Z} are Pauli operators and $\sigma_{\mathrm{Z}}^{env_i} := \mathbb{1}^{\otimes i-1} \otimes \sigma_{\mathrm{Z}}^{i} \otimes \mathbb{1}^{\otimes N-i}$ is an operator acting on only the i^{th} spin in the environment. Assuming that the environment consists of N spins initially in the identity state, evolution under this interaction Hamiltonian will produce correlations between the qubit and the spin environment, which are contained in the following expansion for the total density matrix $\rho_{(t)}$ of the system and environment:

$$\begin{aligned} \rho_{(t)} &= C_0(t)\sigma_{\mathrm{X}}^{qubit} \otimes \mathbb{1}^N \\ &+ C_1(t)\sigma_{\mathrm{Y}}^{qubit} \otimes \sigma_{\mathrm{Z}}^{i} \otimes \mathbb{1}^{N-1} \\ &+ C_2(t)\sigma_{\mathrm{X}}^{qubit} \otimes \sigma_{\mathrm{Z}}^{i} \otimes \sigma_{\mathrm{Z}}^{j} \otimes \mathbb{1}^{N-2} \\ &+ \cdots . \end{aligned} \tag{1.3}$$

Above, $C_0(t)$ is a product of oscillating functions in time that determines the overlap between the initial state of the qubit and its evolved state, and determines the amplitude of the observable signal if the spin system is allowed to evolve with no interruption. It is also known as the Free Induction Decay (FID) of the central spin. The amplitude of multi-spin correlated operators between the qubit and environment spins, $C_n(t) \quad n = 1, 2, 3 \cdots$, are not directly observable via NMR. In this thesis we develop an experimental approach to measuring the amplitudes of these terms based on their response to collective rotations.

The FID of the central spin may be interpreted as the flow of quantum information from the qubit to the spin environment. In this setup initially the central spin and the environment spins are uncorrelated and the central spin contains all of the quantum information while the environment is in the maximally mixed state with no information content

and at its maximum entropy. After the evolution of the central spin and the environment, quantum information is shared with the environment spins in the form of correlations between the central spin and the environment spins, equation 1.3. These correlations can be measured by looking at the composite system-environment state. Since by correlating to the environment spins the von Neumann entropy of the central spin increases, the growth of correlations between the central spin and the environment is associated with the flow of quantum information to the environment. Quantum information left in the environment allows an unspecified observer to learn about the qubit and the results of quantum information processes. On the other hand, because the evolution of the central spin and the environment is a unitary dynamics, the shared quantum information with environment spins can flow back to the qubit. This means that the history of quantum information on the qubit is stored in the environment and can affect its evolution and change the outcome of future quantum processes. Therefore, a complete understanding of the dynamics of the correlations between the central spin and the environment is useful for implementation of quantum information processing.

An important factor in determining the effect of multi-spin correlations on the dynamics of the central spin is their lifetime. If the lifetime of correlated operators is short relative to the time scale of the evolution of the central spin, their influence on the effective dynamics of the central spin will be limited. For example exchanging the spin of environment changes the multi-spin correlated operators and effectively mixes the shared portion of quantum information. With evolution under mixing action the amplitude of an echo experiment decays since the flow of information from the central spin can not be reversed completely. Therefore, the time scale for mixing of quantum information in the environment, relative to the strength of the qubit-environment interaction, determines the effectiveness of mixing in limiting the flow of information from the environment back to the central spin. Characterizing mixing behavior has been a subject of interest in high energy physics and condensed matter physics recently [31, 32].

The central spin problem has been concerned with finding an effective map for the decoherence of the central spin after truncating the environment spins. Ideally a theoretical description for the multi-body dynamics of the central spin would contain the details of correlations between the central spin and the environment. The exact diagonalization solution for the composite Hilbert space of the central spin and the environment is limited

by the size of spin environment. Our solution for understanding the effective dynamics of the central spin is to design experiments for direct observation of correlations between the central spin and the environment spins, using Multiple Quantum Nuclear Magnetic Resonance (MQNMR) techniques. These experiments are used to observe the flow of quantum information from the central spin to the environment and to study the sensitivity of the spin environment to fluctuations in the environment spin state. Results of these experiments lead us to a practical model for multi-spin dynamics of the central spin which is successful in explaining the quantum evolution of the central spin, and provides a picture for understanding the dynamics of the correlation in the environment.

The rest of this chapter gives a review of prior solutions for the decoherence problem, a description of decoherence with the open quantum system formalism and a discussion of recent proposals for making dynamical maps for the central spin problem. Next we provide a short description of Multiple Quantum Nuclear Magnetic Resonance (MQ NMR) techniques and discuss experiments for the detection of correlated spins in solid states samples. Afterwards a pictorial description for the evolution of quantum information in the central spin system is discussed. Chapter two focuses on the experimental techniques, instrumentation, and sample.

In chapter three the experimental design for the main experiment, Multi-spin Correlation Detection (MCD), is discussed. There are simulations of the MCD experiment on a smaller spin system, showing the functionality of the MCD experiment. In addition, a set of operators are defined along with a recipe that can be used to evaluate the amplitude of different sub-spaces of the density matrix. Using these operators, we make a connection between the results of MCD experiment and the evolution of the density matrix. The final part of chapter three presents the results of the MCD experiment and a discussion on quantifying the growth of environment information content. Chapter four introduces the experiment for the detection of quantum information mixing in the system, Multi-spin Correlation Scrambling Detection (MCSD). The results of this experiment paint a full picture of the central spin-environment correlations, which include the detection of information flow from the central spin to the spin environment and also the effect of mixing on the memory state of the environment. The relevance of multi-spin correlation dynamics in giving a complete picture for the evolution of quantum information is revisited by making predictions on the mixing time of the environment. In chapter five we use the Out-of-Time-

Order-Correlation function to analyze the mixing dynamics of multi-spin correlations. In the last chapter we summarize our findings and introduce possible directions for future works.

1.1 Formal interpretation of the central spin problem

The evolution of a central spin may be understood as an evolution under a fluctuating local field caused by dipolar interaction between the central spin and environment spins. Spin flips in the environment from T_1 relaxation and the flip-flop interaction contribute to the fluctuations of the local field. Bloembergen et al [33] used the concept of local field and its perturbations to explain T_2 and T_1 relaxation processes. In particular, they used the local field fluctuations induced by the motion of the spins to explain the changes in the relaxation time and the spectral line-width of nuclear spins versus temperature. The concept of a local field was also used to describe paramagnetic relaxation at low temperature and for different concentrations of paramagnetic salt. Anderson argued that frequency distribution of absorbed and emitted phonons is determined by width of energy levels of lattice spins driven by spin-spin interactions [3]. He showed that for a central spin, variations of the local field are directly induced by dipolar interaction between the spins adjacent to it.

In this section the evolution of a central spin coupled to a spin environment is discussed. Where our interest is to focus on only the dynamics of the central spin we may use the formalism of open quantum system to reduce the system environment unitary dynamics to an open system picture of the central spin. The resultant map of the central spin will only make sense if it reflects the effects of the environmental interactions in the apparent dynamics of the central spin. As a result, correlated spin operators in the environment are incorporated in the construction of a dynamical map for the evolution of the central spin.

In this thesis decoherence refers to a map of Markovian processes for the evolution of the central spin caused by the environment spins. A decoherence map can be described by a quantum dynamics semigroup which accepts the time independent Lindblad generator. In contrast, the interaction between the central spin and the environment spins may lead to a non-Markovian dynamics that produce a memory in the environment. This evolution is reversible and we refer to it as dephasing. Dephasing process can not be described by a

quantum dynamical semigroup and does not have a time independent map.

1.1.1 Non-Interacting Environment

First we consider the simplest form of the central spin problem where a single spin interacts with a spin environment consisting of N non-interacting spins. In this case, there is an analytical solution for the evolution of the system. The Hilbert space of the system-environment composite system is given by the tensor product of the Hilbert spaces of the two subsystems:

$$H_{\text{cs-env}} = H_{\text{cs}} \otimes H_{\text{env}} \tag{1.4}$$

and the dimension of the composite Hilbert space is equal to the product of subsystems' dimensions. The central spin and the environment spins are spin $\frac{1}{2}$ nuclei. The initial state of the system is separable in the system-environment composite Hilbert space. The central spin is quantized along the z axis with $\mathcal{H}_S = \frac{\omega_0^{cs}\sigma_{\text{Z}}}{2}$. Since we are interested in studying the dephasing process, the central spin is initialized in an equal superposition of Zeeman eigenstates, or in σ_{X}. The environment spins are initially in the fully mixed state $(\frac{\mathbb{1}}{2})^{\otimes N}$. The initial density matrix of the composite system is written as

$$\rho_0 = \underbrace{\frac{\mathbb{1} + \sigma_{\text{X}}}{2}}_{\text{cs}} \otimes \underbrace{(\frac{\mathbb{1}}{2})^{\otimes N}}_{\text{env}} \tag{1.5}$$

We will keep this order of spin operators for the composite system throughout this thesis. The identity part of the central spin density matrix does not evolve. To simplify our notation we drop the identity operator in the central spin term and only show the deviation part, although we recall that the density matrix has trace 1.

$$\rho_0 = \frac{1}{2^{N+1}} \sigma_{\text{X}} \otimes \mathbb{1}^{\otimes N}. \tag{1.6}$$

The central spin-environment density matrix evolves under the the system-environment Hamiltonian:

$$\begin{aligned}
\mathcal{H} &= \mathcal{H}_S + \mathcal{H}_E + \mathcal{H}_{SE} && (1.7)\\
\mathcal{H}_S &= \frac{1}{2}\omega^{cs}\sigma_{\mathrm{z}} && (1.8)\\
\mathcal{H}_E &= \frac{1}{2}\sum_{j=1}^{N}\omega_j\sigma_{\mathrm{z}}^j && (1.9)\\
\mathcal{H}_{SE} &= \frac{1}{2}\sum_{j=1}^{N} d_j\sigma_{\mathrm{z}}\otimes\sigma_{\mathrm{z}}^j && (1.10)\\
\sigma_{\mathrm{z}}^j &:= \mathbb{1}^{\otimes j-1}\otimes\sigma_{\mathrm{z}}^j\otimes\mathbb{1}^{\otimes N-j}. && (1.11)
\end{aligned}$$

$\mathcal{H}_S$ and $\mathcal{H}_E$ represent the system Hamiltonian and the environment Hamiltonian terms for the spin's interaction in the main magnetic field or the Zeeman interaction, with the respective Larmor frequencies of ω^{cs} and ω_j. For the moment there are no internal dynamics for environment spins. The system-environment interaction term H_{SE} represents the coupling between the central spin and the environment spins, with d_j representing the coupling constant for each of the environment spins, which is determined by the nature of the H_{SE} interaction and the geometry of spins. σ_{z}^i is a spin operator acting only on the i$^{\mathrm{th}}$ spin in the environment.

First we go to the interaction frame defined by the Zeeman interactions of the central spin and environment. Using the interaction Hamiltonian $\mathcal{H}_0 = \mathcal{H}_S\otimes\mathbb{1}^{\otimes N} + \mathbb{1}^{cs}\otimes\mathcal{H}_E$, $\mathcal{H}_{SE}$ is transformed to the interaction frame with:

$$\mathcal{H}_{SE}^I(t) \equiv e^{(i\mathcal{H}_0 t)}\mathcal{H}_{SE}e^{(-i\mathcal{H}_0 t)} \qquad (1.12)$$

In this case $\mathcal{H}_{SE}$ and $\mathcal{H}_0$ commute and $\mathcal{H}_{SE}^I(t) = \mathcal{H}_{SE}$. As a result the system-environment density matrix evolution in the interaction frame is given by a unitary propagator:

$$\begin{aligned}
\rho(t) &= \mathcal{U}_{SE}(t)\cdot\rho(0)\cdot\mathcal{U}_{SE}^\dagger(t) && (1.13)\\
\mathcal{U}_{SE}(t) &= \mathcal{T}\exp(-i\int_0^t \mathcal{H}_{SE}^I(t)dt)\\
&= \exp(-i\mathcal{H}_{SE}t) && (1.14)
\end{aligned}$$

where $\mathcal{T}$ is Dyson time-ordering operator and we have set $\hbar = 1$. The result of this evolution is a correlation between the central spin and each environment spin with an oscillatory behavior. If d_1 was the only non-zero coupling constant in $\mathcal{H}_{SE}$, then $\rho(t)$ would be:

$$\rho(t) = \frac{1}{2^{N+1}}\{\sigma_{\rm X}\otimes\mathbb{1}^{\otimes N}\cos(d_1 t) + \sigma_{\rm Y}\otimes\sigma_{\rm Z}\otimes\mathbb{1}^{\otimes N-1}\sin(d_1 t)\} \tag{1.15}$$

Note that the central spin and environment spins are uncorrelated at t=0. At short times, the amplitude of this uncorrelated spin term declines while $\sigma_{\rm Y}\otimes\sigma_{\rm Z}$ which is a correlated two-spin operator, is produced. The amplitude of the correlated spin term and the uncorrelated term oscillates and there is a complete revival of the uncorrelated spin term is reached at $t = \frac{n\pi}{d_1}$.

The general solution for the evolution of a central spin interacting with N non-interacting spins in the environment is:

$$\begin{aligned}
\rho(t) = \frac{1}{2^{N+1}} \quad \{ \quad & \sigma_{\rm X}\otimes\mathbb{1}^{\otimes N}\prod_{i=1}^{N}\cos(d_i t) \\
+ \quad & \sum_{j=1}^{N}\sigma_{\rm Y}\otimes\sigma_{\rm Z}^{j}\sin(d_j t)\prod_{i\neq j}^{N}\cos(d_i t) \\
- \quad & \sum_{j,k}^{N}\sigma_{\rm X}\otimes(\sigma_{\rm Z}^{j}.\sigma_{\rm Z}^{k})\sin(d_j t)\sin(d_k t)\prod_{i\neq j,k}^{N}\cos(d_i t) \\
- \quad & \sum_{j,k,l}^{N}\sigma_{\rm Y}\otimes(\sigma_{\rm Z}^{j}.\sigma_{\rm Z}^{k}.\sigma_{\rm Z}^{l})\sin(d_j t)\sin(d_k t)\sin(d_l t)\prod_{i\neq j,k,l}^{N}\cos(d_i t) \\
+ \quad & \ldots\}.
\end{aligned} \tag{1.16}$$

This equation shows the progress of correlations between the central spin and the environment as a result of the evolution with $\mathcal{H}_{SE}$. A drop in the amplitude of the initial uncorrelated spin operator corresponds to the production of correlated spin terms. The fastest growing correlated spin operators are one spin correlations, $\sigma_{\rm Y}\otimes\sigma_{\rm Z}^{i}$. The two-spin correlated operators, $\sigma_{\rm Y}\otimes(\sigma_{\rm Z}^{i}\cdot\sigma_{\rm Z}^{j})$, show up when the evolution time is long enough for two spins in the environment to be correlated with the central spin simultaneously, and higher correlation orders follow suit.

The expectation value of an arbitrary observable A, acting only on the central spin can be evaluated with $\langle A\otimes\mathbb{1}_{env}\rangle = {\rm Tr}[(A\otimes\mathbb{1}_{env})\rho(t)]$. In a composite Hilbert space the

results of measurements on a subsystem can be evaluated by using the reduced density matrix of that subsystem. Thus, the expectation value of operators A can also be written as $\langle A\rangle = \mathrm{Tr}[A\,\mathrm{Tr}_{env}[\rho(t)]]$, where $\mathrm{Tr}_{env}[\rho(t)]$ represents the reduced density matrix of the central spin after tracing over the environment spins.

Starting from the initial density matrix $\rho_0 = \frac{1}{2^{N+1}}\sigma_{\mathrm{X}}\otimes\mathbb{1}^{\otimes N}$ with the system-environment interaction in the equation 1.10

$$\mathcal{H}_{SE} = \frac{1}{2}\sum_{j=1}^{N} d_j\sigma_{\mathrm{Z}}\otimes\sigma_{\mathrm{Z}}^{j}$$

the evolution of the central spin and the environment is described by equation 1.16. Tracing over environment spins will lead to the reduced density matrix of the central spin:

$$\rho^{cs}(t) = \mathrm{Tr}_{env}[\rho(t)] = \frac{1}{2}\begin{pmatrix} 1 & \prod_{i=1}^{N}\cos(d_i t) \\ \prod_{i=1}^{N}\cos(d_i t) & 1 \end{pmatrix} \tag{1.17}$$

Considering this reduced density matrix we explore the result of measurements on the central spin. For example the expectation value of the magnetization along x is

$$\langle M_{\mathrm{X}}^{cs}\rangle = \mathrm{Tr}[\sigma_{\mathrm{X}}\rho^{cs}(t)] = \prod_{i=1}^{N}\cos(d_i t) \tag{1.18}$$

The expectation value of M_{X}^{cs} is a product of the dipolar oscillations of the central spin to each environment spin.

Another interesting observation is that the outcome of measurements on the environment spins do not evolve, since the reduced state of the environment spins stay unchanged in time, $\mathrm{Tr}_{cs}[\rho_{(t)}] = (\frac{\mathbb{1}}{2})^{\otimes N}$. This means that, the result of independent measurements on the environment give zero information about the state of the central spin or the correlations in the environment, since the reduced state of environment is a fully mixed state at all times.

To visualize the correlation between the central spin and the environment spins, and to make a connection to the concept of local field it is useful to rewrite the density matrix in terms of spin projectors on the environment. $E_+ = \begin{pmatrix} 1 & 0 \\ 0 & 0 \end{pmatrix}$ and $E_- = \begin{pmatrix} 0 & 0 \\ 0 & 1 \end{pmatrix}$ are

idempotent operators and they can be used to indicate spins in pure states along the $+z$ and $-z$, respectively. Using $\mathbb{1} = E_+ + E_-$ we can rewrite the initial density matrix in equation 1.6 as:

$$\rho_{(0)} = \frac{1}{2^{N+1}}\sigma_{\mathrm{X}}\otimes(E_+ + E_-)^{\otimes N} \tag{1.19}$$

$$\begin{aligned} = \frac{1}{2^{N+1}} \quad \{ \quad & \sigma_{\mathrm{X}}\otimes \underbrace{E_+\otimes E_+\otimes E_+ \cdots E_+}_{\text{Hw=N}} \\ + \quad & \sigma_{\mathrm{X}}\otimes \underbrace{E_-\otimes E_+\otimes E_+ \cdots E_+}_{\text{Hw=N-2}} \\ & \vdots \\ + \quad & \sigma_{\mathrm{X}}\otimes \underbrace{E_-\otimes E_-\otimes E_+ \cdots E_+}_{\text{Hw=N-4}} \\ & \vdots \\ + \quad & \sigma_{\mathrm{X}}\otimes \underbrace{E_-\otimes E_-\otimes E_- \cdots E_-}_{\text{Hw=-N}} \\ & \} \end{aligned} \tag{1.20}$$

This is equivalent to picturing an ensemble of central spins as isiochromats labeled by the spin state of the environment. The Hamming weight (Hw) is defined here as the number of E_+ minus the number of E_- operators in a multi-spin term. There are $N+1$ different Hamming weights possible for the N environment spins. While $Hw = N$ has only one possible combination, there are N different combinations of environment spins with $HW = N-2$. The multiplicity of a particular Hamming weight is $\binom{N}{n}$ for $Hw = n$. In total there are 2^N different possible combinations for the N spins in the environment. Each central spin in the ensemble sees a local field corresponding to one of these combinations.

Considering that an environmental spin in E_+/E_- state increase/decrease the local field by a value proportional to its dipolar coupling constant to the central spin d_i, equation 1.20 can be used to describe the local field observed by the ensemble of the central spins

from the following 2^N isochromats:

$$\begin{aligned}
\mathbf{H}(0) \propto \quad \{ \quad & d_1 + d_2 + d_3 + \cdots + d_N \\
, \quad & -d_1 + d_2 + d_3 + \cdots + d_N \\
, \quad & d_1 - d_2 + d_3 + \cdots + d_N \\
& \vdots \\
, \quad & -d_1 - d_2 + d_3 + \cdots + d_N \\
, \quad & -d_1 + d_2 - d_3 + \cdots + d_N \\
& \vdots \\
, \quad & -d_1 - d_2 - d_3 - \cdots - d_N \\
\} \quad & .
\end{aligned} \tag{1.21}$$

The line shape of the central spin is the sum over all of these isochromats, figure 1.1. Since for now there are no interactions between the environment spins, there is a static distribution for the local field which is very populated around zero and small values and has low population for large values. In the case of a constant coupling strength where $d_i = d$, equation 1.21 results in a binomial distribution for the local field, which can be approximated by a Gaussian distribution in the limit of large N, using the central limit theorem. Zurek et al. [30] showed that the Gaussian distribution can be used in the general case if the dipolar coupling constants have a finite variance. The line shapes resulting from various distributions of d_i coefficients, have been discussed in more details [27, 34, 30, 35, 36, 37, 38, 39].

This line shape is a simple example of an inhomogeneous line, which is made up of a large number of time-independent isochromatics. It has the important characteristic that evolution under the corresponding spin Hamiltonian can be simply refocused, either by inverting all of the environment spins or the central spin, which lead to an echo. In this work we are interested in exploring the case where the information in the environment is mixed and a complete refocusing is not possible.

1.1.2 Self-Interacting Environment

The evolution of the central spin in a static environment can always be inverted and refocused by evolving under $-\mathcal{H}_{SE}$ in a closed environment. With no interaction between the environment spins, all the correlation terms evolve back to the initial uncorrelated state, making a perfect echo experiment. So if during the evolution there is information flow from the central spin to the environment, during the inverted evolution this information flows back to the central spin and since there is no internal interaction in the environment, the information revival is complete. Contrary to this, in an environment with self interacting spins, the state of information in the environment changes and a perfect echo can no longer be achieved.

In order to observe how self interacting environment spins change the dynamics of an echo experiment, let us follow an example. Consider a case in which all the Hamiltonian terms are the same as equation 1.7 to 1.10 except the Hamiltonian term for environment spins, which is:

$$\mathcal{H}_E = \frac{1}{2}\sum_{j=1}^{N}\omega_j\sigma_{\mathrm{z}}^j + \frac{1}{2}\sum_{i<j}D_{ij}(\sigma_+^i\otimes\sigma_-^j + \sigma_-^i\otimes\sigma_+^j) \tag{1.22}$$

with $\sigma_\pm = \frac{\sigma_{\mathrm{X}}\pm i\sigma_{\mathrm{Y}}}{2}$. The second term on the right-hand side is known as the flip-flop Hamiltonian term which swaps spins in the environment according to their dipolar coupling constants and leads to mixing of the quantum information in the environment. To show its effect, consider a case in which the spin system has evolved under the $\mathcal{H}_{SE}$ in equation 1.10, for time T and its density matrix has the form indicated in equation 1.16:

$$
\begin{aligned}
\rho_{(t)} = \frac{1}{2^{N+1}} \quad \{ \quad & \sigma_{\mathrm{X}} \otimes \mathbb{1}^{\otimes N} \prod_{i=1}^{N} \cos(d_i t) \\
+ \quad & \sum_{j=1}^{N} \sigma_{\mathrm{Y}} \otimes \sigma_{\mathrm{Z}}^{j} \sin(d_j t) \prod_{i \neq j}^{N} \cos(d_i t) \\
- \quad & \sum_{j,k}^{N} \sigma_{\mathrm{X}} \otimes (\sigma_{\mathrm{Z}}^{j} . \sigma_{\mathrm{Z}}^{k}) \sin(d_j t) \sin(d_k t) \prod_{i \neq j,k}^{N} \cos(d_i t) \\
- \quad & \sum_{j,k,l}^{N} \sigma_{\mathrm{Y}} \otimes (\sigma_{\mathrm{Z}}^{j} . \sigma_{\mathrm{Z}}^{k} . \sigma_{\mathrm{Z}}^{l}) \sin(d_j t) \sin(d_k t) \sin(d_l t) \prod_{i \neq j,k,l}^{N} \cos(d_i t) \\
+ \quad & \ldots \}.
\end{aligned}
$$

Assume that the dipolar coupling constant to the central spin is large for the i^{th} spin and is small for the j^{th} spin. Therefore, the spin operators for these two spins may be approximated with $\sigma_{\mathrm{Z}}^{i} \otimes \mathbb{1}^{j}$. At time T the environment interaction $\mathcal{H}_E$ is turned on and the evolution of these two spins under the flip-flop Hamiltonian is:

$$
\mathcal{U}_{\text{flip-flop}}^{ij} = \exp(-i \frac{D_{ij} t}{2} (\sigma_{+}^{i} \otimes \sigma_{-}^{j} + \sigma_{-}^{i} \otimes \sigma_{+}^{j})) \tag{1.23}
$$

$$
\begin{aligned}
\mathcal{U}_{\text{flip-flop}} (\sigma_{\mathrm{Z}}^{i} \otimes \mathbb{1}^{j}) \mathcal{U}_{\text{flip-flop}}^{\dagger} = & \frac{1}{2} \{ \sigma_{\mathrm{Z}}^{i} \otimes \mathbb{1}^{j} + \mathbb{1}^{i} \otimes \sigma_{\mathrm{Z}}^{j} \\
+ & (\sigma_{\mathrm{Z}}^{i} \otimes \mathbb{1}^{j} - \mathbb{1}^{i} \otimes \sigma_{\mathrm{Z}}^{j}) \cos(D_{12} t) + (\sigma_{\mathrm{X}}^{i} \otimes \sigma_{\mathrm{Y}}^{j} - \sigma_{\mathrm{Y}}^{i} \otimes \sigma_{\mathrm{X}}^{j}) \sin(D_{12} t) \}.
\end{aligned} \tag{1.24}
$$

So this evolution under the environment Hamiltonian has two effects: first, is the exchange of the state of spin i and j and the second is, introduction of new correlated spin terms which are not produced in a static environment. This is an indication of richer dynamics in a self-interacting spin environment.The coupling constant for the flip-flop interaction is determined by the geometry of the spin environment and is different from the coupling constants to the central spin. This adds to the complexity of the environment, while a few spins are strongly correlated to the central spin and directly affect its evolution, a larger group of environment spins, coupled with the flip-flop interaction, have an indirect influence on the evolution of the central spin.

The concept of a local field is useful for analyzing central spin dynamics. The flip-flop term in the homonuclear dipolar interaction, leads to the exchange of spin states

in the environment between isochromats with the same Hamming weight, equation 1.23. The exchange between two isochromats in the fast exchange regime results in a weighted average of the two isochromats. If the rate of spin exchange is slow, it broadens the two line shapes and moves them toward each other. In both of these cases the exchange between environment spins result in complexities in the effective local field that can profoundly change the line shape of the central spin, figure 1.1. The exchange rate for two isochromats is determined by the homonuclear dipolar coupling constant of the interacting spins.

Because the Markovian approximation oversimplifies the central spin problem and fails to capture quantum dynamics of the central spin, it does not lead to a reasonable quantum many body theory for this problem. It has been shown that finding a quantum dynamical map for the central spin can only be achieved by taking into account the correlated spin operators and the collection of individual spin fluctuations can not describe the dynamics of the central spin [40, 41, 42, 43, 44]. The pair correlation approximation considers individual pairs of nuclear flip-flop actions as an excitation mode to construct a map for decoherence of the central spin [45]. The linked-cluster approximation goes beyond the correlated spin pairs and uses the Feynman diagram method to calculate the effects of higher order correlated spin terms in the evolution of the central spin [46]. The Cluster Correlation Expansion (CCE) systematically includes higher orders of correlated spin terms in the evolution. This leads to an exact calculation in the case that all possible correlations are included. The effective dynamics of the central spin in the CCE method gives convergent results by truncating the CCE by keeping the multi-spin correlations up to a certain maximum order M. [47, 48].

Ma et al [49] showed that the correlated spin terms calculated using the CCE method produce identifiable signatures in the evolution of the central spin which can be isolated and observed by the application of different control sequences. They discovered that control sequences for refocusing of the dynamics of the environment spins, target different orders of correlations in the environment based on the number of their pulses. As a result, for odd or even number of control pulses the most effective terms in the central spin dephasing are caused by second-order or fourth-order of multi-spin correlations in the environment, respectively. They analyzed the evolution of the central spin induced by various orders of correlated spin clusters and showed that as the CCE method predicts, the changes in the dephasing time of the central spin is determined by the order of the correlations between

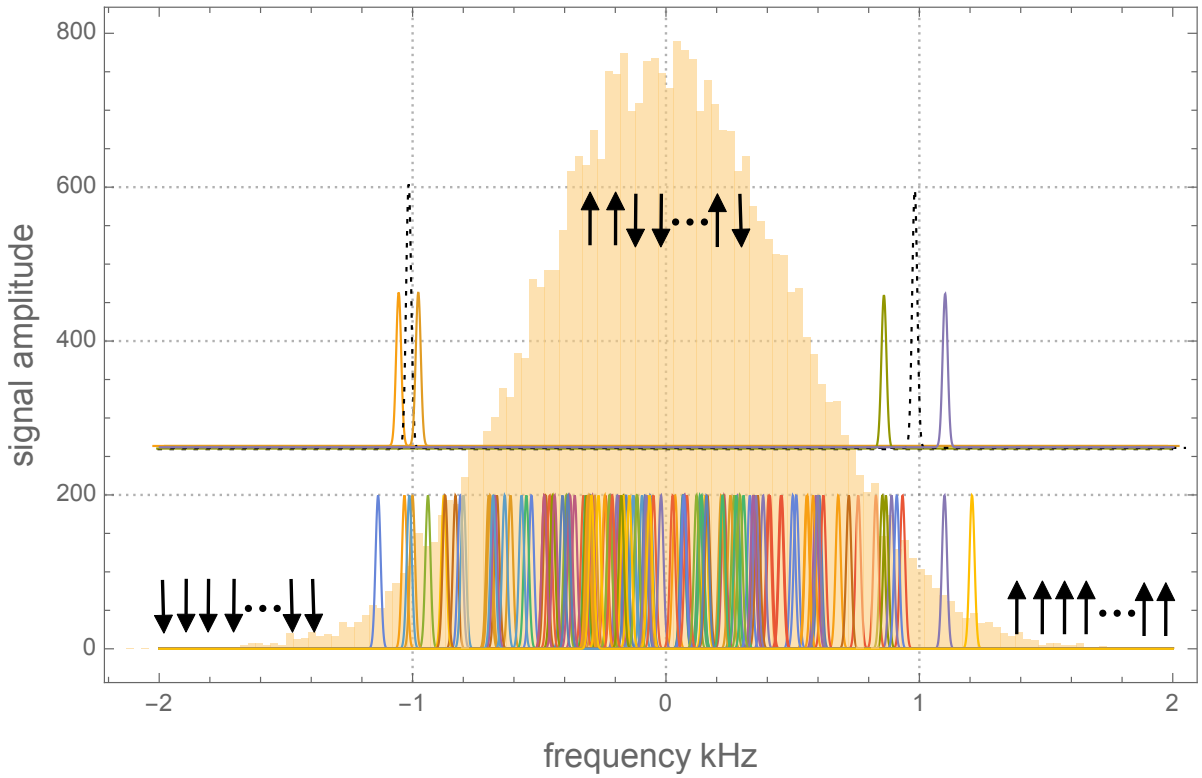

Figure 1.1: For N spins in the environment, there are 2^N possible combinations of E_+ and E_- each inducing a different local field, or 2^N isochromats. In a spin ensemble, the distribution of these isochromats determines the line shape. The extremes of the local field distribution are caused by combinations such as all spins up $Hw = N$ and all spins down $Hw = -N$, terms with small multiplicity, in contrast the center corresponds to combinations with small Hamming weights and large multiplicity. This results in a nearly Gaussian distribution for the local field which is presented here by adding the local field of 2^{15} isochromats. 128 isochromats are also plotted here. The effect of exchange between two isochromats and resulting change in the effective local field is shown in the fast exchange regime.

central spin and the environment. Consequently, they were able to observe and identify the influence of different orders of correlation on the evolution of the central spin.

In this section we emphasized the importance of incorporating multi-spin correlations between the central spin and the environment in evaluation of the evolution of the central spin. A quantum dynamical map for the evolution of the central spin can only be constructed by considering the dynamics of these correlations. The CCE method suggests that effects of multi-spin correlations should be evaluated in the dynamical map. Motivated by this we have designed experiments, using Multiple Quantum NMR (MQNMR) techniques, to directly observe the production and growth of multi-spin correlation between the central spin and the environment. Results of these experiments can be used to make an effective map for evolution of the central spin.

1.2 Underlying structure of the Central Spin problem

The central spin is initially in a separable state from the environment spins and it holds all of the quantum information. The evolution under the system-environment Hamiltonian produces multi-spin correlations between the central spin and environment spins at the expense of the uncorrelated spin term. In a multi-spin correlated operator the quantum information is shared between the central spin and the environment spins. This evolution from uncorrelated spin term to multi-spin correlation is interpreted as a flow of quantum information from the central spin to the environment. Notice that the quantum information is not lost but it is simply being stored in the form of multi-spin correlations between the central spin and the environment spins, and performing an echo experiment will refocus the initial state of the central spin. Examples of echo experiments include Hahn echo for refocusing the heteronuclear dipolar interaction [18], solid echo and magic echo for refocusing the homonuclear dipolar interaction [21, 25]. The revival of the initial state of the central spin in an echo experiment is the result of flow of quantum information from the environment spins back to the central spin. The success of an echo experiment depends on the structure and dynamics of the quantum information in the environment. The goal of our experiments is to provide us with the production and growth rate of multi-spin correlations between the central spin and the environment that are essential for understanding the dynamics of the quantum information flow. In this section we introduce

a pictorial model for the flow of quantum information in the central spin setup based on detection of the multi-spin correlations.

1.2.1 Pictorial representation:

Suppose that we have a central spin surrounded by N non-interacting spins that form a closed spin environment. Initially the central spin and the environment spins are uncorrelated and their composite spin system is described with equation 1.6:

$$\rho(0) = \frac{1}{2^{N+1}} \sigma_{\mathrm{X}} \otimes \mathbb{1}^{\otimes N}.$$

The system-environment Hamiltonian is the same as equation 1.10:

$$\mathcal{H}_{SE} = \frac{1}{2} \sum_{j=1}^{N} d_j \sigma_{\mathrm{Z}} \sigma_{\mathrm{Z}}^{j}.$$

The evolution of the initial density matrix under the interaction Hamiltonian is described by the unitary operator $\mathcal{U}_{SE} = \exp[-i\mathcal{H}_{SE}t]$. Solving the Liouville-Von Neumann equation gives the time evolution of this system-environment density matrix, equation 1.13:

$$\rho_{(t)} = \mathcal{U}_{SE} \cdot \rho_{(0)} \cdot \mathcal{U}_{SE}^{\dagger}.$$

As discussed above, the time evolution of the spin system results in the oscillation of the amplitudes of the initial uncorrelated state and the correlated spin operators, according to equation 1.16:

$$\begin{aligned}
\rho_{(t)} = \frac{1}{2^{N+1}} \quad \{ \quad & \sigma_{\mathrm{X}} \otimes \mathbb{1}^{\otimes N} \prod_{i=1}^{N} \cos(d_i t) \\
+ \quad & \sum_{j=1}^{N} \sigma_{\mathrm{Y}} \otimes \sigma_{\mathrm{Z}}^{j} \sin(d_j t) \prod_{i \neq j}^{N} \cos(d_i t) \\
- \quad & \sum_{j,k}^{N} \sigma_{\mathrm{X}} \otimes (\sigma_{\mathrm{Z}}^{j} . \sigma_{\mathrm{Z}}^{k}) \sin(d_j t) \sin(d_k t) \prod_{i \neq j,k}^{N} \cos(d_i t) \\
- \quad & \sum_{j,k,l}^{N} \sigma_{\mathrm{Y}} \otimes (\sigma_{\mathrm{Z}}^{j} . \sigma_{\mathrm{Z}}^{k} . \sigma_{\mathrm{Z}}^{l}) \sin(d_j t) \sin(d_k t) \sin(d_l t) \prod_{i \neq j,k,l}^{N} \cos(d_i t) \\
+ \quad & \ldots \}.
\end{aligned}$$

This equation gives us the framework for the flow of quantum information from the central spin to the environment and production of multi-spin correlation between them. We observe that at short evolution times the uncorrelated spin term is dominant. The spins with the strongest coupling to the central spin will establish their correlations with it in the form of first order correlation operators. As a consequence the quantum information is no longer exclusively contained in the state of the central spin and is shared in the form of correlated operators of the central spin and the environment spins. Production of multi-spin correlations between the central spin and the environment is equivalent to the flow of quantum information from the central spin to the environment. Increasing the evolution time results in production of additional correlations with larger orders of correlated operators. Our pictorial model for this situation is shown in figure 1.2.

For a short evolution time T, the density matrix does not greatly deviate from its initial form and the uncorrelated spin term has a large weight while all the correlated spin terms are small and unobservable. This situation is depicted in figure 1.2a. Notice that all the environment spins are uncorrelated with the central spin and their state has not changed from the maximally mixed. In the intermediate evolution time, figure 1.2b, there are visible differences between the states of environment spins. This state has achieved correlations of third order with the central spin. The initial information of the central spin is now shared with three spins in the environment, in the form of a correlated spin operator. Consequently, there is a distribution of quantum information over the environment spins, although a measurement performed only on the environment spins will not reveal that information. Figure 1.2c shows a more complicated correlated state with 7 spins involved in the correlation to the central spin, for the case of the longest evolution time T.

This pictorial representation may be used to explain the echo experiment as well. Figure 1.3a represents the result of an echo experiment for an environment with three correlated spins at an intermediate evolution time. Application of a π pulse results in a sign change for the heteronuclear dipolar interaction, in the interaction frame of the pulse. Because there is no self-interaction between the environment spins, after evolution for time T, if the second evolution period is sandwiched between two π pulses, a complete revival of the initial state of the central spin is observed at time $2T$. In other words, there will be a Loschmidt echo in which all the information returns to the central spin. The same applies for any evolution time T, figure 1.3b. Although the quantum information may be

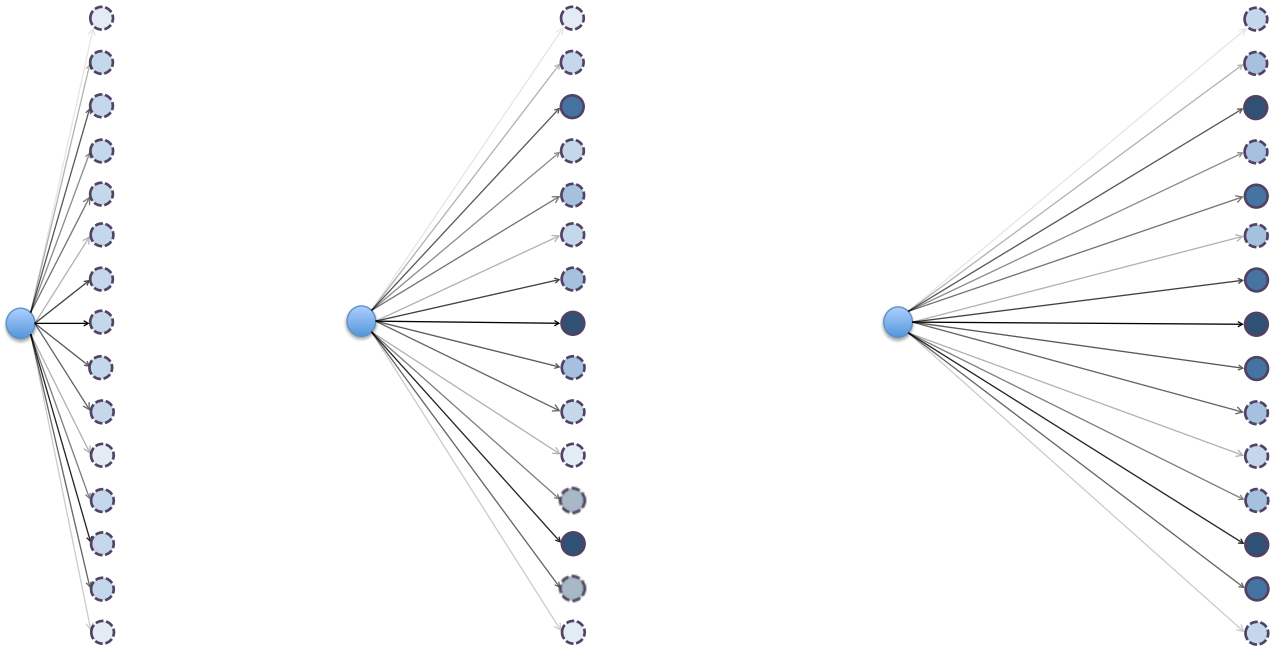

(a) Short evolution time T (b) Intermediate evolution time T (c) Long evolution time T

Figure 1.2: The large blue dot represents the central spin and the smaller dots indicate the environment spins for a closed environment with $N = 15$. Arrows are indicative of the strength of couplings between the central spin and environment spins with a bolder arrow indicating a larger absolute value for the dipolar coupling constant. The distance between the central spin and the environment spins changes according to the evolution time T. Spins in the environment are presented in 4 different shades of blue, depicting the amplitude of their correlated spin operator with the central spin. Lighter shades are used when the correlated states have a smaller weight, which are not observable. If the correlation between an environment spin and the central spin is observable in the experiment, that spin is presented with a solid border line. This picture indicates that the environment spins become correlated with the central spin as the evolution time increases which corresponds to the flow of quantum information from the central spin to the environment.

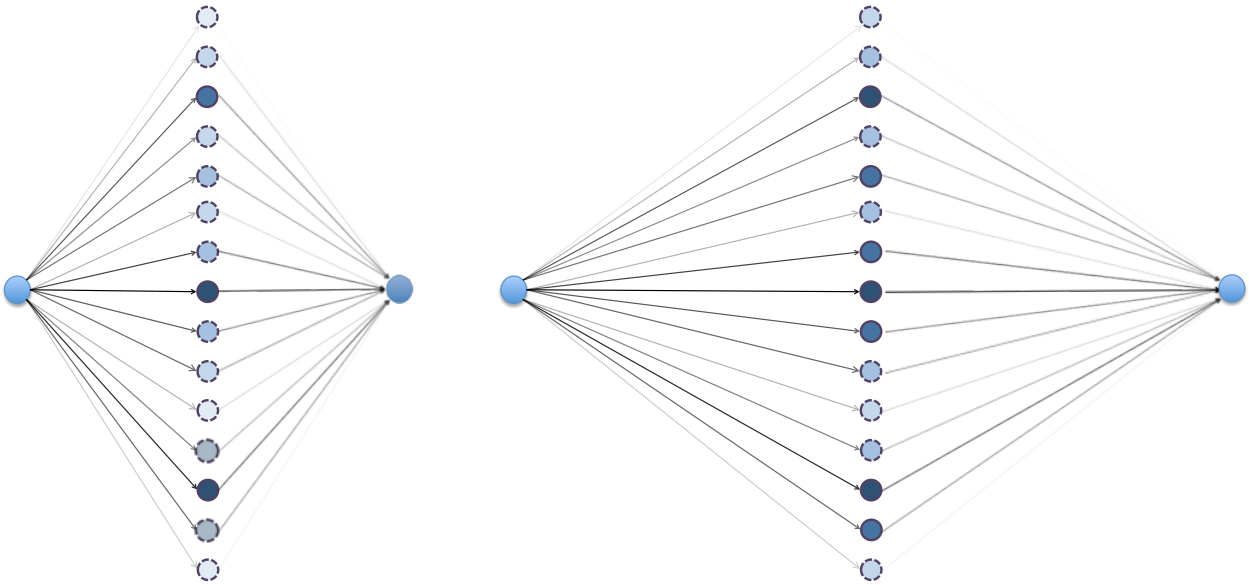

(a) Intermediate evolution time T (b) Long evolution time T

Figure 1.3: Diagram of an echo in the case of a static environment. Increasing the evolution time results in larger multi-spin correlations between the central spin and environment. As long as the environment spins only interact with the central spin, an echo experiment will perfectly refocus the initial state of the central spin, a Loschmidt echo.

distributed over a more complicated correlated state, because of the static nature of the environment, it can be perfectly refocused to the initial uncorrelated state of the central spin.

Here the message is that for an environment with no self-interaction, the quantum information flow to the environment becomes encoded in the multi-spin correlated states, which can be refocused back to the central spin. In other words the environment keeps a perfect record of the initial quantum information of the central spin. In this picture we have neglected the T_1 effects which can randomly flip the environment spins and decrease the amplitude of revival signal in the spin ensemble.

Let us relax one of these two conditions and allow the environment spins to interact with each other for a time interval that we call the mixing window. The interaction of the environment spins during this window is described by the homonuclear dipolar inter-

action that contains the flip-flop term, equation 1.22. The evolution under the flip-flop term exchanges the state of interacting spins, equation 1.23, and cause a mixing in the multi-spin correlated terms that mixes the quantum information in the environment. The mixing window is positioned after the evolution time T, when the production of multi-spin correlated operators between the central spin and the environment has completed, and immediately before the refocusing step. If the mixing window is short, distribution of correlations between the central spin and the environment doesn't change significantly and refocusing step will be successful in reviving the central spin initial state, figure 1.4a. By increasing the length of mixing window, the exchange interaction between environment spins will effectively mix the multi-spin correlations in the environment, figure 1.4b. Notice that each spin may go through multiple exchanges of state and end up with a completely different correlation state with the central spin at the end of the mixing window. Because the strength of heteronuclear dipolar coupling to the central spin is different for the environment spins, mixing them will result in correlated states that can only be partially refocused. As an example consider the case that a spin which is strongly correlated with the central spin, depicted with a dark blue circle and a solid border, undergoes an exchange interaction with a spin with weak coupling to the central spin, represented in light blue and dashed border. After the exchange we have a spin in dark blue with dashed border and weak coupling to the central spin, and also a light blue spin with solid border and strong coupling to the central spin. None of these two spins will contribute effectively in revival of the initial state of the central spin, which results in a partial echo signal.

This pictorial representation is useful for understanding the significance of the environment information content on the effectiveness of the mixing process. For very short evolution times when the environment has only a small number of correlations to the central spin, the environment has a low information content and exchanging the state of its spins cannot effectively change the distribution of information. As a result the amplitude of an echo experiment remains unchanged after introduction of a mixing window. In contrast, an environment with many correlations to the central spin has a large information content and is more sensitive to the mixing process. Consequently, we expect that the sensitivity of the environment to the mixing Hamiltonian depend on its information content, and this impacts the amplitude of the echo signal.

This pictorial model is a simple representation of the complex dynamics of multi-spin

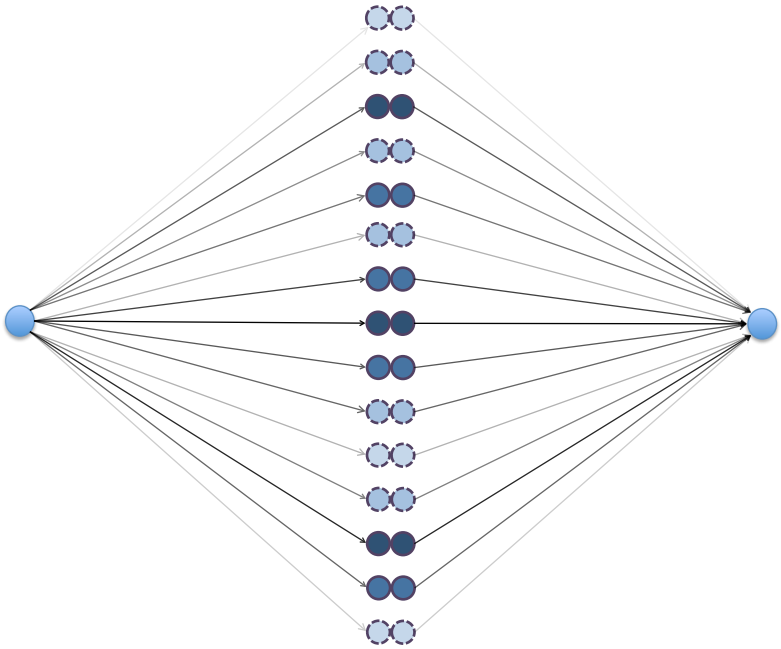

(a) Very short mixing window

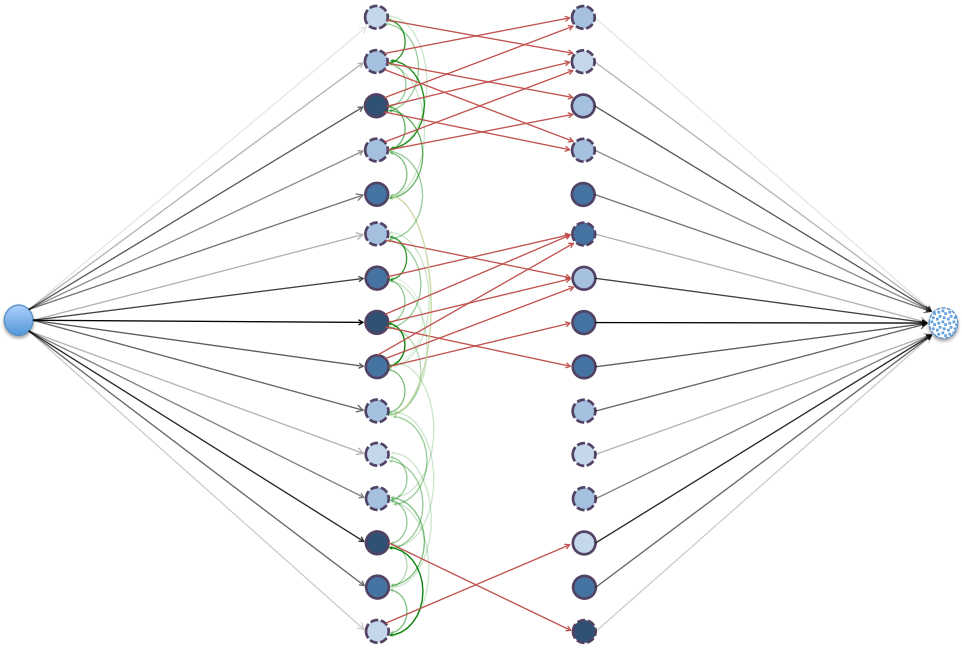

(b) Longer mixing window

Figure 1.4: Introducing a mixing window will result in partial refocusing of the central spin initial state.

correlations between the central spin and environment for explaining the flow of quantum information in the central spin problem. In chapter four we present the results of experiments which were designed to record the dynamics of multi-spin correlations in the central spin system, and connect to this picture of quantum information flow.

1.3 Multi-spin dynamics of solid state NMR

To construct a model for the evolution of a central spin enclosed by a spin environment, we need to go beyond the static picture of spin correlations and induced local field, and construct a dynamic model of evolution for the multi-spin physics of the central spin. Multiple Quantum (MQ) NMR has the right toolbox to enable discovery of the multi-spin dynamics as a spin system evolves in time. In this section we introduce the MQ NMR technique and describe previously performed experiments with this method.

1.3.1 Spin counting experiment

The early works in MQ NMR were developed for observation of the quantum coherence transitions in a multi-spin systems, including the so called spin counting experiment [50, 51, 52, 53, 54, 55, 56, 57, 58]. In that experiment a pulse sequence is applied to convert the dipolar Hamiltonian to a grade raising Hamiltonian , $((\sigma_+ \otimes \sigma_+) + (\sigma_- \otimes \sigma_-))$, and growth of multi-coherence spin operators in a network of dipolar connected spins is observed. Investigation of MQ coherences with spin counting experiment has been valuable in giving insight into the spatial state of spins in polymers and crystalline samples.

The idea behind discovering the multi-spin correlated operators, or the MQ coherences, is to utilize the rotational symmetry of different parts of the density matrix, since operators with the same coherence order follow the same transformation under a collective rotation. As an example, consider N spin $\frac{1}{2}$ nuclei in a strong magnetic field along the z axis. The total magnetization is determined by difference between the number of spins pointing towards z and the number of spins pointing to $-z$:

$$M_z = \sum_i m_{zi} = \frac{1}{2}(P_{|+1/2\rangle} - P_{|-1/2\rangle}) \tag{1.25}$$

where $m_{zi} = \pm 1/2$ is the eigenvalue of i^{th} spin in the magnetic field and P_i shows population of each state. The off-diagonal components of the density matrix for this spin system $\langle Z_i|\rho|Z_j\rangle$ for $i \neq j$, with $\{|Z_i\rangle\}$ being a set of eigenbases for the Z quantization axis, are called Multiple Quantum Coherences. The order of MQC is defined as $n = M_z(Z_i) - M_z(Z_j)$. If we express the density matrix as a sum over multi-spin operators, having a component with the coherence order n means that the difference between the number of σ^+ operators and σ^- operators in that particular multi-spin operator is n. All parts of the density matrix with the coherence order n have the same response to collective rotation along the quantization axis $R_{\text{z}}(\phi) = \exp(-i\phi\frac{1}{2}\sum_i \sigma^i_{\text{z}})$:

$$\langle Z_i|R_{\text{z}}(\phi)\rho_n R_{\text{z}}(\phi)^\dagger|Z_j\rangle = e^{in\phi}\langle Z_i|\rho_n|Z_j\rangle \tag{1.26}$$

where ρ_n represents a part of density matrix with the coherence order n operators.

This is the basis for distinguishing different coherence orders or different correlated spin terms. All the spins belonging to the same coherence order n, have the same symmetry with respect to $R_{\text{z}}(\phi)$ collective rotations and they gain the same phase factor $e^{in\phi}$. The density matrix of the spin system may be expanded based on this symmetry in the Liouville space:

$$\rho = \sum_{k,n,p} C_{knp} T_{knp} \tag{1.27}$$

Where T_{knp} represents a basis operator made by a product of k single spin operators. In this expression n represents the coherence order, k indicates the number of spins involved in the multi-spin correlated operator and p accounts for number of different permutations in individual spin operators which will have the same k and n.

Figure 1.5 shows the pulse sequence for the spin counting experiment. Consider a sample with an ensemble of protons placed in a strong magnetic field and they evolve under the secular part of homonuclear dipolar interaction:

$$\begin{aligned} \mathcal{H}_D &= \sum_{j<k} D_{jk}(\sigma^j_{\text{z}}\sigma^k_{\text{z}} - \frac{1}{4}(\sigma^j_+\sigma^k_- + \sigma^j_-\sigma^k_+)) \\ D_{jk} &= \frac{\gamma^2\hbar^2}{r^3_{jk}}(1 - 3\cos\theta^2_{jk}) \end{aligned} \tag{1.28}$$

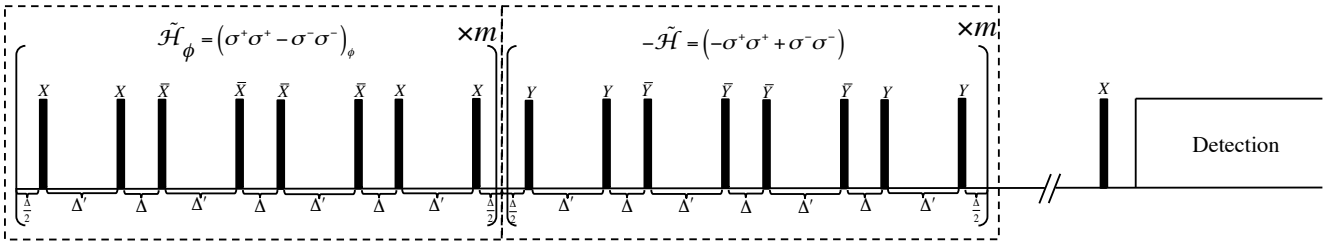

Figure 1.5: Pulse sequence for the spin counting experiment. Black lines present the $\frac{\pi}{2}$ pulses with the noted phase. The first dashed box shows the pulses for the evolution step in which the MQ coherence orders grow, equation 1.29. With the application of pulses in the second dashed box, this evolution is inverted to make the resulting density matrix observable. By repeating 8 pulses in each box, with the loop counter m, the evolution step can be extended to increase the production of MQ coherence orders. The ϕ phase shift between these two boxes implements the collective rotation along the z axis necessary for encoding the MQ coherence orders, equation 1.26.

where γ is the gyromagnetic ratio, r_{jk} is the vector connecting the two spins j and k which makes an angle θ_{jk} to the direction of Zeeman field B_0. Average Hamiltonian Theory may be used to describe an effective Hamiltonian on average of a periodic modulation scheme [59, 60]. The zeroth order average Hamiltonian term for the homonuclear dipolar interaction, in the toggling frame of 8-pulse cycle in figure 1.5 is:

$$\widetilde{\mathcal{H}_D} = -\frac{1}{2}\sum_{j<k} D_{jk}(\sigma_+^j\sigma_+^k - \sigma_-^j\sigma_-^k). \tag{1.29}$$

This effective Hamiltonian increases the order of coherence in the density matrix by ± 2. Collective rotations along the z axis is implemented by shifting the phase of all pulses for ϕ, and results in encoding the coherence order of correlated spin terms with $\mathrm{e}^{in\phi}$ phase factor, equation 1.26. After the encoding step, application of a phase shifted 8-pulses sequence, refocuses the evolution of the density matrix and results in single-spin terms which are observable. This signal at the end of experiment carries the encoded phase factor and may be Fourier transformed to show the weight of MQ coherence orders.

The result of spin counting experiment on the protons in Triphenylphosphine molecule is presented in figure 1.6.

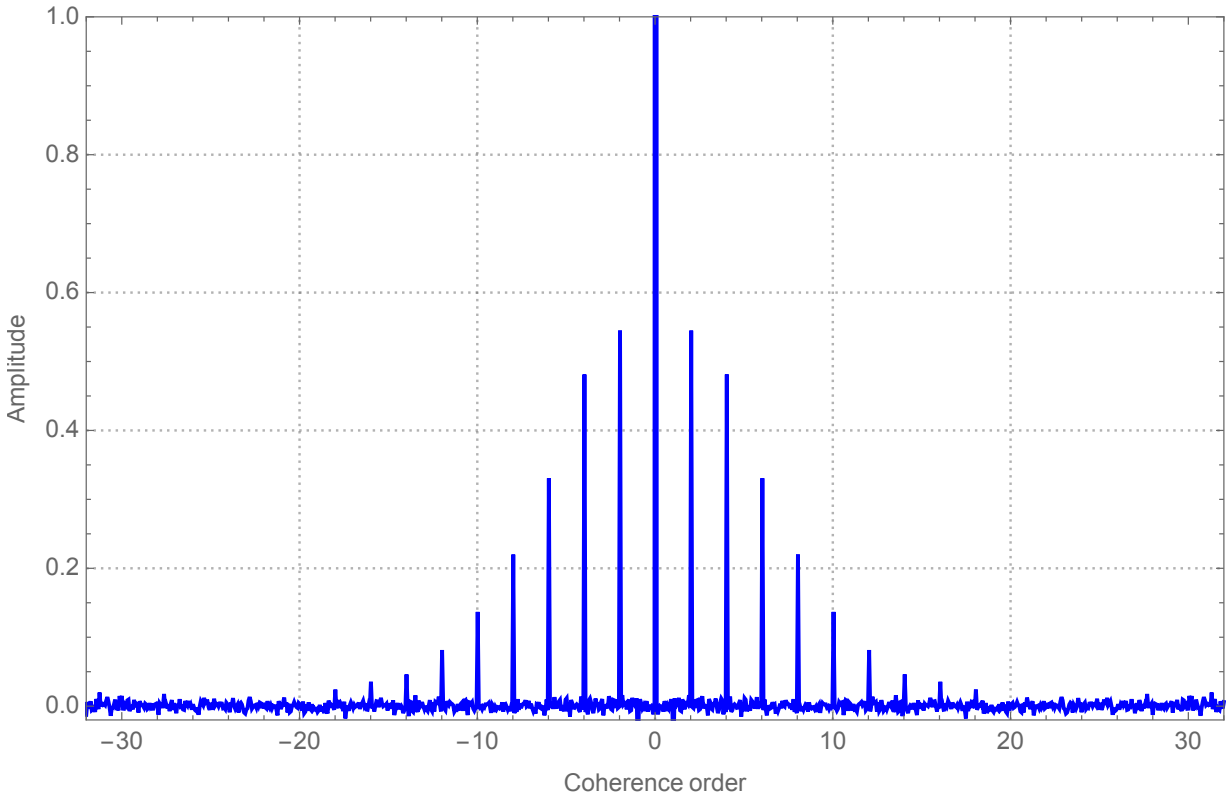

Figure 1.6: Experimental results for the spin counting experiment. Weight of multi-coherence correlated terms in Triphenylphosphine $P(C_6H_5)_3$. Sample at room temperature, $\Delta = 3.5\mu s$, $m = 7$, $\frac{\pi}{2}$ pulse length: $1.99\mu s$ and 64 increments for ϕ.

1.3.2 MQ NMR technique for homonuclear dipolar network

The idea of encoding coherence orders with the use of collective rotations, has been generalized to the other quantization axes, such as x, to uncover different rotational symmetries. x quantization axis has previously used for exploring the growth of coherence orders in a network of spins with homonuclear dipolar interaction [61, 2, 62]. When a collective rotation is used to encode the multi-spin correlations, the preferred basis for representation of the density matrix is also set by the symmetry of that rotation. This is equivalent to the representation of a spin system in a different effective quantization axis which is determined by the rotation axis. This representation can be obtained with a similarity transform from the original basis. In this case the density matrix in the x quantization axis, ρ_{x}, is described as:

$$\rho_{\mathrm{x}} = U^{-1}\rho_{\mathrm{z}}U \tag{1.30}$$

where U indicates the unitary for the similarity transform from the z basis to the x basis. The density matrix elements in each representation are defined as:

$$\{\rho_{\mathrm{z}}\}_{ij} = \langle z_i|\rho|z_j\rangle \tag{1.31}$$

$$\{\rho_{\mathrm{x}}\}_{ij} = \langle x_i|\rho|x_j\rangle \tag{1.32}$$

where $\{z_i\}$ represents a set of basis operators in the z basis, e.g. the set of four Pauli operators, and $\{x_i\}$ represents a set of basis operators for x basis. We choose the following set operators: σ_{X}, the ladder operators in the x basis defined as $\sigma_{\mathrm{X}\pm} = \sigma_{\mathrm{Y}} \pm i\sigma_{\mathrm{Z}}$ and the identity operator. The following commutation relation describes the evolution of the density matrix in this basis:

$$[\sigma_{\mathrm{X}}, \sigma_{\mathrm{X}\pm}] = \pm 2\sigma_{\mathrm{X}\pm}$$
$$[\sigma_{\mathrm{X}+}, \sigma_{\mathrm{X}-}] = 4\sigma_{\mathrm{X}} \quad .$$

Consequently, the result of a collective rotation along the x axis can be represented as:

$$R_{\mathrm{X}}(\theta).\rho.R_{\mathrm{X}}(\theta)^{\dagger} = R_{\mathrm{X}}(\theta).\rho_{\mathrm{x}}.R_{\mathrm{X}}(\theta)^{\dagger} \tag{1.33}$$

$$= \langle x_i|\exp(-i\frac{\theta}{2}\sum_i \sigma_{\mathrm{X}}^i).\rho.\exp(i\frac{\theta}{2}\sum_i \sigma_{\mathrm{X}}^i)|x_j\rangle \tag{1.34}$$

$$= \sum_n \mathrm{e}^{in\theta}\langle x_i|\rho_{\mathrm{X}}^n|x_j\rangle \tag{1.35}$$

where n represents the coherence order along x axis. This shows that a rotation along x axis introduces $e^{in\theta}$ phase factor with n coherence order in the x quantization axis defined as $n = N(\sigma_{x+}) - N(\sigma_{x-})$. As a result in this representation, there is a clear relation between the coherence order and the phase factor introduced by the rotation.

Munowitz et al. used vectors in the Liouville space to represent the density matrix in the z quantization axis [52]. Similar expansion may be done using the set of $\{x_i\}$ operators in the x quantization axis for the density matrix:

$$\rho_x(t) = \sum_{k=0}^{N} \sum_{n=-k}^{k} \sum_{p} g_{knp}(t) \hat{P}_{knp} \tag{1.36}$$

where N is the number of spins, $\hat{P}_{knp}$ is a basis operator constructed by product of k single spin operators in x basis, n indicates the coherence order in the x basis and p identifies the different permutations of k spins with the coherence order n. Although rotations along the x axis can reveal the coherence order n, they cannot give direct information about the number of spins k involved in a correlated multi-spin term, nor they distinguish the specific order of the multi-spin terms, p. This means that in order to define the operators to reflect the time evolution of the density matrix as they are distinguished by the x rotations, we should sum over k and p degrees of freedom:

$$\rho_x(t) = \sum_{n=-k}^{k} C_n(t) \hat{P}_n \tag{1.37}$$

$$C_n(t) = \sum_{k=0}^{N} \sum_{p} g_{knp}(t) \tag{1.38}$$

$$\hat{P}_n = \sum_{k=0}^{N} \sum_{p} \hat{P}_{knp} \tag{1.39}$$

Encoding the coherence order in the x quantization axis, has proven to be a powerful tool for investigation of the multi-spin dynamics in the solid-state spin systems. Cho et al. [2] used this technique to study the mechanism of Free Induction Decay (FID) in a solid state sample with a network of spin $\frac{1}{2}$ particles interacting with the homonuclear dipolar interaction. For a system of homonuclear dipolar connected spins in a large magnetic field

B_0 along the z axis the initial density matrix in thermal equilibrium, is:

$$\rho_{initial} = \frac{\mathbb{1} + \epsilon\sigma_{\mathrm{Z}}}{2} \tag{1.40}$$

which is a diagonal matrix containing only population terms and no coherence components. ϵ is the nuclear spin polarization which is proportional to $\frac{\gamma B_0}{K_B T}$ and is of order 10^{-6}. The Identity part of this density matrix will not evolve and we focus our attention on the deviation part $\rho_{(0)} = \sum_i \sigma^i_{\mathrm{Z}}$. At $t = 0$ a $\frac{\pi}{2})_{\bar{Y}}$ pulse rotates $\rho_{(0)}$ to $\rho_{(0^+)} = \sum_i \sigma^i_{\mathrm{X}}$. This density matrix then evolves under the homonuclear dipole interaction. The formal equation of motion for this time independent Hamiltonian is given by the Liouville-von Neumann equation:

$$\rho_{(t)} = e^{-iH_D t}\rho_{(0^+)}e^{iH_D t} \tag{1.41}$$

which does not have an exact solution, as discussed in the previous section. Expanding this equation using power series gives an insight for understanding the multi-spin dynamics in this system at short times:

$$\begin{aligned}
\rho_{(t)} &= \rho_{(0)} + \frac{i}{\hbar}t[\rho_{(0)}, H_D] - \frac{t^2}{2\hbar^2}[[\rho_{(0)}, H_D], H_D] + \cdots \\
&= \frac{1}{2}\sum_j (\sigma^j_+ + \sigma^j_-) + \frac{3}{2}it\sum_{jk} D_{jk}(\sigma^j_{\mathrm{Z}}\sigma^k_+ - \sigma^j_{\mathrm{Z}}\sigma^k_-) \\
&+ \frac{3}{4}t^2\sum_{jkl} D_{lk}D_{jk}(\sigma^j_{\mathrm{Z}}\sigma^l_{\mathrm{Z}}\sigma^k_+ + \sigma^j_{\mathrm{Z}}\sigma^l_{\mathrm{Z}}\sigma^-_k) + \cdots .
\end{aligned} \tag{1.42}$$

Note that in NMR inductive detection is used and the observable operator is σ_+ and the NMR signal is evaluated as $S_{(t)} \propto \sum_i \mathrm{Tr}[\sigma^i_+\rho_{(t)}]$. Only the single-spin and single-coherence terms have non-zero trace and contribute to NMR signal. Evolution of the spin system produces the multi-spin correlated operators in the density matrix, indicated in equation 1.42. For longer evolution times the correlated spin terms gain more weight relative to the weight of the initial single spin term, this results in loss of the observable signal in FID [2].

Using the MQ techniques we can have a detailed understanding of the decay of observable signal, corresponding to the growth of the MQ terms. The homonuclear dipolar Hamiltonian in the basis vectors of the x quantization axis or x basis with defining

$\sigma_{\mathrm{X}\pm} = \sigma_{\mathrm{Y}} \pm i\sigma_{\mathrm{Z}}$, is written as:

$$\begin{aligned} \mathcal{H}_D^{\mathrm{X}} &= -\frac{1}{2}\sum_{j<k} D_{jk}(\sigma_{\mathrm{X}}^j\sigma_{\mathrm{X}}^k - \frac{1}{4}(\sigma_{\mathrm{X}+}^j\sigma_{\mathrm{X}-}^k + \sigma_{\mathrm{X}-}^j\sigma_{\mathrm{X}+}^k)) \\ &- \frac{3}{8}\sum_{j<k} D_{jk}(\sigma_{\mathrm{X}+}^j\sigma_{\mathrm{X}+}^k + \sigma_{\mathrm{X}-}^j\sigma_{\mathrm{X}-}^k). \end{aligned} \tag{1.43}$$

The density matrix may also be evaluated by transforming equation 1.42 to the x basis:

$$\begin{aligned} \rho^{\mathrm{X}}(t) &= \sum_j \sigma_{\mathrm{X}}^j + \frac{3}{4}it\sum_{jk} D_{jk}(\sigma_{\mathrm{X}+}^j\sigma_{\mathrm{X}+}^k - \sigma_{\mathrm{X}-}^j\sigma_{\mathrm{X}-}^k) \\ &- \frac{3}{8}t^2\sum_{jkl} D_{lk}D_{jk}(\sigma_{\mathrm{X}+}^j\sigma_{\mathrm{X}}^k\sigma_{\mathrm{X}+}^l - \sigma_{\mathrm{X}+}^j\sigma_{\mathrm{X}}^k\sigma_{\mathrm{X}-}^l - \sigma_{\mathrm{X}-}^j\sigma_{\mathrm{X}}^k\sigma_{\mathrm{X}+}^l + \sigma_{\mathrm{X}-}^j\sigma_{\mathrm{X}}^k\sigma_{\mathrm{X}-}^l) + \cdots . \end{aligned} \tag{1.44}$$

Considering equation 1.27 which describes the density matrix of a spin system as a sum over terms with the spin number k and the coherence order n, one can define a selection rule for evolution under the homonuclear Hamiltonian in the z basis, equation 1.28, and in the x basis, equation 1.43. Projection of the Liouville space into the k and n axes [52] for both of these two Hamiltonian representations, reveals a set of available paths in the Liouville space that may be taken by the density matrix, figure 1.7. A selection rule can be associated with the available paths in the Liouville space for homonuclear dipolar Hamiltonian in the Zeeman basis representation:

$$\Delta k = \pm 1, \qquad \Delta n = 0. \tag{1.45}$$

This is depicted in figure 1.7a which indicates that in the Zeeman basis, the time evolution under the homonuclear dipolar interaction produces correlated spin terms and increases the number of correlated spins k which results in a decrease in the weight of observable operators. The coherence order n on the other hand, does not show any changes when the density matrix is expressed in the Zeeman basis. The selection rules for the evolution under the same Hamiltonian transformed to the x basis is:

$$\Delta k = \pm 1, \qquad \Delta n = 0, \pm 2. \tag{1.46}$$

Figure 1.7b shows the available multi-spin operators in the Liouville space in the x basis. In this representation both spin number k and coherence number n change as a result of

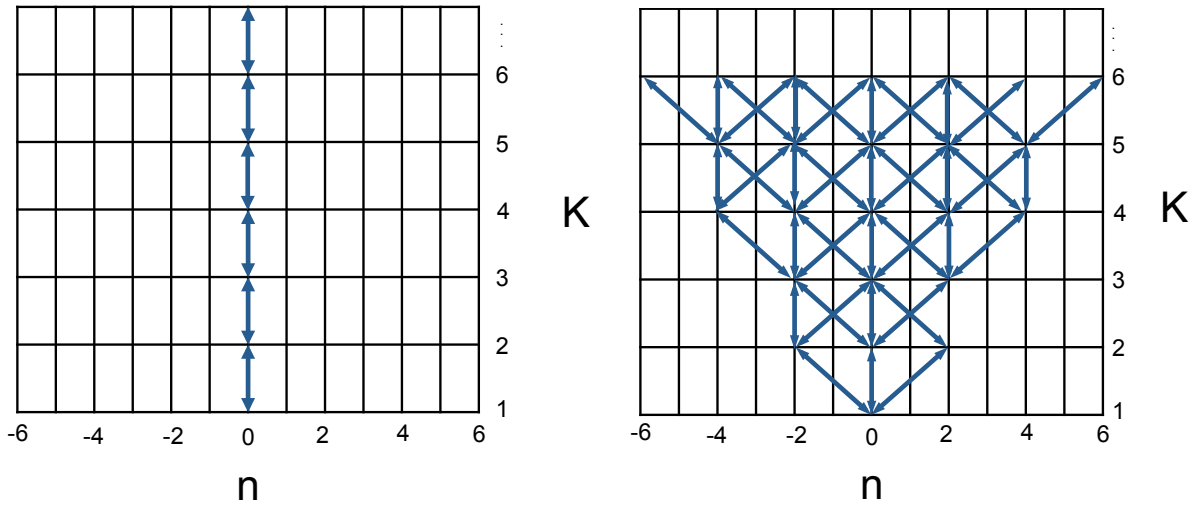

(a) Zeeman basis

(b) X basis

Figure 1.7: The Liouville space is projected on to the multi-spin operators with the number of spins k and the coherence order n. The space spanned by the homonuclear dipolar interaction in the Zeeman basis and in the x basis is presented.

evolution under homonuclear dipolar interaction. Note that the increase in the coherence order n happens in the steps of two units, so the evolution under the homonuclear dipolar interaction will not change the parity coherence orders in the density matrix.

This progress in the population of multi-spin correlated terms during the FID may be detected with an NMR experiment presented in figure 1.8. After the initial evolution of spins under the homonuclear dipolar interaction, a collective rotation about the x axis encodes the coherence orders of correlated operators as a phase factor, as discussed in equation 1.35. Next, the spin system evolves under the inverted dipolar interaction to its initial single spin state which is observable, while the encoded phase factor is preserved and will be detected.

Equation 1.35 indicates that a Fourier relation exist between the coherence order n and the angle of the encoding pulse, which suggests that with the detection of data along the ϕ axis one can find the weight of correlated spin terms along the n or number of coherence axis. The standard way to perform this experiment is to implement the encoding rotations

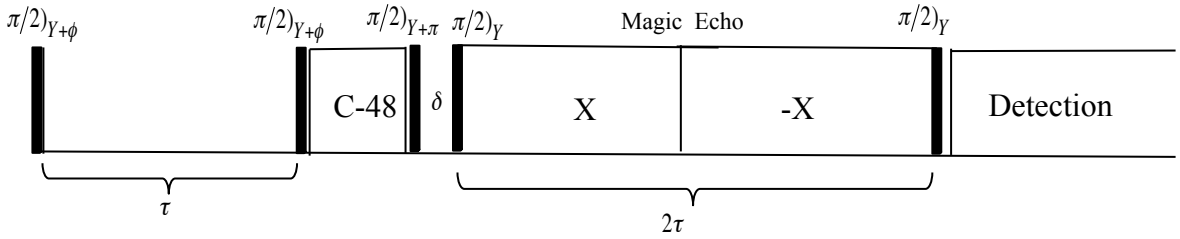

Figure 1.8: Pulse sequence for detection of the growth of MQ coherence orders with evolution under homonuclear dipolar interaction. During the first τ period, the dipolar evolution creates multi-spin correlated terms. The two pulses with a C-48 sequence between them represent a robust way of applying the collective ϕ encoding pulse along the x axis. C-48 is a 48-pulse sequence for evolution suspension [1]. With the application of RF radiation for 2τ the dipolar evolution is inverted and the observable signal can be detected at the end of the sequence.

with incremental values for ϕ, going from 0 to 2π in $2n_{max}$ steps. n_{max} indicates the maximum coherence number that the experiment can detect. This is to comply with the Nyquist-Shannon sampling theorem which states that: the sampling frequency should be at least twice the highest frequency contained in the signal. Integrating over the frequency domain signal for each of these encoding steps yields one data point along the ϕ axis. The Fourier transform of these points with respect to n reveals the weight of each coherence order. Figure 1.9 indicates the result of such an experiment carried out on a crystal of CaF_2, taken from [2]. Performing this experiment for different values of τ reveals the progress of multi-spin coherence spin term production as the system evolves under the homonuclear dipolar interaction during FID [2].

Cho et al went one step further and followed the dynamics of individual multi-spin correlated terms as they changed the time of evolution τ. Their results are presented in figure 1.10 which shows the decay of the zeroth coherence term while the higher coherence order terms are being produced. There is an onset time for each of these coherence terms to become observable, which is determined by the geometry of the spin system. The initial growth of multi coherence terms is fitted with a sigmoidal function:

$$S_n(t) = \frac{C_n}{1 + \exp[-\alpha_n(t - t_n^{onset})]} \tag{1.47}$$

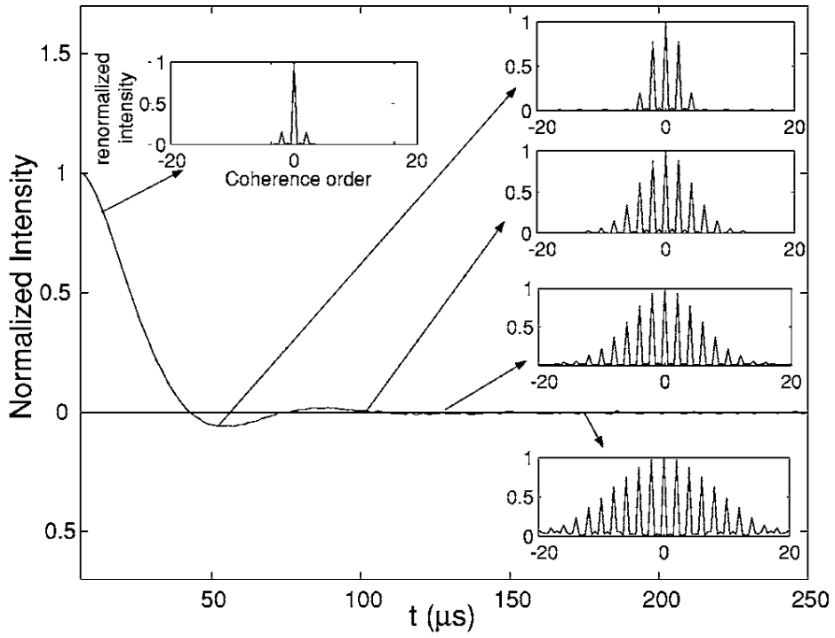

Figure 1.9: Experimental results from [2] indicating the overlay of the Free Induction Decay curve and the growth of multiple quantum coherence terms in CaF_2. The FID is a result of the evolution under homonuclear dipolar interaction.

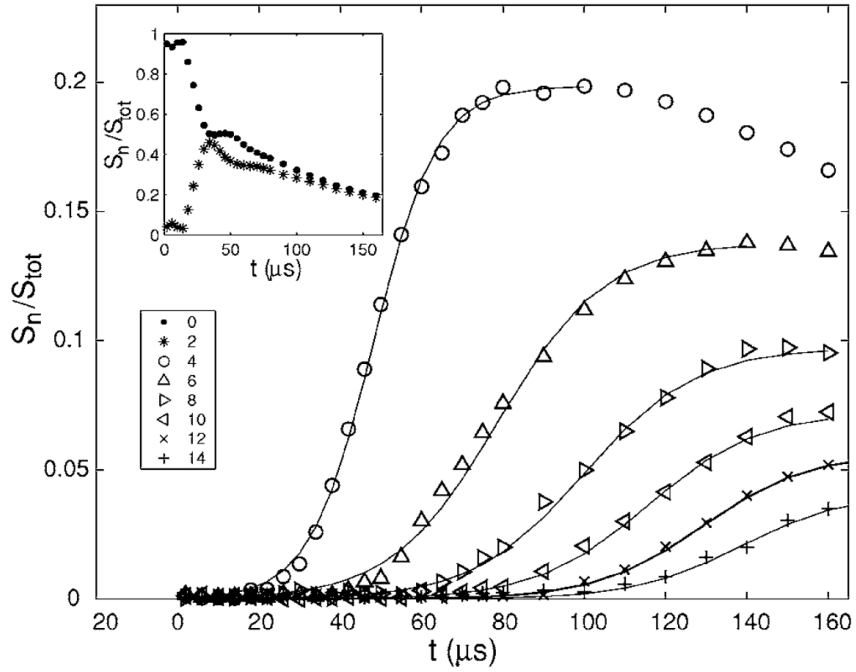

Figure 1.10: Growth of the multi-spin correlated terms in CaF_2 . The inset shows the evolution of zero and double quantum terms [2].

where α_n represents the rate of transformation of the different coherence orders which should be mostly determined by the strength of the dipolar coupling constants. The dynamics of Multiple Quantum Coherence terms are in agreement with the theory proposed by Gleason et al [63].

To summarize, using the symmetry of the density matrix with respect to collective rotations along the quantization axis, an experiment has been designed to uncover the multi-spin dynamics of Free Induction Decay in a solid state spin system with homonuclear dipolar interaction. Direct experimental results indicate that the decay of single-coherence single-spin terms in the density matrix are accompanied by the growth of multi-spin cor-

related operators. As was discussed in the previous sections, understanding multi-spin dynamics requires a clear picture of the production, growth and decay of the correlated spin terms. We show that the same ideas may be utilized in the central spin problem where the evolution of quantum information is determined by the dynamics of the environment spins.

1.4 Quantum dynamical map for the central spin problem

The evolution of the central spin may be described as a quantum dynamical map. Quantum dynamical maps are a general form of physical transformation for a quantum state. They are Completely Positive and Trace Preserving (CPTP) maps. Map Λ acting on A subsystem is completely positive if:

$$\rho_{AB}(t) = \Lambda \otimes \mathbb{1}_B(\rho_{AB}(0)) \text{is positive if} \rho_{AB}(0) \text{is positive} \tag{1.48}$$

and trace preserving maps preserve normalization $\mathrm{Tr}(\rho(t)) = \mathrm{Tr}(\rho(0))$. The Kraus representation theorem and Stinespring's Dilation theorem may be used to construct such a map for the evolution of the central spin [64, 65].

Kraus Representation Theorem: [66] *A superoperator Λ is a CPTP map iff it admits an operator-sum decomposition.*

Stinespring's Dilation Theorem [67]: *Any map $\Lambda : \mathcal{L}(H_A) \to \mathcal{L}(H_A)$ can be expressed as the reduced action of a unitary operator acting on an extended Hilbert space $U : \mathcal{H}_A \otimes \mathcal{H}_B \to \mathcal{H}_A \otimes \mathcal{H}_B$, i.e.*

$$\Lambda(\rho) = \mathrm{Tr}_B[U \rho \otimes \sigma U^\dagger] \tag{1.49}$$

where the initial state for an ancilla Hilbert space $\sigma \in \mathcal{L}(H_B)$ is uncorrelated with the initial system state $\rho \in \mathcal{L}(H_A)$

This means that the reduced action of a unitary evolution in a system-environment composite Hilbert space can be expressed as the application of a CPTP map on the reduced Hilbert space of the central spin. To construct such a transformation map we use the

"operator-sum decomposition "a.k.a. "Kraus decomposition ":

$$\Lambda(\rho) = \sum_k A_k(t)\rho_{(0)}A_k^\dagger(t)$$
$$\sum_k A_k^\dagger(t)A_k(t) = \mathbb{1}$$

where $\{A_k\}$ is a set of linear bounded operators known as Kraus operators.

In an environment without memory or without long-lasting correlations between the central spin and the environment spins, finding an evolution map independent of environment degrees of freedom may be possible. In our case, if the multi-spin correlations between the central spin and the environment get mixed such that the refocusing of the central spin becomes impossible, the evolution of the central spin can be explained with a map independent of the size of the environment.

In general, if a linear map Λ_t satisfies the following three conditions it is a quantum dynamical semigroup.

- Λ_t is a CPTP map
- $Tr[\Lambda_t(\rho)A]$ is a continuous function of t for any ρ and A
- $\Lambda_{t+s} = \Lambda_t \circ \Lambda_s$ for every $s, t > 0$ and $\Lambda_0 = \mathbb{1}$

The third condition states that a map should be divisible in time, or its dynamics should be time local with no memory, to be a semigroup. A Markovian process is defined as a stochastic process with a short memory that is independent of its history and the third condition suggests that the semigroup structure can only be used for Markovian processes [65]. A quantum dynamical semigroup admits a generator such that

$$\Lambda_t = \exp(Lt) \tag{1.50}$$

and $\rho(t) = \Lambda_t\rho_{(0)}$. These dynamics can be presented with a master equation:

$$\frac{d}{dt}\rho(t) = L\rho(t). \tag{1.51}$$

The assumption of Markovian dynamics is an oversimplification for the central spin problem and the long term dynamics of the central spin cannot be explained using the quantum dynamical semigroups. To quantify the non-Markovian characteristic of the central spin problem Breuer et al. [68] suggested using the trace distance as a metric. The trace distance is defined as:

$$D[\rho_1, \rho_2] = \frac{1}{2} \operatorname{Tr} |\rho_1 - \rho_2| \tag{1.52}$$

If Alice prepares the central spin in one of the two initial density matrices ρ_1 or ρ_2 with the probability of $\frac{1}{2}$, Bob can identify them with the probability of $\frac{1}{2}(1 + D[\rho_1, \rho_2])$ which shows that the trace distance is a measure of the distinguishability of two density matrices. ρ_1 and ρ_2 become continuously less distinguishable under Markovian processes, whereas the evolution under a non-Markovian dynamics may have time intervals with increased distinguishability. For the central spin problem they realized that the trace distance oscillates between a maximum and minimum value which can be interpreted as an oscillation of distinguishability. Assuming that the desired quantum information is encoded in the central spin, the loss of distinguishability is associated with the flow of information from the central spin to the environment, and its increase is a result of quantum information flow from environment back to the central spin, a signature of non-Markovian dynamics. As a consequence, the description of the central spin problem in the open quantum system formalism, should be carried out using non-divisible dynamical maps suitable for non-Markovian dynamics. Such a description have terms that depend on the history of the central spin evolution, known as memory kernels.

1.5 Conclusion

There is a renewed interest in understanding the evolution of the central spin due to its relevance in the quantum information processing. In particular our current understanding of the Quantum Error Correction is built upon the assumption that the quantum noise have Markovian characteristics and at acts locally, and in addition there is no long-range memory in the environment. We can experimentally test these by investigating the multi-spin correlations between the central spin and the environment.

The remainder of the thesis will describe how we develop experiments to explore the

flow of quantum information between the central spin and the environment and the effects of perturbing the environment on the dynamics of quantum information.

Chapter 2

Experimental

2.1 Instrument

All the solid state measurements presented in this thesis were performed on a Bruker Avance AV 300 MHz spectrometer. We used a two channel, static, solid-state probe tuned to protons at 300 MHz and ^{31}P at 121 MHz. Variable temperature capabilities in the probe were extended to record 140 K by the addition of a vacuum jacket glass chamber.

The NMR coil is wound from rhodium flashed copper wire to match the magnetic susceptibility of air [69, 70]. Our coil consists of 5 turns with a length of 5.7 mm and inner diameter of 5 mm, which leads to an inductance of 97 nH [71]. To wind the coil we used the recipe from [72] to have high B_1 field homogeneity.

In our probe the pulse length for a $\frac{\pi}{2}$ pulse in proton channel is 1.99 μs with 150 Watts of power. The same pulse length can be achieved in ^{31}P channel as well. The efficiency of multi-pulse control sequences increase by reducing their cycle length. By over-coupling we can reduce the quality factor of the NMR circuit and its ring down time, and with the help of a duplexer circuit for fast switching between the transmission and receiver mode, the cycle time for the WAHUHA pulse sequence [23, 73, 74, 75] is measured to be 18.80 μs for our probe [76, 77, 78, 79, 80, 81, 82, 83, 84, 85].

2.2 Sample

Our goal is to investigate the quantum evolution of a central spin using the methods based on the MQ NMR technique, in a solid state NMR setup. To achieve this we need a sample which resembles the structure of the central spin problem, i.e. a spin system in the center of a molecular structure, enclosed by a different species of magnetic nuclei preferably located in a symmetric orientation, acting as the spin environment. It is an advantage to find molecules with similar structures but different number of spins, to have the possibility of performing experiments varying the size of the spin environment. A natural choice for the environment spins is Hydrogen nuclei. The ^{1}H nucleus is 99.99 % abundant with the spin quantum number of $\frac{1}{2}$. The central spin should also be a magnetic nucleus with high abundance and preferably high gyro-magnetic ratio and ^{31}P is the most promising nuclei with an 100 % abundance of spin $\frac{1}{2}$ nuclei.

Triphenylphosphine (PPh_3) with the molecular formula $P(C_6H_5)_3$ meets all of these conditions. There are three phenyl groups surrounding a central ^{31}P nuclei in this molecule, which gives us a central spin system with the bath size of 15, figure 2.1. Triphenylphosphine is a common organophosphorous compound, our sample was obtained from SIGMA-ALDRICH with 99% purity. (PPh_3) is a white powder soluble in organic solvents and its melting point is 80 ℃. To prepare the NMR sample tube solid particles of PPh_3 were compressed into a NMR-sphere sample tube which was flame sealed to best preserve the contents.

To continue this work we plan to run experiments with samples containing higher number of the Hydrogen nuclei and also the molecular structures with more than one spin in the center. Tri-tert-butylphosphine $C_{12}H_{27}P$ and 1,2-Bis(diphenylphosphino)ethane (dppe) $C_{26}H_{24}P_2$ are our candidate samples for the larger spin environment and the larger central spin system, respectively.

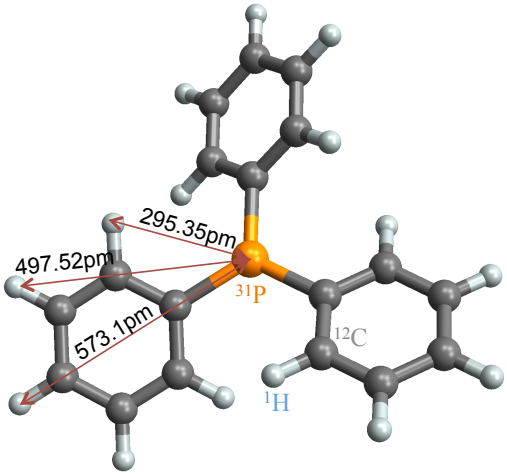

Figure 2.1: Triphenylphosphine structure with the ^{31}P positioned as the central spin and the Hydrogen nuclei in three phenyl groups acting as the spin environment. The largest heteronuclear dipolar interaction coupling constant is 11.8 kHz and the strongest homonuclear dipolar coupling between environment spins is 49.8 kHz.

2.2.1 Spin environment characterization

Our spin environment consists of a network of Hydrogen nuclei with a strong homonuclear dipolar interaction which homogeneously broadens the Hydrogen's NMR resonance line, resulting in a line-width of 32.5 ±0.2 kHz, figure 2.3. This is by far the fastest interaction in our spin system and to have a high fidelity experiment we need to be able to control this interaction.

The MREV-8 consists of eight $\frac{\pi}{2}$ pulses in the form of four solid echo pulse pairs. It refocuses the zeroth order of average Hamiltonian terms of the homonuclear dipolar interaction and all of the odd orders are also get canceled due to its symmetry, figure 2.2a. It also compensates for effects of RF inhomogeneity and finite pulse width [86, 80, 73]. Under the MREV8 cycle the zeroth order average of σ_{z} operator for the environment spins is a vector pointing at the $(1, 0, 1)$ direction with te scaling factor α for its magnitude:

$$\alpha = \frac{\sqrt{2}(1 + 2\frac{3t_p}{\tau_c}(\frac{4}{\pi} - 1))}{3} \tag{2.1}$$

where t_p is the pulse length and τ_c is the length of MREV-8 sequence. In our experiment the scaling factor is $\alpha = 51.00\%$. All interactions linear in σ_{z} will be transformed with the same scaling factor. Therefore, the zeroth order of average Hamiltonian for heteronuclear dipolar interaction in the toggling frame of the MREV-8 pulse sequence is:

$$\mathcal{H}_{SE} = \sum_i d_i \sigma_{\mathrm{z}}^{cs} \otimes \sigma_{\mathrm{z}}^{i} \Rightarrow \widetilde{\mathcal{H}_{SE}} = \frac{1.17}{3} \sum_i d_i (\sigma_{\mathrm{z}}^{cs} \otimes \sigma_{\mathrm{x}}^{i} + \sigma_{\mathrm{z}}^{cs} \otimes \sigma_{\mathrm{z}}^{i}). \tag{2.2}$$

Figure 2.2b shows the decay of proton NMR signal during application of the MREV-8 pulse sequence.

For the PPh_3 sample we measure a proton T_1 relaxation time of 630 ±30 seconds. This is inconveniently long for these studies so we prepared a sample with Chromium(III) acetylacetonate as a relaxation agent. With the relaxation agent the T_1 is reduced to 2.5 s.

(a)

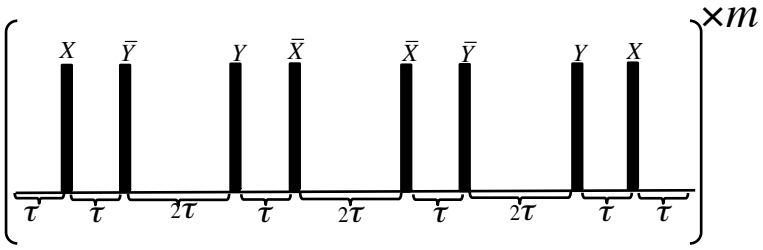

(b)

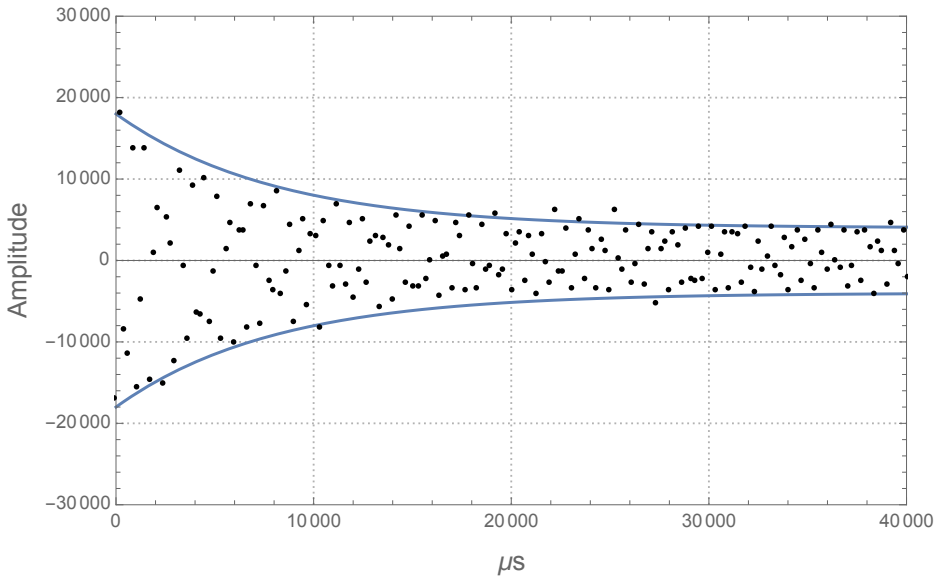

Figure 2.2: (a) The MREV8 pulse sequence cancels the homonuclear dipolar interaction up to the first order of average Hamiltonian. All the pulses are $\frac{\pi}{2}$ rotations along indicated axis. (b) Experimental data recorded during the application of an MREV-8 pulse sequence on protons in PPH_3 sample. The continuous lines are exponential decays with characteristic decay time of 8 ms.

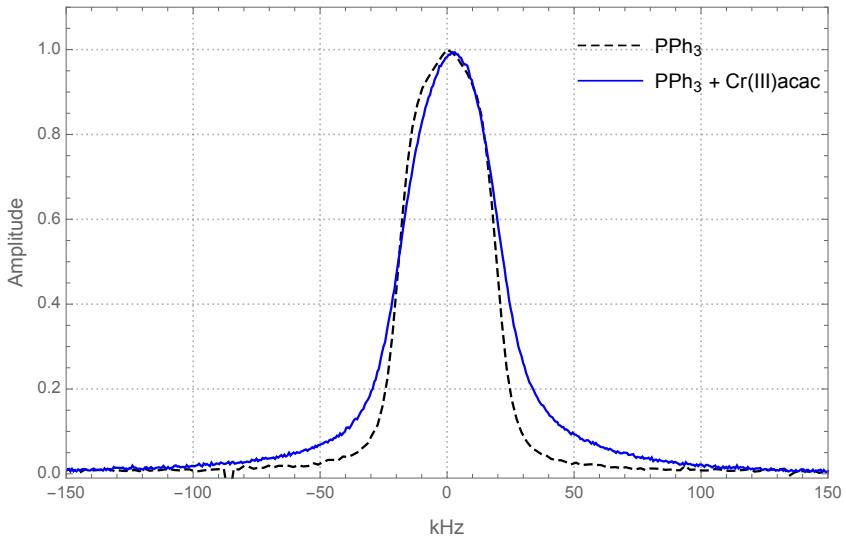

Figure 2.3: Comparison between PPh_3 proton spectra before (dashed line) and after adding $Cr(acac)_3$ relaxation agent(solid line). Solid state line shape for proton shows the expected susceptibility broadening.

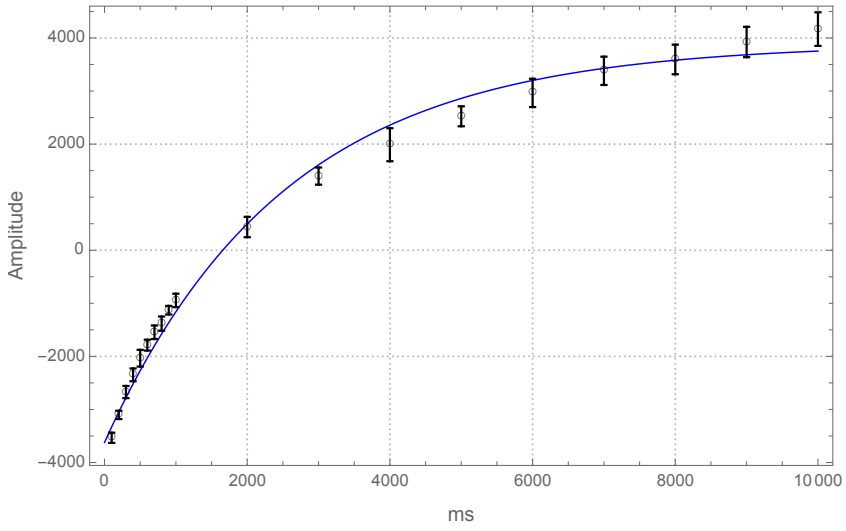

Figure 2.4: Exponential fit to the inversion recovery experimental data with the characteristic time of 2.5 ±0.2 s.

2.2.2 Central spin characterization

The most important interactions for the evolution of phosphorous nuclei in our sample are the heteronuclear dipolar interaction with the environment spins and the chemical shift anisotropy (CSA). The homonuclear dipolar interaction between the phosphorous nuclei causes a line broadening of less than 200 Hertz.

The Chemical Shift Anisotropy (CSA) tensor components for PPh_3 measured by Duncan [87] are $\delta_X = \delta_Y = 17$ ppm and $\delta_Z = -34$ ppm. Figure 2.5 presents the phosphorous line-shape observed with decoupling the proton environment. Addition of the relaxation agent broadens the line as expected. Note that the CSA is static and thus always refocusable.

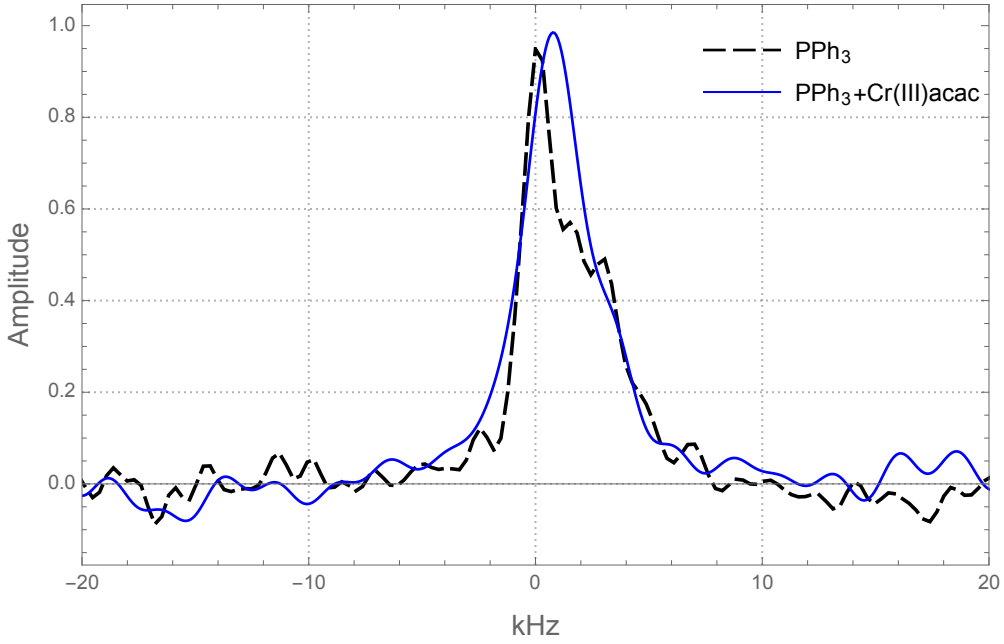

Figure 2.5: The black-dashed line shows the ^{31}P line shape caused by the CSA with decoupling the heteronuclear dipolar interaction, before addition of the relaxation agent. The blue line shows the CSA line shape after adding the relaxation agent.

The heteronuclear dipolar interaction in the sample may be as strong as 11 kHz depending on the orientation of the protons with respect to static magnetic field, figure 2.6, but

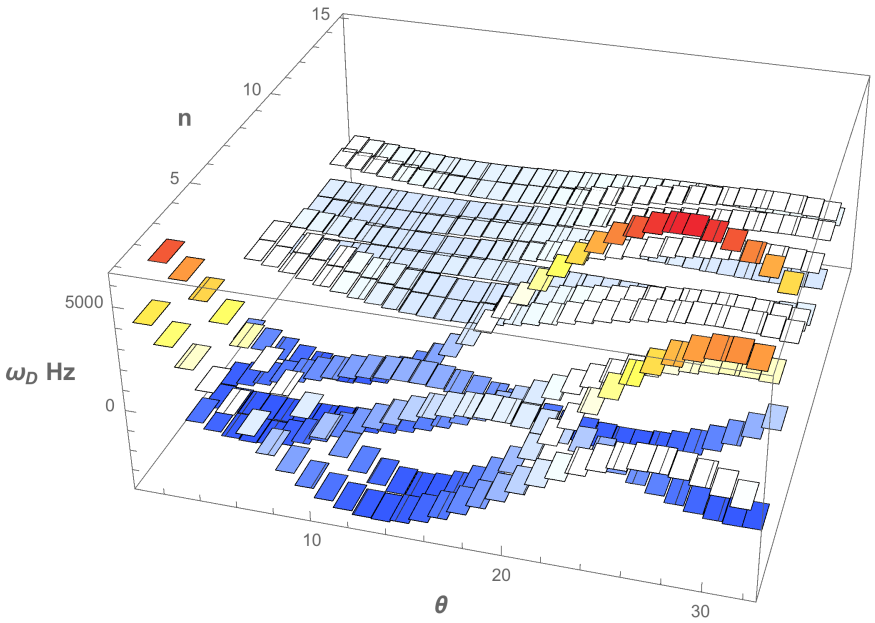

Figure 2.6: Coupling constants for the heteronuclear dipolar interaction between the central spin and 15 protons in the environment, 32 different azimuthal angle relative to the external field are examined.

results in an approximate 1 kHz line-broadening in the ^{31}P resonances. Figure 2.7 shows a comparison of the ^{31}P line shape when its coupled to protons and when its decoupled from them with application of a 50 kHz Continuous Wave (CW) decoupling.

In order to explore the quantum evolution of the central spin it is necessary to have control over the dynamics of environment spins as well as the central spin [88, 89]. The CSA and the heteronuclear dipolar interaction with the environment spins are the two important interactions for the central spin and both can be refocused with the application of the Carr-Purcell-Meiboom-Gill or CPMG sequence, which is a train of π pulses. Each π pulse inverts the sign of these Hamiltonian and results in an echo signal. The problem is that spins in the environment evolve under the homonuclear dipolar interaction and this prevents a complete reversal of the evolution under the heteronuclear interaction resulting in partial revival of the central spin signal. Alternatively, if the dynamics of the environment can be frozen, the amplitude of echo signal will decay slower. To verify this we compare three

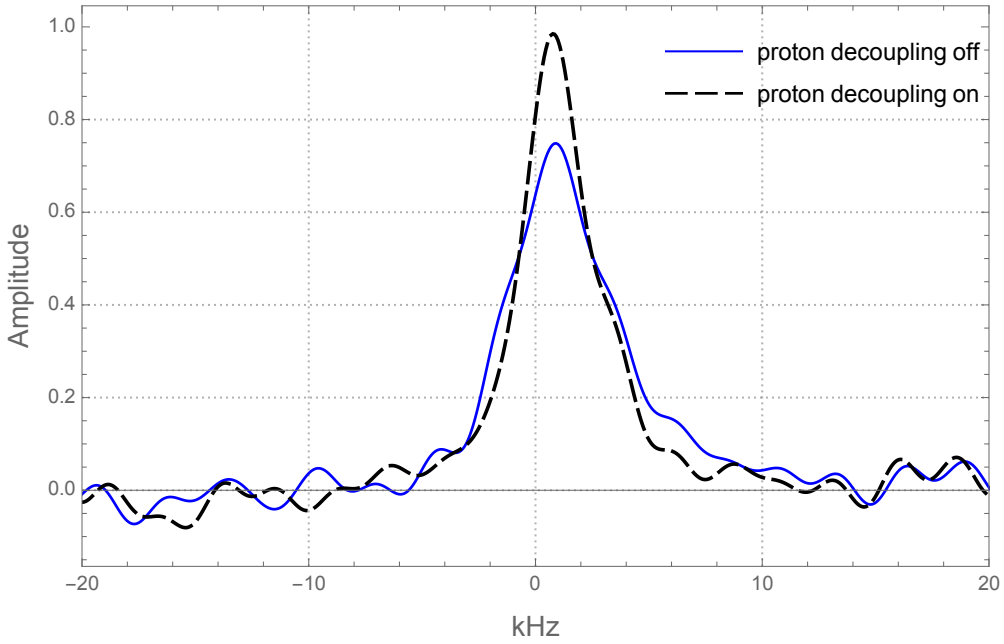

Figure 2.7: Phosphorous line shape with and without decoupling of the heteronuclear dipolar interaction with the protons. The major line-width is due to the CSA.

experiments in which the central spin is completely decoupled from the environment, the internal interaction in the environment is turned off, and a case with no modification of the environment. To implement the first experiment, the Continuous Wave (CW) decoupling is used to completely remove effects of the environment on the evolution of the central spin, figure 2.8. The result is a decaying echo signal with decay characteristic time of 13.2 $\pm$0.3 milliseconds, which corresponds to a Lorentzian line with the linewidth of around 24 Hz at half height. To freeze the dynamics of environment spins under the homonuclear dipolar interaction the MREV-8 sequence is used. The result is a decay with characteristic time of 11.6 $\pm$0.4 milliseconds corresponding to a linewidth about 27 Hz. Consequently, the effects of environment on the evolution of the central spin can be refocused very efficiently for a static environment. In comparison, if the environment evolves with no manipulation, the result of CPMG is a decaying curve with characteristic time of 1.10 $\pm$0.02 milliseconds corresponding to a linewidth of around 312 Hz.

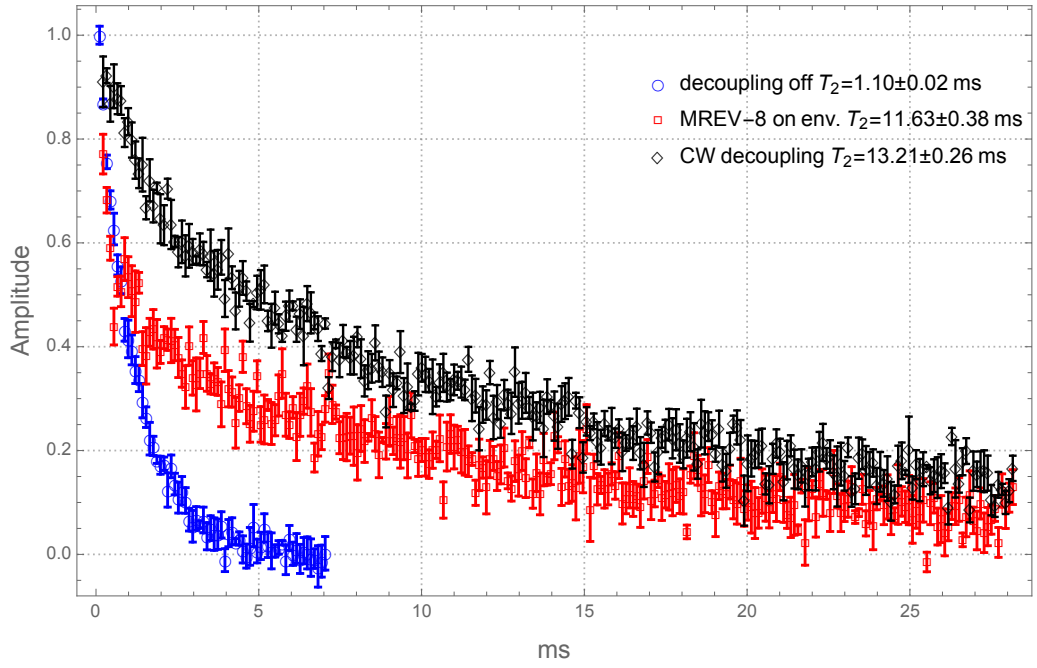

Figure 2.8: ^{31}P signal while the CSA effect has been refocused by the CPMG sequence. Blue circles indicate the decay in amplitude while the interaction with the environment is not modified. Red squares are the result of refocusing the homonuclear interaction in the environment using the MREV-8 sequence. Black diamonds present the result of the experiment with decoupled environment using the continuous wave decoupling. The characteristic decay times for these experiments are indicated in the legends.

The results of characterization experiments are summarized in table 2.1.

Table 2.1: Characteristic parameters for PPh_3 sample

Parameter	Value
Proton T_1	2.5 ±0.2 s
Proton Dipolar Broadening	32.54 ±0.02 kHz
Proton T_2 with MREV-8	8.0 ±0.5 ms
^{31}P T_1	61 ±4 s
^{31}P line-width	1 kHz
^{31}P CS [87]	$\delta_{iso} = -10$ ppm
^{31}P CSA [87]	$\delta_{11} = \delta_{22} = 9$ ppm , $\delta_{33} = -42$ ppm
^{31}P T_2 CPMG	1.10 ±0.02 ms
^{31}P T_2 CPMG MREV-8 dec	11.6 ±0.4 ms
^{31}P T_2 CPMG CW dec	13.2 ±0.4 ms

2.2.3 Cross Polarization

We use cross-polarization to increase the Signal to Noise Ratio or SNR of the ^{31}P detection [27, 90, 91, 92]. The gain comes from two factors, a thermal polarization which is proportional to the gyromagnetic ratios of proton and phosphorous nuclei:

$$\frac{\mathrm{P_{in}}(^1H)}{\mathrm{P_{in}}(^{31}P)} = \frac{\gamma_{^1H}}{\gamma_{^{31}P}} = 2.47\cdot \tag{2.3}$$

In addition, a decrease in T_1 will help in increasing the SNR by $\frac{T_1(^{31}P)}{T_1(^1H)} = 42.15$. Overall using cross polarization provides a signal increase of 104 times.

Cross polarization requires application of a long locking pulse allowing the thermal equilibrium between the two spin species. Any initial correlation between the central spin and the environment will have the form of $(\sigma_{\mathrm{Z}}\otimes\sigma_{\mathrm{Z}})$ which does not commute with the locking pulse $(\sigma_{\mathrm{X}}\otimes\mathbb{1} + \mathbb{1}\otimes\sigma_{\mathrm{X}})$. Consequently, even if correlation terms between the central spin and the environment exist, the application of long locking pulse ensures that the initial state of the central spin and the environment is uncorrelated:

$$\rho_{(0)} = \frac{1}{2^{N+1}}\sigma_{\mathrm{X}}\otimes\mathbb{1}\otimes\mathbb{1} \tag{2.4}$$

Chapter 3

Direct detection of system-environment correlations

In this chapter an experimental design for the detection of multi-spin dynamics in the central spin model is introduced. The results of such an experiment are presented and analyzed to characterize the extent of quantum information flow to the environment and the information content of the environment. Furthermore, a set of projective operators is introduced to facilitate the study of multi-spin dynamics in the central spin model.

3.1 Central spin: A probe for correlation detection

The simplest form of the correlation detection is performed on a static environment (no self-interaction). Assuming that there are N non-interacting spins in the environment, the evolution of central spin is determined with the system-environment Hamiltonian:

$$\mathcal{H}_{SE} = \frac{1}{2}\sum_{j=1}^{N} d_j \sigma_{\rm z} \otimes \sigma_{\rm z}^j \tag{3.1}$$

$$\sigma_{\rm z}^j := \mathbb{1}^{\otimes j-1} \otimes \sigma_{\rm z}^j \otimes \mathbb{1}^{\otimes N-j}. \tag{3.2}$$

As a result the initially uncorrelated state of the central spin and environment, $\rho_0 = \frac{1}{2^{N+1}}\sigma_{\rm X}\otimes\mathbb{1}^{\otimes N}$, evolves in a correlated state with different correlation orders:

$$\begin{aligned}\rho_{(t)} &= C_0(t)\sigma_{\rm X}^{qubit}\otimes\mathbb{1}^N \\ &+ C_1(t)\sigma_{\rm Y}^{qubit}\otimes\sigma_{\rm Z}^i\otimes\mathbb{1}^{N-1} \\ &+ C_2(t)\sigma_{\rm X}^{qubit}\otimes\sigma_{\rm Z}^i\otimes\sigma_{\rm Z}^j\otimes\mathbb{1}^{N-2} \\ &+ \cdots .\end{aligned} \tag{3.3}$$

Here, the order of correlation in each multi-spin operator is determined by the number of environment spin operators. Measurement of correlation order weights, $C_n(t)$, leads to evaluation of the state of the environment. There are two important points in the design of an experiment for detecting these correlations. First, collective rotations along the x axis can be used to encode the order of correlation in the environment. Second, the experiment is designed to use the central spin as a probe for correlations between the system and environment spins. By refocusing the system-environment interaction the central spin state revives, carrying the encoding factors.

3.1.1 Multi-spin Correlation Detection experiment (MCD)

Figure 3.1 presents the necessary steps for the Multi-spin Correlation Detection or MCD experiment in the central spin model and Figure 3.2 shows the pulse sequence for the implementation of this experiment.

Application of the cross polarization technique in preparation of the initial state increases the initial polarization of the central spin by a factor of 104. The spin locking field for cross polarization is applied with spin temperature alteration phase shifts to remove Bloch decay components and phase glitches [91].

After the preparation step, evolution under the system-environment interaction for time T results in multi-spin correlations. Environment spins are coupled with the homonuclear dipolar interaction that should be refocused in order to provide a static environment. This is done by application of an MREV-8 sequence which removes the zeroth and first order terms in the average Hamiltonian of the homonuclear dipolar interaction. As a consequence, the magnitude of Hamiltonian terms linear in $\sigma_{\rm Z}$ scale down to 51.00% while they rotate to

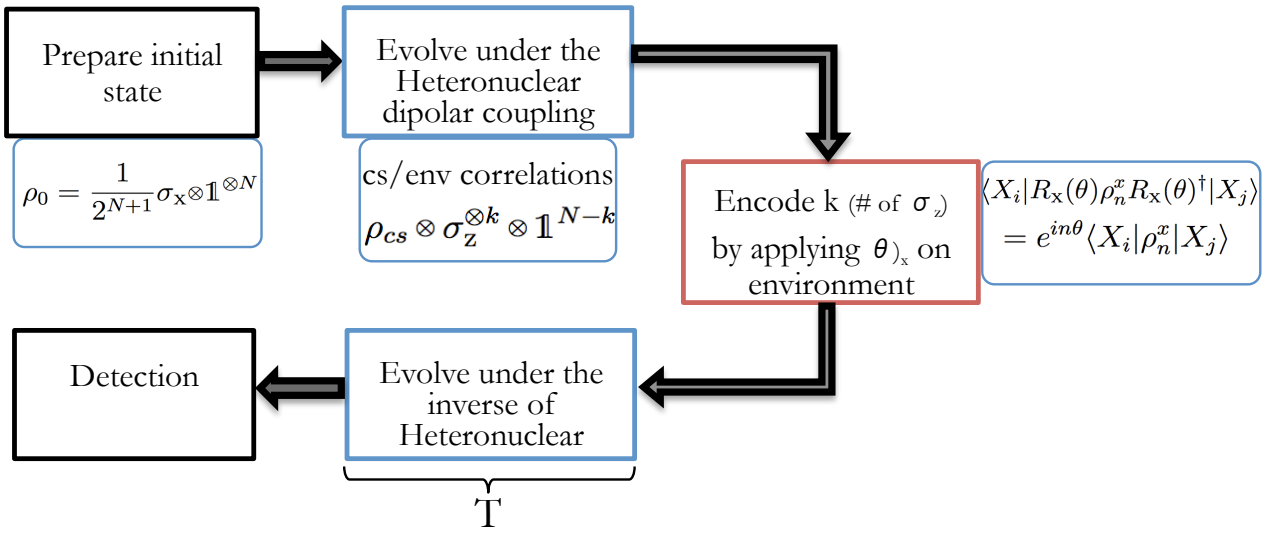

Figure 3.1: Multi-spin Correlation Detection or MCD experiment is designed to probe the correlations between the central spin and environment spins.

the [1,0,1] axis [86, 73]. This means that during the evolution time T, while the interaction between environment spins averages to zero for a full cycle of MREV-8, the heteronuclear dipolar incineration between the central spin and the environment spins is transformed to $\widetilde{\mathcal{H}_{SE}} = \frac{1.17}{3}\sum_i(\sigma_z^{cs}\otimes\sigma_x^i + \sigma_z^{cs}\otimes\sigma_z^i)$.

The encoding step consists of a collective rotation of the environment spins along the x axis $R_x(\theta)$ to encode the number of correlated spins into a phase factor:

$$\langle X_i|R_x(\theta)\rho_n^x R_x(\theta)^\dagger|X_j\rangle = e^{in\theta}\langle X_i|\rho_n^x|X_j\rangle \tag{3.4}$$

The encoding rotation is implemented with a composite pulse $(\frac{\pi}{2})_\theta - (\frac{\pi}{2})_Y$ which provides a robust rotation with a fixed length [93]. The sign of heteronuclear dipolar interaction can be virtually changed by sandwiching the evolution period with π rotations on the central spin, which results in an echo signal after the second evolution period at time $2T$. During the encoding step, the density matrix terms gain phase factors proportional to the number of their correlated spins $e^{in\theta}$. These phase factors are observed at the end of the experiment. A decoupling sequence is applied to remove environment interactions during the detection to achieve the maximum signal-to-noise ratio.

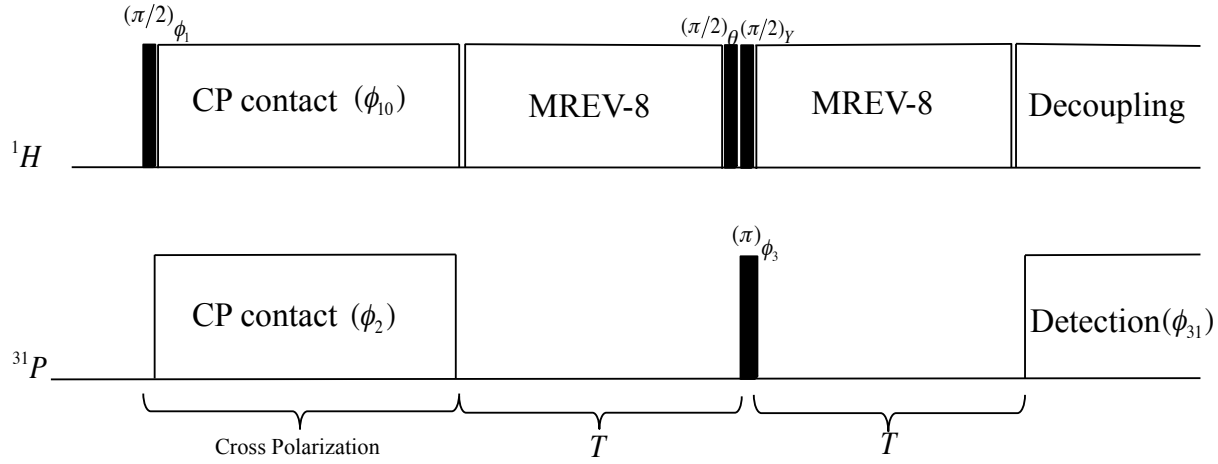

Figure 3.2: Pulse program for implementing the MCD experiment.

Table 3.1: Phase table shows phase cycling implementation of cyclops and spin temperature alteration. ^{31}P phase indicates the phase of central spin after cross polarization step.

ϕ_1	ϕ_{10}	ϕ_2	^{31}P phase	ϕ_3	ϕ_{31}
Y	X	X	X	X	X
$\bar{\text{Y}}$	X	X	$\bar{\text{X}}$	X	$\bar{\text{X}}$
Y	X	Y	Y	X	$\bar{\text{Y}}$
$\bar{\text{Y}}$	X	Y	$\bar{\text{Y}}$	X	Y
Y	X	X	X	Y	$\bar{\text{X}}$
$\bar{\text{Y}}$	X	X	$\bar{\text{X}}$	Y	X
Y	X	Y	Y	Y	Y
$\bar{\text{Y}}$	X	Y	$\bar{\text{Y}}$	Y	$\bar{\text{Y}}$
Y	X	X	X	$\bar{\text{X}}$	X
$\bar{\text{Y}}$	X	X	$\bar{\text{X}}$	$\bar{\text{X}}$	$\bar{\text{X}}$
Y	X	Y	Y	$\bar{\text{X}}$	$\bar{\text{Y}}$
$\bar{\text{Y}}$	X	Y	$\bar{\text{Y}}$	$\bar{\text{X}}$	Y
Y	X	X	X	$\bar{\text{Y}}$	$\bar{\text{X}}$
$\bar{\text{Y}}$	X	X	$\bar{\text{X}}$	$\bar{\text{Y}}$	X
Y	X	Y	Y	$\bar{\text{Y}}$	Y
$\bar{\text{Y}}$	X	Y	$\bar{\text{Y}}$	$\bar{\text{Y}}$	$\bar{\text{Y}}$

Table 3.1 indicates the phase cycling for cyclops, exorcycle and spin temperature alteration phase shifts. These phase cycles help with suppression of the imbalances in quadrature detection, eliminate π pulse refocusing imperfections and remove the spurious signal from direct polarization, respectively.

3.1.2 Analysis of the MCD experiment

To understand the spin physics of the MCD experiment we can look at an example of a central spin model with two spins in the environment $N = 2$. After the cross polarization step the density matrix for the central spin and the environment can be written as

$$\rho_{(0)} = \frac{1}{2^3}\sigma_{\mathrm{X}}\otimes\mathbb{1}\otimes\mathbb{1}. \tag{3.5}$$

The initial state of system-environment is uncorrelated because pre-existing correlations between the central spin and the environment spins disappear during the spin locking pulse.

Assuming that during the evolution step the homonuclear dipolar interaction in the environment is completely turned off and the central spin evolves under the heteronuclear dipolar interaction:

$$\mathcal{H}_{SE} = \frac{1}{2}d_1\{\sigma_{\mathrm{Z}}\otimes\sigma_{\mathrm{Z}}\otimes\mathbb{1}\} + \frac{1}{2}d_2\{\sigma_{\mathrm{Z}}\otimes\mathbb{1}\otimes\sigma_{\mathrm{Z}}\} \tag{3.6}$$

After the evolution time T the density matrix is:

$$\begin{aligned}\rho_{(T)} &= \frac{1}{8}\{\sigma_{\mathrm{X}}\otimes\mathbb{1}\otimes\mathbb{1}\cos(d_1T)\cos(d_2T) \\ &+ \sigma_{\mathrm{Y}}\otimes\sigma_{\mathrm{Z}}\otimes\mathbb{1}\sin(d_1T)\cos(d_2T) + \sigma_{\mathrm{Y}}\otimes\mathbb{1}\otimes\sigma_{\mathrm{Z}}\cos(d_1T)\sin(d_2T) \\ &- \sigma_{\mathrm{X}}\otimes\sigma_{\mathrm{Z}}\otimes\sigma_{\mathrm{Z}}\sin(d_1T)\sin(d_2T)\}.\end{aligned} \tag{3.7}$$

Collective rotation of environment spins by θ about the x axis will add powers of factors

of $\cos(\theta)$ according to the number of $\sigma_{\rm Z}$ operators:

$$
\begin{aligned}
R_{\rm X}(\theta) &= \exp(i\frac{\theta}{2}\sum_i \sigma_{\rm X}^i) && (3.8)\\
\rho_\theta &= R_{\rm X}(\theta).\rho_{(T)}.R_{\rm X}^\dagger(\theta) && (3.9)\\
&= \frac{1}{8}\Big\{\sigma_{\rm X}\otimes\mathbb{1}\otimes\mathbb{1}\cos(d_1T)\cos(d_2T) && (3.10)\\
&+ \sigma_{\rm Y}\otimes\{\sigma_{\rm Z}\cos(\theta)+\sigma_{\rm Y}\sin(\theta)\}\otimes\mathbb{1}\sin(d_1T)\cos(d_2T)\\
&+ \sigma_{\rm Y}\otimes\mathbb{1}\otimes\{\sigma_{\rm Z}\cos(\theta)+\sigma_{\rm Y}\sin(\theta)\}\cos(d_1T)\sin(d_2T)\\
&- \sigma_{\rm X}\otimes\{\sigma_{\rm Z}\cos(\theta)+\sigma_{\rm Y}\sin(\theta)\}\otimes\{\sigma_{\rm Z}\cos(\theta)+\sigma_{\rm Y}\sin(\theta)\}\sin(d_1T)\sin(d_2T)\Big\}\\
&= \frac{1}{8}\Big\{\sigma_{\rm X}\otimes\mathbb{1}\otimes\mathbb{1}\cos(d_1T)\cos(d_2T) && (3.11)\\
&+ \cos(\theta)\{\sigma_{\rm Y}\otimes\sigma_{\rm Z}\otimes\mathbb{1}\sin(d_1T)\cos(d_2T)+\sigma_{\rm Y}\otimes\mathbb{1}\otimes\sigma_{\rm Z}\cos(d_1T)\sin(d_2T)\}\\
&+ \sin(\theta)\{\sigma_{\rm Y}\otimes\sigma_{\rm Y}\otimes\mathbb{1}\sin(d_1T)\cos(d_2T)+\sigma_{\rm Y}\otimes\mathbb{1}\otimes\sigma_{\rm Y}\cos(d_1T)\sin(d_2T)\}\\
&- \{\cos(\theta)^2\sigma_{\rm X}\otimes\sigma_{\rm Z}\otimes\sigma_{\rm Z}+\sin(\theta)^2\sigma_{\rm X}\otimes\sigma_{\rm Y}\otimes\sigma_{\rm Y}\}\sin(d_1T)\sin(d_2T)\\
&- \cos(\theta)\sin(\theta)\{\sigma_{\rm X}\otimes\sigma_{\rm Z}\otimes\sigma_{\rm Y}+\sigma_{\rm X}\otimes\sigma_{\rm Y}\otimes\sigma_{\rm Z}\}\sin(d_1T)\sin(d_2T)\Big\}.
\end{aligned}
$$

Notice that the density matrix terms have gained a $\cos(\theta)^n$ factor where n shows the

number of their $\sigma_{\rm Z}$ operators. At $2T$ this density matrix evolves to:

$$
\begin{aligned}
\rho_{(2T)} &= \frac{1}{8}\Big\{\sigma_{\rm X}\otimes\mathbb{1}\otimes\mathbb{1}\cos(d_1T)^2\cos(d_2T)^2 \\
&+ \cos(d_1T)\cos(d_2T)\Big(\sigma_{\rm X}\otimes\sigma_{\rm Y}\otimes\mathbb{1}\sin(d_1T)\cos(d_2T) + \sigma_{\rm X}\otimes\mathbb{1}\otimes\sigma_{\rm Y}\cos(d_1T)\sin(d_2T)\Big) \\
&+ \sigma_{\rm X}\otimes\sigma_{\rm Y}\otimes\sigma_{\rm Y}\cos(d_1T)\cos(d_2T)\sin(d_1T)\sin(d_2T) \\
&+ \cos(\theta)\{\sigma_{\rm X}\otimes\mathbb{1}\otimes\mathbb{1}\sin(d_1T)^2\cos(d_2T)^2 + \sigma_{\rm X}\otimes\mathbb{1}\otimes\mathbb{1}\cos(d_1T)^2\sin(d_2T)^2\} \\
&+ \cos(\theta)\{\sigma_{\rm Y}\otimes\sigma_{\rm Z}\otimes\mathbb{1}\sin(d_1T)\cos(d_1T)\cos(2d_2T) \\
&+ \sigma_{\rm Y}\otimes\mathbb{1}\otimes\sigma_{\rm Z}\cos(2d_1T)\sin(d_2T)\cos(d_2T)\} \\
&+ 2\cos(\theta)\sin(d_1T)\cos(d_1T)\sin(d_2T)\cos(d_2T)\{\sigma_{\rm X}\otimes\sigma_{\rm Z}\otimes\sigma_{\rm Z}\} \\
&- \sin(\theta)\sin(d_1T)\cos(d_2T)\Big(\sigma_{\rm Y}\otimes\sigma_{\rm Y}\otimes\mathbb{1}\cos(d_1T)\cos(d_2T) + \sigma_{\rm X}\otimes\sigma_{\rm X}\otimes\mathbb{1}\sin(d_1T)\cos(d_2T) \\
&- \sigma_{\rm X}\otimes\sigma_{\rm Y}\otimes\sigma_{\rm Z}\cos(d_1T)\sin(d_2T) + \sigma_{\rm Y}\otimes\sigma_{\rm X}\otimes\sigma_{\rm Z}\sin(d_1T)\sin(d_2T)\Big) \\
&- \sin(\theta)\cos(d_1T)\sin(d_2T)\Big(\sigma_{\rm Y}\otimes\mathbb{1}\otimes\sigma_{\rm Y}\cos(d_1T)\cos(d_2T) - \sigma_{\rm X}\otimes\sigma_{\rm Z}\otimes\sigma_{\rm Y}\sin(d_1T)\cos(d_2T) \\
&+ \sigma_{\rm X}\otimes\mathbb{1}\otimes\sigma_{\rm X}\cos(d_1T)\sin(d_2T) + \sigma_{\rm Y}\otimes\sigma_{\rm Z}\otimes\sigma_{\rm X}\sin(d_1T)\sin(d_2T)\Big) \\
&+ \cos(\theta)^2\sin(d_1T)\sin(d_2T)\Big(-\sigma_{\rm X}\otimes\sigma_{\rm Z}\otimes\sigma_{\rm Z}\cos(d_1T)\cos(d_2T) \\
&+ \sigma_{\rm Y}\otimes\mathbb{1}\otimes\sigma_{\rm X}\sin(d_1T)\cos(d_2T) - \sigma_{\rm Y}\otimes\sigma_{\rm Z}\otimes\mathbb{1}\cos(d_1T)\sin(d_2T) \\
&+ \sigma_{\rm X}\otimes\mathbb{1}\otimes\mathbb{1}\sin(d_1T)\sin(d_2T)\Big) \\
&+ \sin(\theta)^2\sin(d_1T)\sin(d_2T)\Big(-\sigma_{\rm X}\otimes\sigma_{\rm Y}\otimes\sigma_{\rm Y}\cos(d_1T)\cos(d_2T) \\
&+ \sigma_{\rm Y}\otimes\sigma_{\rm X}\otimes\sigma_{\rm Y}\sin(d_1T)\cos(d_2T) + \sigma_{\rm Y}\otimes\sigma_{\rm Y}\otimes\sigma_{\rm X}\cos(d_1T)\sin(d_2T) \\
&+ \sigma_{\rm X}\otimes\sigma_{\rm X}\otimes\sigma_{\rm X}\sin(d_1T)\sin(d_2T)\Big) \\
&- \sin(\theta)\cos(\theta)\sin(d_1T)\sin(d_2T)\Big(\sigma_{\rm X}\otimes\sigma_{\rm Z}\otimes\sigma_{\rm Y}\cos(d_1T)\cos(d_2T) \\
&+ \sigma_{\rm Y}\otimes\mathbb{1}\otimes\sigma_{\rm Y}\sin(d_1T)\cos(d_2T) - \sigma_{\rm Y}\otimes\sigma_{\rm Z}\otimes\sigma_{\rm X}\cos(d_1T)\sin(d_2T) \\
&+ \sigma_{\rm X}\otimes\mathbb{1}\otimes\sigma_{\rm X}\sin(d_1T)\sin(d_2T)\Big) \\
&- \sin(\theta)\cos(\theta)\sin(d_1T)\sin(d_2T)\Big(\sigma_{\rm X}\otimes\sigma_{\rm Y}\otimes\sigma_{\rm Z}\cos(d_1T)\cos(d_2T) \\
&- \sigma_{\rm Y}\otimes\sigma_{\rm X}\otimes\sigma_{\rm Z}\sin(d_1T)\cos(d_2T) + \sigma_{\rm Y}\otimes\sigma_{\rm Y}\otimes\mathbb{1}\cos(d_1T)\sin(d_2T) \\
&- \sigma_{\rm X}\otimes\sigma_{\rm X}\otimes\mathbb{1}\sin(d_1T)\sin(d_2T)\Big)\Big\}
\end{aligned}
\tag{3.12}
$$

Out of all these terms only uncorrelated spin terms, indicated in the first and fourth line, will contribute to an observable signal. These terms are:

$$\sigma_{\mathrm{X}}\otimes\mathbb{1}\otimes\mathbb{1}\cos(d_1T)^2\cos(d_2T)^2$$
$$\cos(\theta)\{\sigma_{\mathrm{X}}\otimes\mathbb{1}\otimes\mathbb{1}\sin(d_1T)^2\cos(d_2T)^2+\sigma_{\mathrm{X}}\otimes\mathbb{1}\otimes\mathbb{1}\cos(d_1T)^2\sin(d_2T)^2\}$$

The signal amplitude is evaluated by the inner product with the observable operator $\hat{O}$ at time $2T$.

$$\begin{aligned}
S_{(2T)} &= \mathrm{Tr}[\rho_{(2T)}\hat{O}] \\
&= \frac{1}{8}\,\mathrm{Tr}\Big[\{\sigma_{\mathrm{X}}\otimes\mathbb{1}\otimes\mathbb{1}\}.\{\sigma_{\mathrm{X}}\otimes\mathbb{1}\otimes\mathbb{1}\}\Big(\cos(d_1T)^2\cos(d_2T)^2 \qquad (3.13)\\
&+ \cos(\theta)\{\cos(d_1T)^2\sin(d_2T)^2+\sin(d_1T)^2\cos(d_2T)^2\}+\cos(\theta)^2\sin(d_1T)^2\sin(d_2T)^2\Big)\Big] \\
&= \cos(d_1T)^2\cos(d_2T)^2 \qquad (3.14)\\
&+ \cos(\theta)\{\cos(d_1T)^2\sin(d_2T)^2+\sin(d_1T)^2\cos(d_2T)^2\} \\
&+ \cos(\theta)^2\sin(d_1T)^2\sin(d_2T)^2
\end{aligned}$$

Consequently, the correlations between the central spin and environment spins are encoded in the final signal with the encoding factor $\cos(\theta)^n$, where $n = 0, 1, 2$ represents order of multi-spin correlated operators.

The data set containing amplitudes of each of these experiments may be Fourier transformed to evaluate the weight of each coherence order term:

$$\begin{aligned}
\mathbb{F}[S_{2T}] &= \cos(d_1T)^2\cos(d_2T)^2\delta(n) \qquad (3.15)\\
&+ \{\cos(d_1T)^2\sin(d_2T)^2+\sin(d_1T)^2\cos(d_2T)^2\}[\frac{1}{2}\delta(n-1)+\frac{1}{2}\delta(n+1)] \\
&+ \sin(d_1T)^2\sin(d_2T)^2[\frac{1}{4}\delta(n-2)+\frac{1}{2}\delta(n)+\frac{1}{4}\delta(n+2)].
\end{aligned}$$

This indicates that the amplitude of each coherence order is equal to the square of the density matrix coefficients, equation 3.7.

Note that all even/odd powers of $\cos(\theta)$ produce Fourier components at lower even/odd

orders since we can expand powers of $\cos(\theta)^n$ as $\cos(n\theta)$:

$$\cos(\theta)^n = \frac{2}{2^n}\sum_{k=0}^{\frac{n-1}{2}}\binom{n}{k}\cos((n-2k)\theta) \qquad \text{n odd} \tag{3.16}$$

$$\cos(\theta)^n = \frac{1}{n}\binom{n}{\frac{n}{2}} + \frac{2}{2^n}\sum_{k=0}^{\frac{n}{2}-1}\binom{n}{k}\cos((n-2k)\theta) \qquad \text{n even} \tag{3.17}$$

One can construct a map to transfer the amplitudes of Fourier transformed signal to weights of correlated spin terms. While this is a valuable calculation, we have developed a more general interpretation of correlation orders that is not limited to counting the number of σ_z operators and will be discussed in detail in next section.

3.1.3 Simulation

PPh_3 has three phenyl rings with 5 hydrogen atoms on each ring. For this simulation we consider the protons on one ring as the environment. Using the ChemicalData package in Mathematica we can find the relative positions of the nuclei. PPh_3 is a molecule with cylindrical symmetry and we use rotations with varying azimuthal angle relative to the external field to access different orientations of the molecule in the powder and calculate the dipolar coupling constants, figure 2.6. For these simulations the central spin interaction with protons from one phenyl ring has been averaged over 128 randomly picked azimuthal angles.

For the purpose of this simulation we assume that the MREV-8 pulse sequence completely removes the homonuclear dipolar interaction and the environment spins have no interaction with each other. The average heteronuclear dipolar interaction in the interaction frame of MREV-8 pulse sequence is:

$$\sigma_z \otimes \sigma_z \Rightarrow \frac{1.17}{3}(\sigma_z \otimes \sigma_x + \sigma_z \otimes \sigma_z). \tag{3.18}$$

Since in this simulation of 6 spins the maximum number of achievable correlations in the system is 5, the encoding pulse θ is incremented in 12 steps from 0 to 2π. The observed signal at time $2T$ is Fourier transformed with respect to the encoding angle to extract the amplitude of multi-correlation spin terms, figure 3.3. As expected initially we start

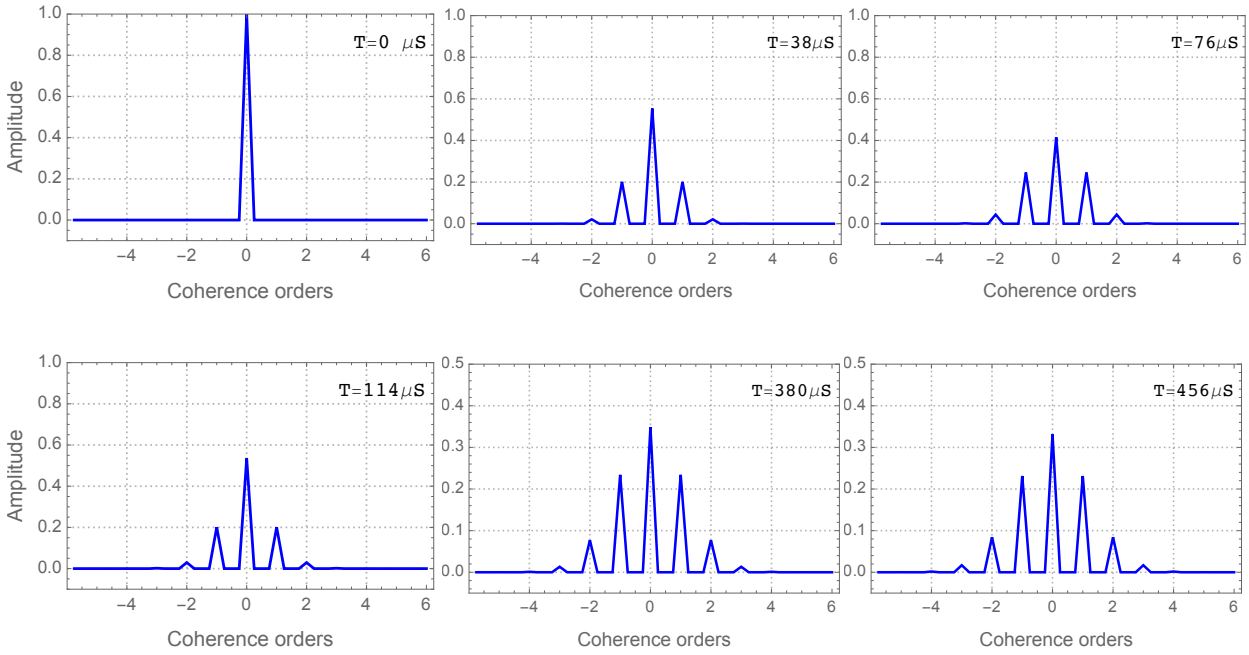

Figure 3.3: Simulation of the MCD experiment for one phosphorous nuclei connected to a ring of 5 protons, averaged over 128 values of azimuthal angle θ. Amplitudes of multi-spin correlations are presented for 6 evolution times T.

with all the weight in the uncorrelated spin term and multi-spin correlations are created as evolution time T increases.

$A_0 - A_5$ amplitudes are associated with the multi-spin correlated terms with correlation order 0-5, respectively. Figure 3.4 shows the growth curves for these amplitudes as the evolution time increases. Note that these amplitudes are the square of the weight of their corresponding multi-spin terms in the $\rho_{(T)}$ and they provide a picture of the rate of production and the evolution of multi-spin correlations in the spin system. As expected, the reduction in the amplitude of the zero correlation spin terms leads to a rise in multi-spin correlation orders. Notice that this simulation is done on a closed spin system and its dynamics can be described by a set of unitary operations. As a result the purity of the composite spin system, $\mathrm{Tr}[\rho^2(t)]$, remains constant and the integral of A_n amplitudes doesn't change. This will be helpful in normalizing the experimental data for the MCD

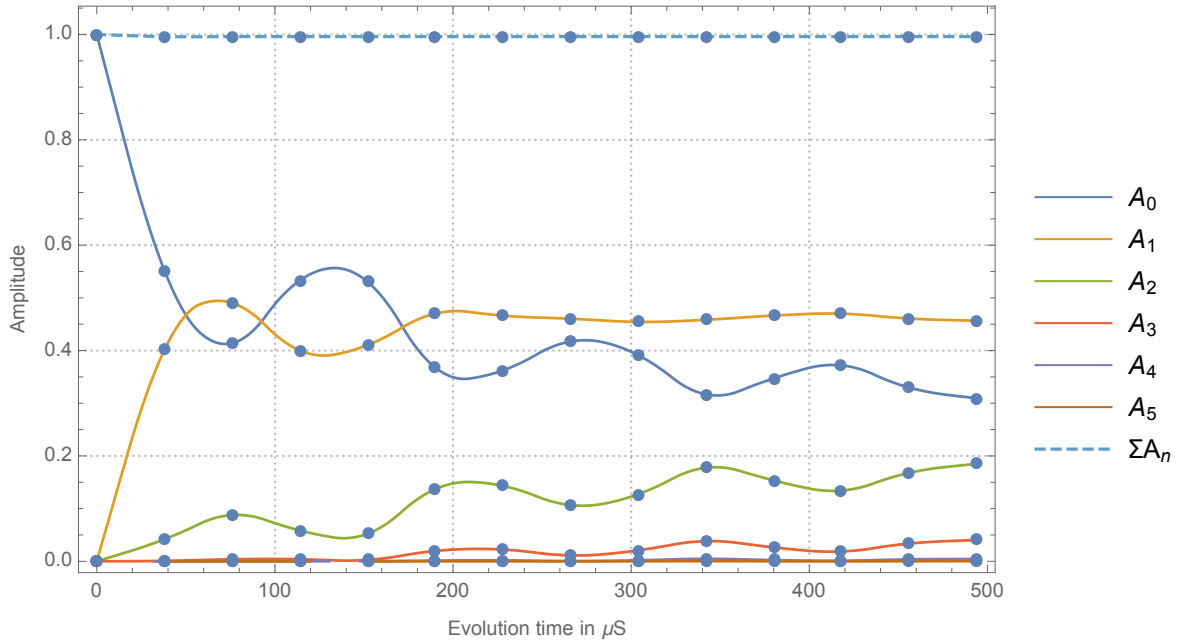

Figure 3.4: Simulation of the MCD experiment on one phosphorous nuclei connected to one ring of Hydrogen nuclei in an arbitrary orientation. A_0-A_5 are amplitudes of multi-spin correlated spin terms for correlation orders 0-5 between the central spin and environment spins. The growth of multi-spin correlated terms with the evolution time T, is indicated. Since this is a simulation of a closed spin system, $\sum_{n=0}^{5} A_n$ = cons.. The oscillations between the A_n amplitudes at larger evolution times also result from simulating a closed spin system.

experiment.

3.2 MCD experiment: analysis in the X quantization axis

In the last section we showed that by using the MCD experiment, the number of σ_z operators in multi-spin correlations can be encoded with a phase factor containing powers of $\cos(\theta)$. Because Fourier transformation of $\cos^n(\theta)$ results in Dirac delta functions positioned

at integer values lower than n, (for odd n see equation 3.16 and for even n see equation 3.17) analyzing such spectra is not straight forward. In this section we look at the concept of coherence order in a more general form and use an alternative quantization axis to represent our experimental data more clearly.

In section 1.3.2 we discussed the potential of encoding multi-spin correlations in the x quantization axis and showed that a density matrix can be transformed to the x basis:

$$\rho_{\mathrm{x}}(t) = \sum_{n=-k}^{k} C_n(t)\hat{P}_n \tag{3.19}$$

$$C_n(t) = \sum_{k=0}^{N}\sum_{p} g_{knp}(t) \tag{3.20}$$

$$\hat{P}_n = \sum_{k=0}^{N}\sum_{p} \hat{P}_{knp}. \tag{3.21}$$

The observed amplitudes in the MCD experiment are related to the weight of different multi-spin correlation operators $A_n = |C_n|^2$. We can introduce a set of basis vectors $\hat{P}_n$ that can be used to project the density matrix to obtain the $C_n(t)$ coefficients.

Consider the central spin setup used for the simulation of the MCD experiment in the previous section, which contains a ^{31}P spin and five ^{1}H spins in the environment. In this case the $\hat{P}_n$ operators are used to represent correlated spin terms in the environment part of density matrix with $N = 5$. This means that the number of spin operators k can be an integer from zero to five with $k = 0$ representing the uncorrelated spin term (i.e. the central spin is correlated with 0 spins in the environment). The correlation order n can go from $-k$ to k and p depends on the number of possible permutations for specific k and n. For example for the cases with $n = 5, -5$ the projective operators are:

$$\hat{P}_{n=5} = \sigma_{\mathrm{x}+}\otimes\sigma_{\mathrm{x}+}\otimes\sigma_{\mathrm{x}+}\otimes\sigma_{\mathrm{x}+}\otimes\sigma_{\mathrm{x}+} \tag{3.22}$$

$$\hat{P}_{n=-5} = \sigma_{\mathrm{x}-}\otimes\sigma_{\mathrm{x}-}\otimes\sigma_{\mathrm{x}-}\otimes\sigma_{\mathrm{x}-}\otimes\sigma_{\mathrm{x}-} \tag{3.23}$$

or $k = 5$ and $p = 1$ since there is only one permutation for the spin operators in this case. Also notice that the number of operators are the same for $n, -n$.

Next consider the multi-spin correlation order $n = 4$, which accepts operators with

$k = 4, 5$. The projective operators in this case are:

$$n = 4, k = 4, p = 5 \;\Rightarrow\; \hat{P}_{4,1:5} : \text{Permutations}\{\sigma_{\text{x}+}\otimes\sigma_{\text{x}+}\otimes\sigma_{\text{x}+}\otimes\sigma_{\text{x}+}\otimes\mathbb{1}\} \tag{3.24}$$

$$n = 4, k = 4, p = 5 \;\Rightarrow\; \hat{P}_{4,6:10} : \text{Permutations}\{\sigma_{\text{x}+}\otimes\sigma_{\text{x}+}\otimes\sigma_{\text{x}+}\otimes\sigma_{\text{x}+}\otimes\sigma_{\text{x}}\} \tag{3.25}$$

Each of these multi-spin operators can have 5 different orders which means that $p = 5$ and as a result the set of $\hat{P}_5$ operators has 10 members. The number of operators increases for $n = 3$:

$$n = 3, k = 3, p = 10 \Rightarrow \hat{P}_{3,1:10} : \text{Permutations}\{\sigma_{\text{x}+}\otimes\sigma_{\text{x}+}\otimes\sigma_{\text{x}+}\otimes\mathbb{1}\otimes\mathbb{1}\} \tag{3.26}$$

$$n = 3, k = 4, p = 20 \Rightarrow \hat{P}_{3,11:30} : \text{Permutations}\{\sigma_{\text{x}+}\otimes\sigma_{\text{x}+}\otimes\sigma_{\text{x}+}\otimes\sigma_{\text{x}}\otimes\mathbb{1}\} \tag{3.27}$$

$$n = 3, k = 5, p = 10 \Rightarrow \hat{P}_{3,31:40} : \text{Permutations}\{\sigma_{\text{x}+}\otimes\sigma_{\text{x}+}\otimes\sigma_{\text{x}+}\otimes\sigma_{\text{x}}\otimes\sigma_{\text{x}}\} \tag{3.28}$$

$$n = 3, k = 5, p = 5 \Rightarrow \hat{P}_{3,41:45} : \text{Permutations}\{\sigma_{\text{x}+}\otimes\sigma_{\text{x}+}\otimes\sigma_{\text{x}+}\otimes\sigma_{\text{x}+}\otimes\sigma_{\text{x}-}\} \tag{3.29}$$

So for the $n = 3$ basis operator set in the case of $N = 5$ contains 45 members in total. The number of basis operators grow as n becomes smaller. For the $n = 2$ case there are 120 operators and for the $n = 1$ case there are 210 operators in the basis set. Zero correlation terms $n = 0$ have a total of 252 multi-spin operators in their basis set.

To find the $\hat{P}_n$ operators for negative values of n we just need to exchange the $\sigma_{\text{x}+}$ operators with the $\sigma_{\text{x}-}$ and vice versa, and in general $C_n(t)$ is symmetric; $C_n(t) = C_{-n}(t)$. To build a set for all of these multi-spin operators we use the Permutation function in Mathematica. The code for generating $\hat{P}_n$ operators with $N = 5$ is attached in Appendix A.2. These operators are constructed to act as a projector on the composite spin system with dimension 2^{5+1}. Projection of the density matrix $\rho(t)$ with these operators can be used to determine the weights of different multi-spin correlated terms, $C_n(t)$:

$$C_n(t) := \sum_{i}^{\hat{P}_n \text{Dimension}} \sqrt{\text{Pu}[\text{Tr}_{\text{env}}[(\rho(t) - \frac{\mathbb{1}^{\otimes 6}}{2^6}).\hat{P}_{n,i}]]} \tag{3.30}$$

The purity of a density matrix is defined as $\text{Pu}[\rho(t)] = \text{Tr}[\rho(t)^2]$ and is used as the result of the MCD experiment is the absolute value of multi-spin amplitudes. A detailed Mathematica code for evaluation the $C_n(t)$ is included in appendix A.2. Evaluated $C_n(t)$ coefficients for the simulated density matrix can be compared with the $A_n(t)$ values from the simulation of the MCD experiment, figure 3.5. The two simulated values follow each

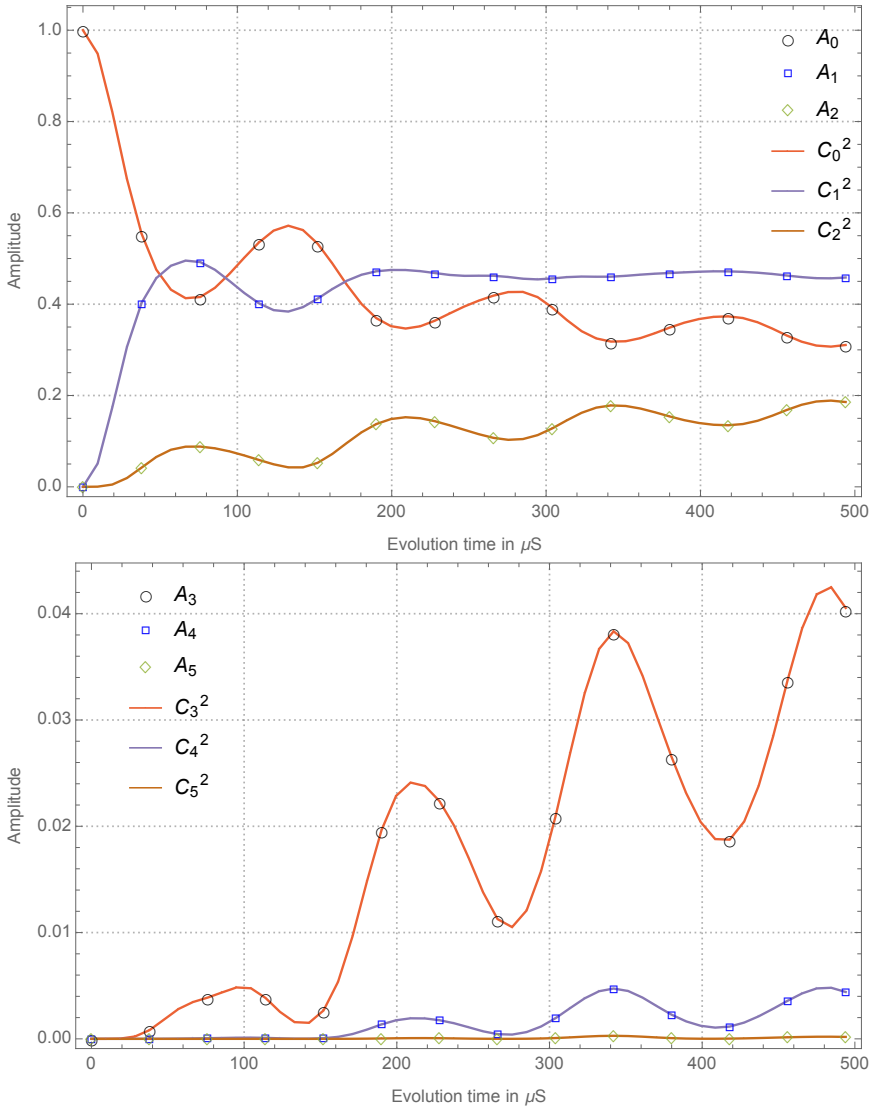

Figure 3.5: $A_n(t)$ obtained by Fourier transforming the MCD experiment signal. $C_n(t)$ are evaluated by projection of $\rho(t)$ to basis operators of the effective x quantization axis. That $A_n(t) = |C_n(t)|^2$ reassures us that the MCD experiment correctly encodes multi-spin correlated terms.

other very closely, and this confirms the utility of MCD experiment in the detection of multi-spin correlations between a central spin and its environment.

As the last example in this section we can investigate the dephasing of the central spin. We are interested in understanding the results of the Free Induction Decay (FID) of the central spin. The FID is a decaying signal that results from the loss of the magnetization vector of the central spin due to fluctuations of the local field induced by the environment spins. It can be determined by looking at the polarization of the uncorrelated central spin terms along the x axis. Any correlation between the central spin and the environment spins results in the loss of observable signal.

$$\mathrm{FID}(t) = \mathrm{Tr}[\sigma_{+} \otimes \mathbb{1}^{5} . \rho(t)] \tag{3.31}$$

The MCD experiment measures the amplitude of zero correlation order terms that consist of both uncorrelated spin terms $n = 0, k = 0$ and correlated spin terms with $n = 0, k \neq 0$, such as $\sigma_{\mathrm{X}+} \otimes \sigma_{\mathrm{X}-} \otimes \mathbb{1}^{3}$. Only the uncorrelated spin terms, $k = 0$, contribute to the FID signal and as a result, the decay of uncorrelated spin terms and the FID signal diverge from each other when the contribution of the $k \neq 0$ terms in A_0 become significant, see figure 3.6.

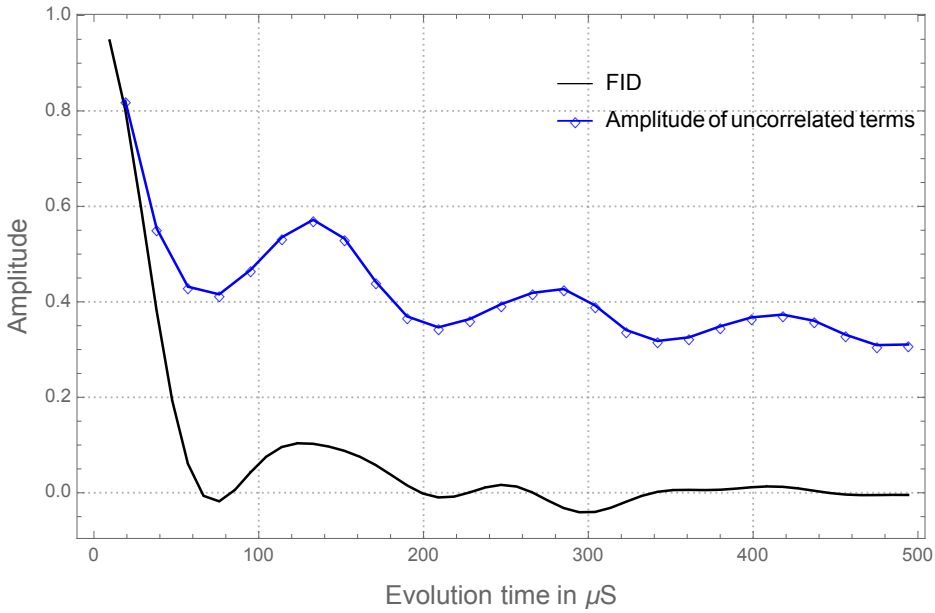

Figure 3.6: Simulation of the MCD experiment on one phosphorous nuclei connected to one ring of protons averaged over 128 orientations. The FID signal corresponds to the decay of uncorrelated terms. A_0 amplitude on the other hand consists of the contributions from the uncorrelated spin terms $n = 0, k = 0$ as well as the terms with $n = 0, k \neq 0$.

3.3 MCD Experimental results

The MCD experiment was performed using 32 steps to increment encoding rotations θ which, according to Nyquist theorem, allows for detection of multi-spin correlations up to order 16. The experiment was carried out with 12 different evolution times T, covering the production of multi-spin correlated terms up to 532 μs. The step size in evolution time is set by the length of MREV-8 sequence, which is $38\mu s$ in our experiment; using RF pulses $\frac{\pi}{2}$: $1.99\mu s$ and $3.2\mu s$ delays, figure 2.2a. A fast Analogue to Digital Converter (FADC) provide us with a sampling rate of $10MHz$. The scans are accumulated with a 10 s relaxation delay, which is almost four times longer than the proton T_1. Data recorded after each θ step were Fourier transformed and integrated to find the signal amplitude $S_{(2T)}$, plotted in figure 3.7.

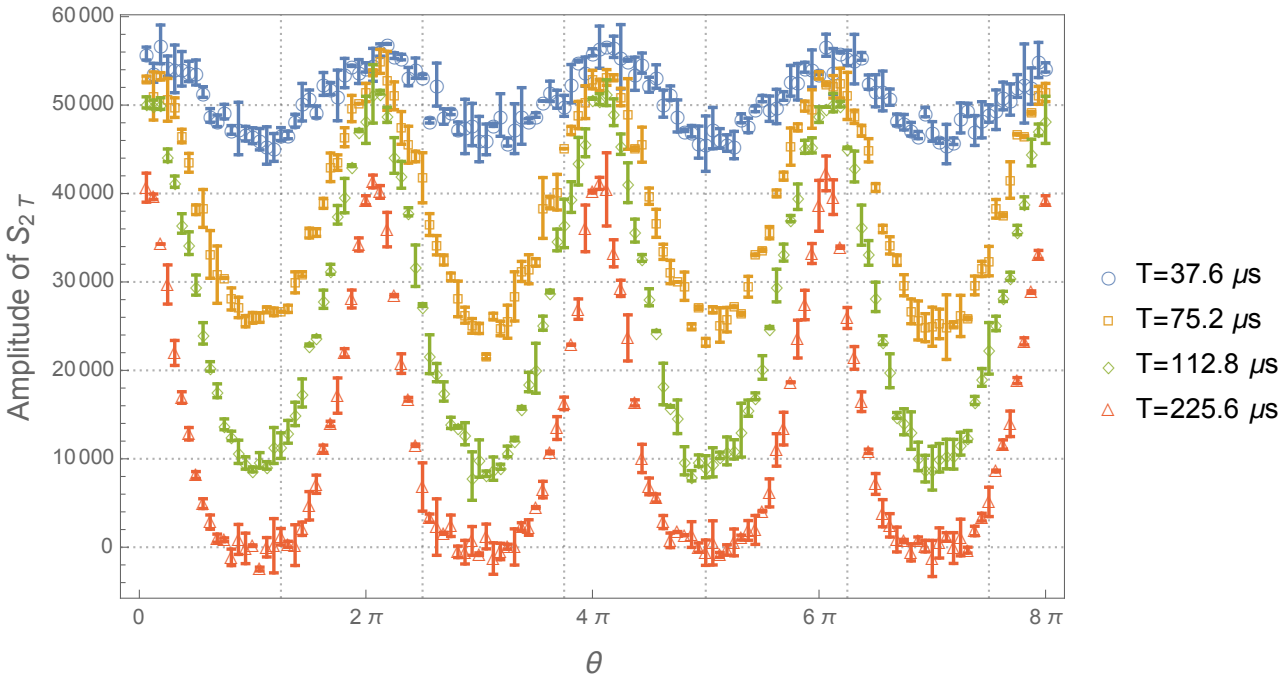

Figure 3.7: Four sets of the MCD experimental results are presented. Data points indicate the amplitude of signal S_{2T}, accumulated in 16 scans for a designated θ and T value. θ is changed from 0 to 8π in 128 steps. Errors bars are determined with the inverse of SNR.

Fourier transforming this data set with respect to the encoding pulse θ returns the amplitudes for different correlated spin terms A_n, figure 3.8. In these plots the amplitude of the integer values of n are the weights of the correlation orders and all non-integer values are noise. Note that correlation orders are symmetric, $A_n = A_{-n}$, as expected.

Consequently, the evolution of the central spin and the spin environment is captured in these plots. The MCD results provide a snapshot of the correlations of the central spin and the environment at various points during the evolution. Using the MCD experiment, one can directly observe the the progress in production of correlations between the central spin and the environment and map the complexity of the environment in time. At a short evolution times, where correlations are not yet developed, the MCD results indicate that a large number of spins in the environment are not correlated to the central spin, $n = 0$, and only clusters of one correlated spin $n = 1$ exist. As the evolution goes on, larger correlations are produced while the amplitude of smaller correlations increase, resulting in a broadening of the A_n distribution.

There are some imperfections in the MCD experiment. The PPh_3 molecules are not isolated and a weak homonuclear dipolar interaction between ^{31}P nuclei exists. In addition, the MREV-8 sequence does not remove the second order and higher order terms of homonuclear dipolar interaction in the environment. Random spin flips, i.e. T_1 relaxation, can also reduce the amplitude of the final signal. All of these factors make the detection of correlation amplitudes A_n noisy, with increasing noise levels for longer evolution times. As a consequence, in the experiments with short evolution times T, the maximum observed correlation order n_{max} corresponds to the maximum number of correlated spins in the environment, while in the experiments with long evolution times, the observed n_{max} sets a lower limit for existing multi-spin correlations between the central spin and environment.

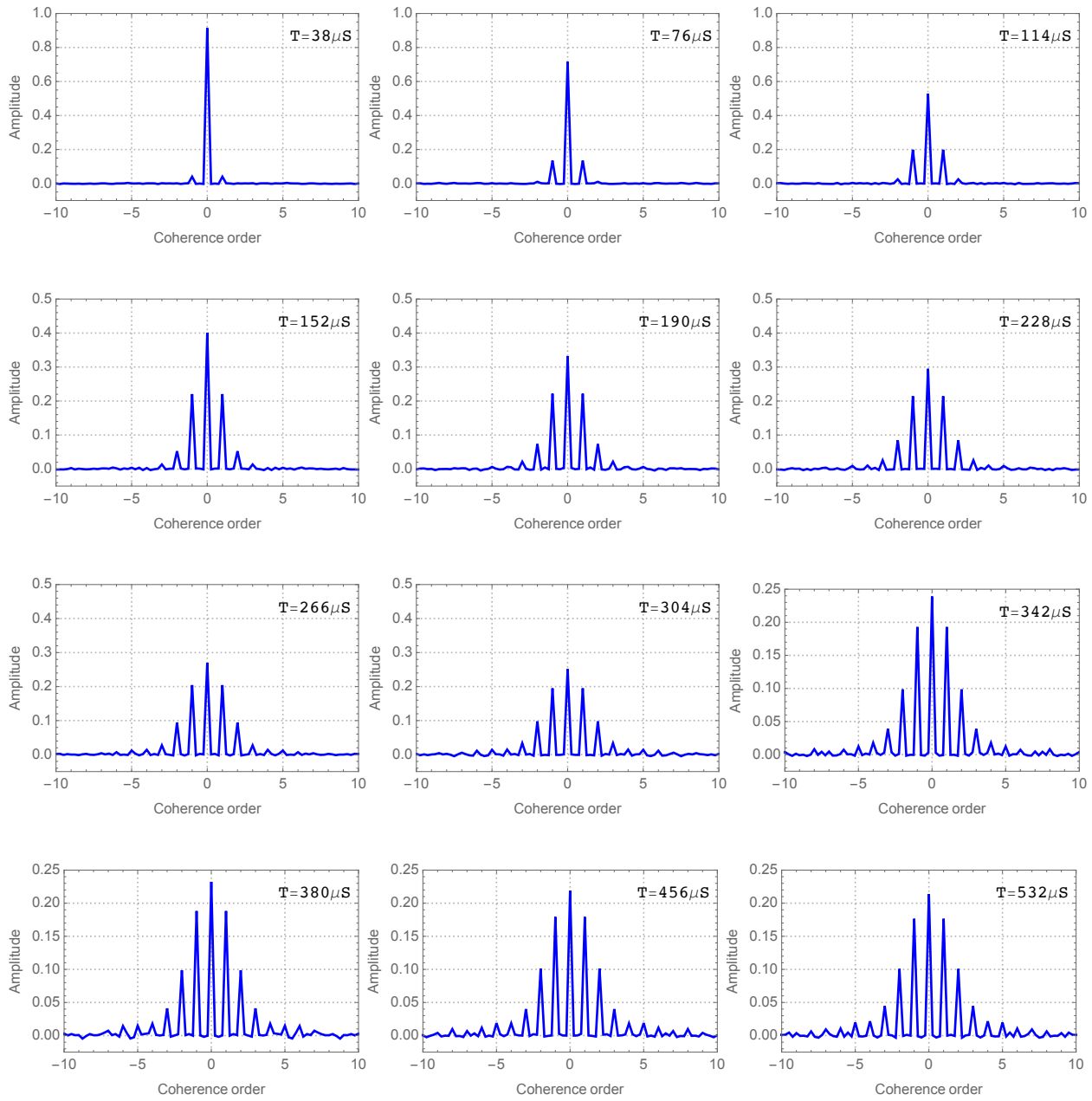

Figure 3.8: Multi-spin correlation detection (MCD) experimental results show the growth of correlation between the central spin and the environment.

3.3.1 MCD growth curves

These MCD results may be plotted to show the dynamics of each correlated spin term as a function of the evolution time T. Figure 3.9 shows the decay of $n = 0$ or uncorrelated spin terms along with the growth of multi-spin correlations $n = 1, 2, 3, \cdots$, as the evolution time T is increased. The maximum number of correlated spins observed in this experiment is $n = 9$.

Notice that all of the correlation orders show a decaying trend at large evolution times. This decay results from imperfections in the implementation of the MCD experiment. The extent of this unwanted decay of observable signal can be characterized by looking at the decay of the correlation amplitudes $\sum A_n(T)$. Recall that for a perfectly closed spin system with the unitary dynamics the purity of the density matrix, which is evaluated by a sum over all A_n amplitudes, stays constant. Figure 3.10 shows the decay of this sum as a function of the evolution time which has Gaussian characteristics. A Gaussian decay function is fitted to the $\sum A_n(T)$ data points with characteristic decay time of $470 \pm 8\mu s$, which corresponds to a characteristic decay time of $T_2 = 940 \pm 20\mu s$ for the Carr-Purcell echo experiment and a Gaussian spectrum with a line-width of 339 Hz.

Assuming that all of the multi-spin correlation terms are affected equally by imperfections in the experiment and decay with the same rate, one can use the $\sum A_n(T)$ data to normalize the growth curves. These normalized growth curves show the progress in correlation of the environment spins to the central spin, figure 3.11.

These growth curves reveal interesting features of the multi-spin correlation dynamics. First of all, notice that the larger correlations are produced from the smaller ones. In the initial density matrix $\rho_{(T=0)}$ the central spin is uncorrelated to the environment and all of the multi-spin correlations except $n = 0$, have zero weight. The evolution under the system-environment Hamiltonian results in a loss of weight for uncorrelated central spins while the number of central spin correlated with one environmental spin, A_1, increases rapidly. At the same time there is an increase in the weight of $n = 2$ correlations although with a smaller slope. Correlation orders $n = 3$ and 4 seem to have no activity initially but gain weight at larger evolution times. The existence of an onset time for larger correlation orders has been observed before in a network of spins connected by homonuclear dipolar interactions [2]. The onset time indicates the time needed to reach correlation orders

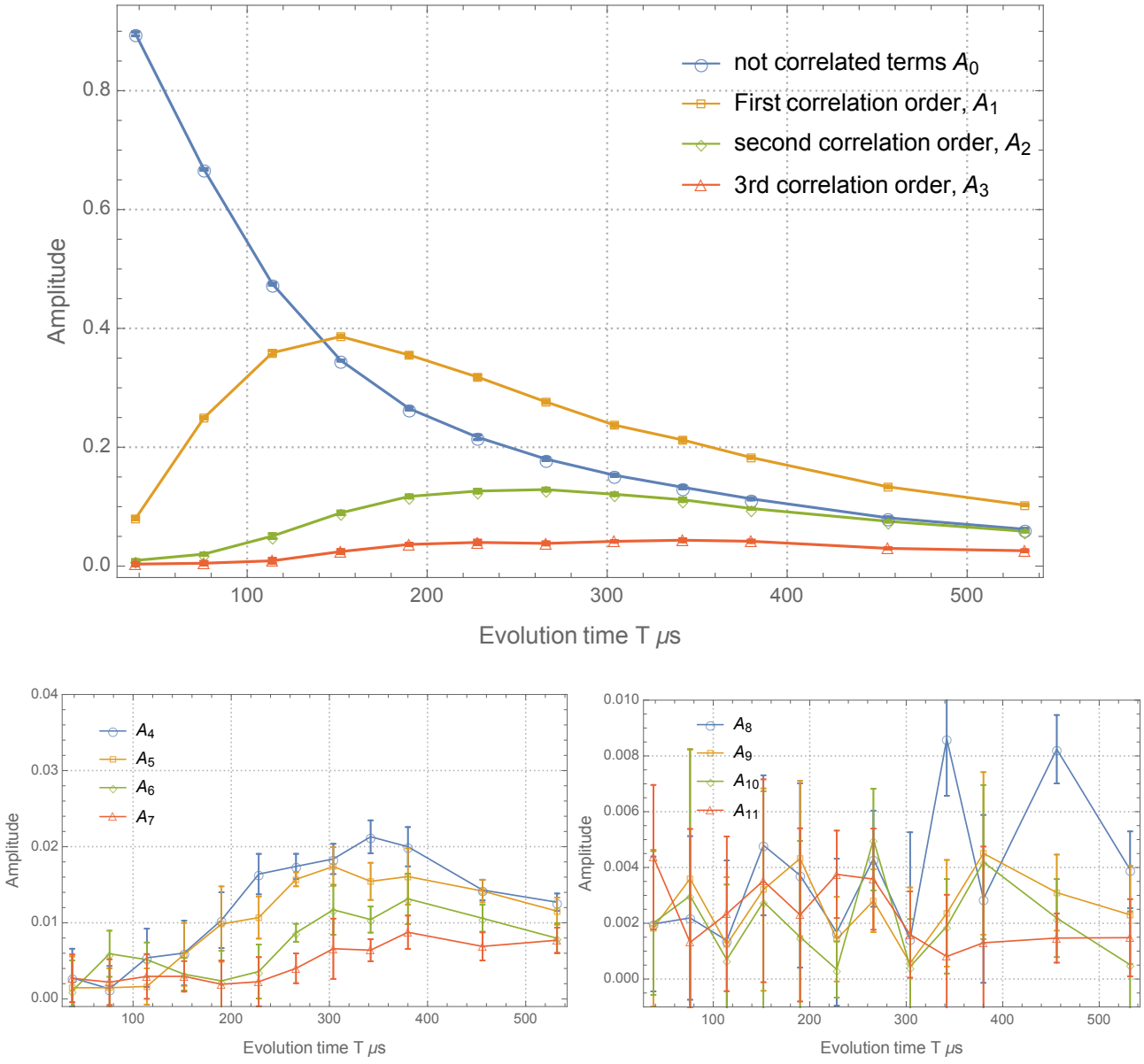

Figure 3.9: MCD experimental results, showing the growth of multi-spin correlations between the system and the environment. Higher correlation orders become observable at longer evolution times. Error bars are determined using the SNR.

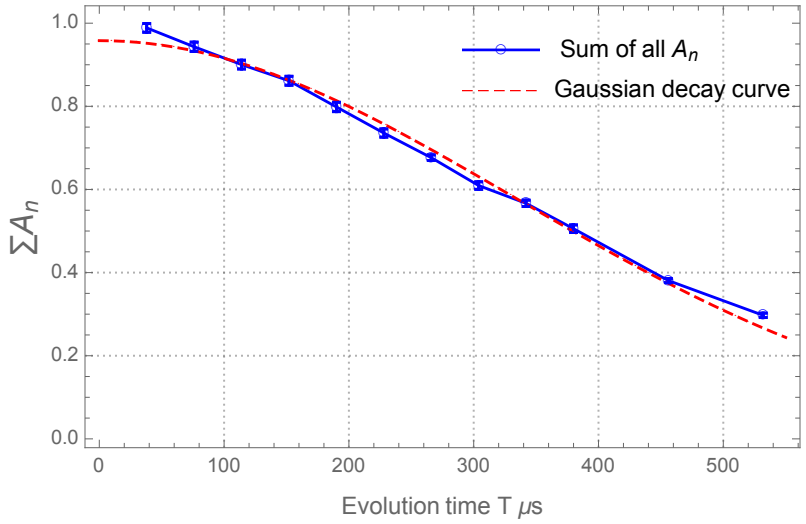

Figure 3.10: In the MCD experiment, the total observed correlation amplitude $\sum A_n(T)$ decay due to imperfections in the experiment. A Gaussian decay curve is fitted to the data with a characteristic decay time of 470 μs. This corresponds to a characteristic decay time of $T_2 = 940\mu s$ for the Carr-Purcell echo experiment and a line-width of 339 Hz for the Gaussian spectrum.

in the system and depends on the coupling strength between the central spin and the environment.

Another interesting feature of correlation growth curves in figure 3.11 is their long time behavior. The correlation amplitudes A_0 and A_2 have similar values at long evolution times. The long time amplitude of A_0 and A_2 are both around 20% while about 35% of spins have one correlation and about 10% are in $n = 3$ clusters. Initially all of the central spins in the ensemble are uncorrelated with the environment, i.e. $A_0 = 1$. The density matrix of the central spin goes from uncorrelated towards having first order correlations, $n = 1$ terms, due to interaction with the most strongly coupled spin in the environment. This cause a decay in A_0 amplitude and an increase in A_1. Although the majority of uncorrelated central spins vanish due to their interaction with the environment, the amplitude of A_0 does not go to zero. This can be understood by following the dynamics of spins in $n = 1$ clusters. Assume that the correlation between the central spin and the environment is

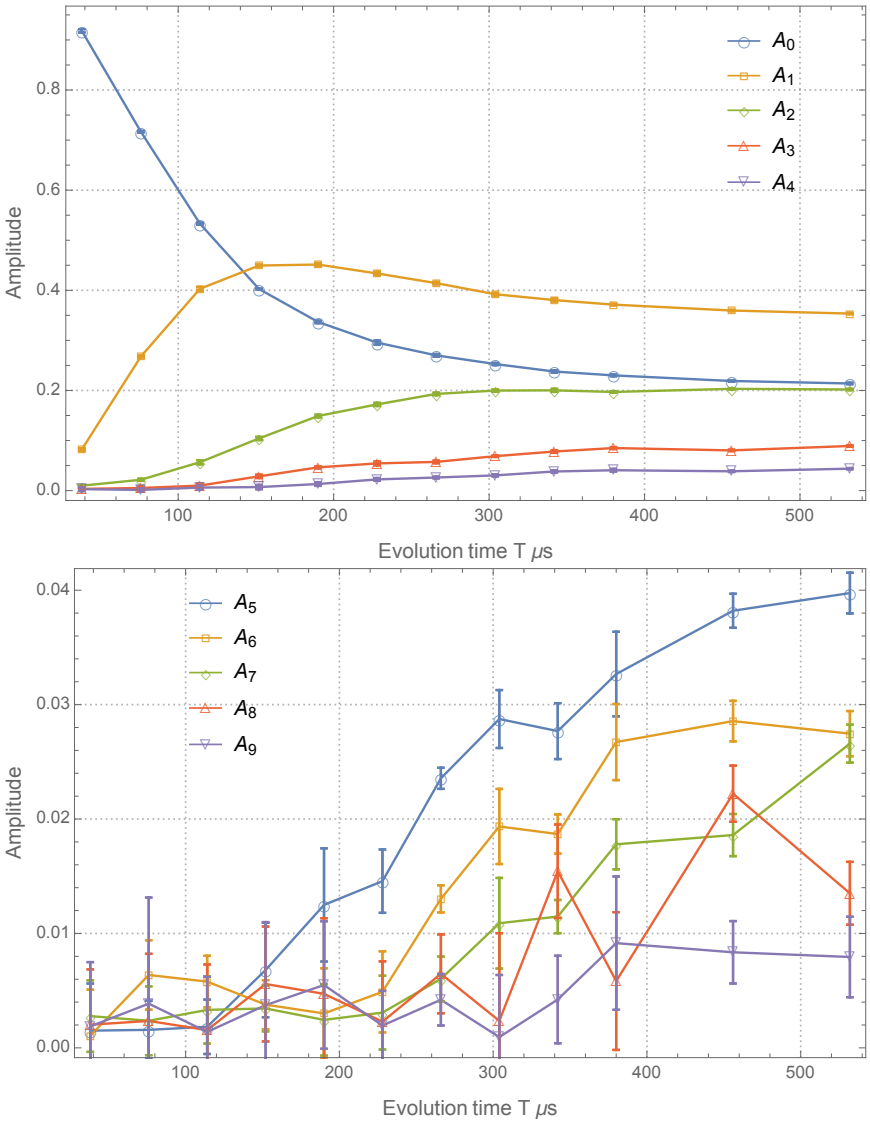

Figure 3.11: Growth of multi-spin correlations in the MCD experiment. Data is normalized to $\sum A_n(T) = 1$.

$\sigma_{\mathrm{x}}^{cs}\sigma_{\mathrm{x}+}$. Adding another spin will produce four terms:

$$\begin{aligned}
&\sigma_{\mathrm{x}}^{cs} \quad \sigma_{\mathrm{x}+}\sigma_{\mathrm{x}+}\\
&\sigma_{\mathrm{x}}^{cs} \quad \sigma_{\mathrm{x}-}\sigma_{\mathrm{x}-}\\
&\sigma_{\mathrm{x}}^{cs} \quad \sigma_{\mathrm{x}+}\sigma_{\mathrm{x}-}\\
&\sigma_{\mathrm{x}}^{cs} \quad \sigma_{\mathrm{x}-}\sigma_{\mathrm{x}+}
\end{aligned}$$

where the first two terms belong to $n = 2$ correlations and the last two terms are from $n = 0$ clusters. Adding one spin to $n = 1$ operator will result in equal production of $n = 0$ and $n = 2$, and this translates into similar values for these correlation orders. Consequently, we observe that the decay of uncorrelated terms causes the growth of A_1, which in turn gives its weight to $n = 0$ and $n = 2$ terms while A_1 slightly drops. On the other hand, although all the uncorrelated spins become correlated to the environment, the decay of A_0 slows down due to production of $n = 0$ alongside $n = 2$ correlations. Next, $n = 3$ correlations arise from $n = 2$ terms in a process that also produce $n = 1$ terms.

The MCD experiment reveals the multi-spin dynamics of the central spin evolution by detection of multi-spin correlation amplitudes. When the central spin becomes correlated with a spin in the environment, their correlated state contains the initial quantum information encoded on the central spin. Consequently, the rate of production for different orders of correlated states between the central spin and the environment can map the flow of quantum information from the central spin to the environment.

3.4 Quantifying the information content of the environment

An important step in understanding the flow of quantum information to the environment is to have a metric for the information content of the environment. Initially at the fully mixed state, the environment has no correlation to the central spin and it is at maximum entropy. The interaction of the central spin with the environment produces clusters of multi-spin correlations with growing orders and amplitudes. A good metric for quantifying the information content of the environment is the number of environment spins in the largest observable cluster in the environment.

One of the advantages of encoding the correlation order in the x quantization axis is that in this frame the maximum number of correlated spins is equal to the largest correlation order, n_{max}. Since the encoding of quantum correlations is done with rotations along the x axis, the number of spins is detectable as long as the correlated operator contains only σ_{Z} and σ_{Y} operators. In our experiment the evolution Hamiltonian is:

$$\widetilde{\mathcal{H}_{SE}} = \frac{1.17}{3} \sum_i d_i (\sigma_{\mathrm{Z}}^{cs} \otimes \sigma_{\mathrm{X}}^i + \sigma_{\mathrm{Z}}^{cs} \otimes \sigma_{\mathrm{Z}}^i) \tag{3.32}$$

This Hamiltonian is symmetric and always produce the same number of σ_{Z} and σ_{X} operators in the environment. To demonstrate how rotation along x axis can reveal the maximum number of correlated spins, lets follow encoding of a density matrix term with n_{max} correlated spins.

$$\sigma_{\mathrm{X}}^{cs} \otimes \underbrace{\sigma_{\mathrm{Z}} \otimes \sigma_{\mathrm{Z}} \cdots \sigma_{\mathrm{Z}}}_{n_{max}} \tag{3.33}$$

Application of the encoding pulse θ_{x} on the environment spins results in the following terms:

$$\begin{aligned}
&\sigma_{\mathrm{X}}^{cs} \quad \otimes \sigma_{\mathrm{Z}} \otimes \sigma_{\mathrm{Z}} \cdots \sigma_{\mathrm{Z}} \cos(\theta)^{n_{max}} \\
&\sigma_{\mathrm{X}}^{cs} \quad \otimes \sigma_{\mathrm{Y}} \otimes \sigma_{\mathrm{Z}} \cdots \sigma_{\mathrm{Z}} \cos(\theta)^{(n_{max}-1)} \sin(\theta) \\
&\vdots \\
&\sigma_{\mathrm{X}}^{cs} \quad \otimes \sigma_{\mathrm{Y}} \otimes \sigma_{\mathrm{Y}} \cdots \sigma_{\mathrm{Y}} \sin(\theta)^{n_{max}}
\end{aligned}$$

After the evolution under the inverted Hamiltonian all of the spin terms refocus to the initial density matrix while they carry their θ dependent coefficients. Assuming that n_{max} is an even number, Fourier transforming $\cos(\theta)^{n_{max}}$ leads to:

$$\begin{aligned}\mathbb{F}[\cos(\theta)^{n_{max}}] = \sqrt{\frac{\pi}{2}}2^{(1-n_{max})}\{ \quad & \binom{n_{max}}{0} \quad (\delta[n-n_{max}]+\delta[n+n_{max}]) \\ + \quad & \binom{n_{max}}{2} \quad (\delta[n-n_{max}+2]+\delta[n+n_{max}-2]) \\ & \vdots \\ + \quad & \binom{n_{max}}{n_{max}} \quad \delta[n]\}.\end{aligned} \tag{3.34}$$

Therefore, the result of Fourier transforming the encoded signal has a peak at $n = n_{max}$. A similar result is reached for odd correlation orders as well.

Figure 3.12 indicates the progress of n_{max} with the evolution time. The linear increase in the environment size is a result of limited resolution due to the fact that the cluster size is an integer value. In addition, as the correlation order increases the correlation amplitudes become smaller in general, and it becomes more challenging to distinguish them from the noise. As a result, the size of the maximum observable correlation stays constant for large evolution times.

In order to improve the metric for information content of the environment we may look at the distribution of the correlation orders. Note that in figure 3.12 while the size of the largest spin cluster stays the same after $350\mu s$, the distribution of correlation orders in these experiments are still changing in figure 3.8. Previously, the full-width at half height (FWHH) of the distribution of coherence orders was proposed as a measure for the average size of the correlated spin clusters or k, where FWHH$= 2\sqrt{(\ln 2)k}$ for large numbers of correlated spins [51, 94]. In other words, the variance, or the second moment of the distribution of the multi-spin correlation orders, is linearly proportional to the number of correlated spins k. We are going to refer to this quantity as the "average cluster size" or "Average Hamming weight" of the environment. Figure 3.12 is a comparison between the average cluster size of the environment and the maximum observed correlation order for the MCD data.

There are two interesting features in this plot. First consider the initial growth of the average cluster size which shows a parabolic behavior. The rate of growth for a spin

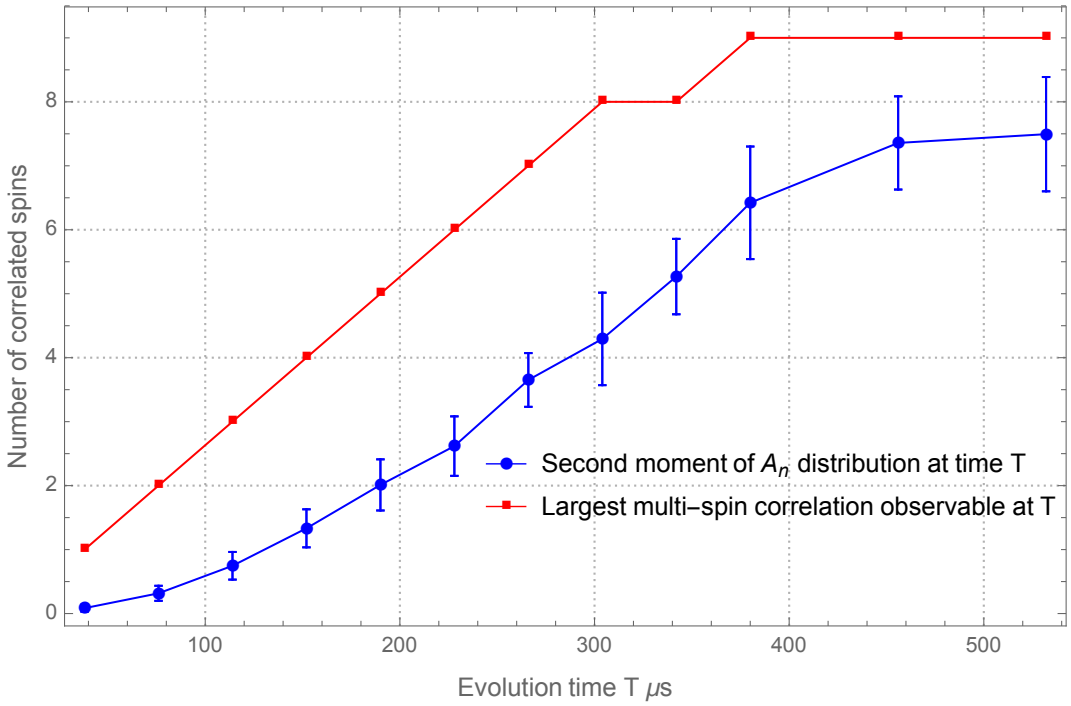

Figure 3.12: Measuring correlated spin cluster size in the MCD experiment. The red dots represent the maximum correlation order observed for each evolution time of the MCD experiment. The blue dots indicate the second moment of the correlation order distribution evaluated up to the maximum cluster size. The second moment of the correlation order distribution, is linearly proportional to the number of correlated spins.

cluster is a function of its dimension. A one-dimensional spin system shows a linear rate while the two and three-dimensional systems grow with increasing growth rates [63, 2, 95]. Comparing the growth rate in this case with the growth rate of a three-dimensional network of homonuclear-coupled spins may lead to a characterization of the dimension of the environment for a given central spin system. In contrast to a very large environment, in our experiment the growth of correlation orders slows down due to the limited numbers of spins in the environment.

3.5 Conclusion

Detection of the correlations between the central spin and the environment helps in understanding the evolution of quantum information in the central spin model. Here we have directly measured this via the Multi-spin Correlation Detection or MCD experiment. By running a set of MCD experiments with increasing evolution time we demonstrate the growth of correlations between the central spin and the environment. The shape of this growth for multi-spin correlations may be used to map the flow of quantum information from the central spin to the environment. The extent of the growth may also be used as a measure of the information content of the environment.

Chapter 4

Quantum information dynamics in the environment

In the last chapter we established an experimental method to directly detect multi-spin correlations between the central spin and its environment. When the central spin is correlated with environment spins its quantum information is shared with them in the form of multi-spin operators. Evolution of the central spin system from a separable state to a correlated state with the environment spins may be considered as flow of quantum information from the central spin to the environment.

In this chapter, we focus on the sensitivity of the environment, particularly the multi-spin correlations between the central spin and the environment, to a perturbation. Here the perturbation is caused by the homonuclear dipolar interaction between the environment spins. We wish to learn how this perturbation influences the different orders of multi-spin operators and if the effect of the perturbation changes depending on the state of the environment. Particularly we would like to know if the higher orders of correlated spins are more sensitive to perturbation. To address these questions we probe the evolution of multi-spin correlations between the central spin and the environment under the internal dynamics of the environment.

Understanding the sensitivity of multi-spin correlated operators to a perturbation will also help in explaining the role of internal interactions of the environment in the decoherence process.

Interference between the memory of environment and the central spin is another important problem that can be studied here. If the multi-spin correlated terms, which contain the shared information of the central spin and the environment, are long-lasting under the internal interactions of the environment, they can interfere with the evolution of the quantum information on the central spin. On the other hand if during the mixing processes the correlations between the central spin and the environment get mixed in short times relative to the central spin-environment interaction, the interference with the quantum information on the central spin is expected to be very small.

4.1 The Multi-spin Correlation Scrambling Detection (MCSD) Experiment

The Multi-spin Correlation Scrambling Detection or MCSD experiment is designed to observe the mixing of quantum information in the environment. The MCSD is an extension of the MCD experiment which enables us to directly detect the dynamics of individual correlated operators in the environment.

Figure 4.1 shows the various steps of the experiment. The general idea is to have an echo signal which is encoded by the order of correlations between the central spin and the environment similar to the MCD experiment, while we perturb the environment at some point. To do this a mixing window is introduced after the first evolution step and before the encoding pulses are applied, in which the central spin is decoupled and the homonuclear dipolar interaction between environment spins is turned on.

$$\begin{aligned} \mathcal{H}_D &= \sum_{j<k} D_{jk}(\sigma_{\mathrm{z}}^j\sigma_{\mathrm{z}}^k - \frac{1}{4}(\sigma_+^j\sigma_-^k + \sigma_-^j\sigma_+^k)) \\ D_{jk} &= \frac{\gamma^2\hbar^2}{r_{jk}^3}(1 - 3\cos\theta_{jk}^2). \end{aligned} \tag{4.1}$$

Notice that the coupling constants for homonuclear dipolar interaction D_{jk} are completely different from the heteronuclear coupling constants to the central spin, and that there are spins strongly coupled to the other spins in the environment which have a weak coupling to the central spin. Evolution under the flip-flop term of the homonuclear dipolar coupling

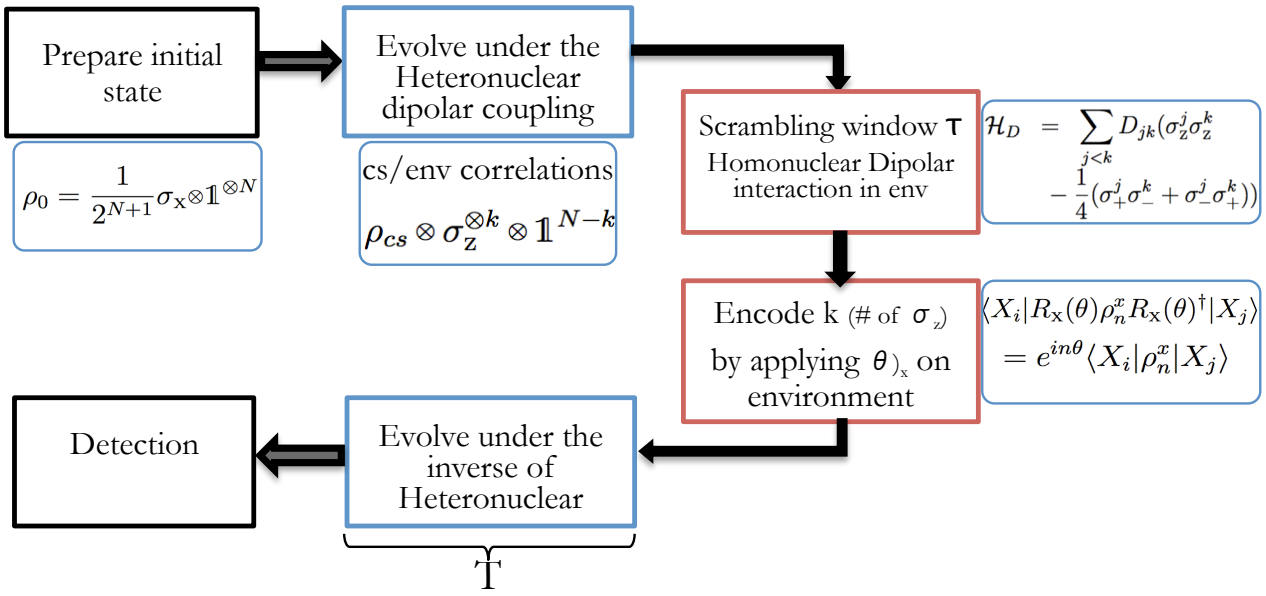

Figure 4.1: Multi-spin Correlation Scrambling Detection or MCSD experiment is designed to probe the decay of correlation orders caused by mixing in the environment.

exchanges the state of these spins in the environment:

$$\mathcal{U}_{\text{flip-flop}} = \exp(-i\frac{D_{jk}t}{4}(\sigma_+^j\sigma_-^k + \sigma_-^j\sigma_+^k)) \tag{4.2}$$

$$\begin{aligned}\mathcal{U}_{\text{flip-flop}}(\sigma_z^j \otimes \mathbb{1}^k)\mathcal{U}_{\text{flip-flop}}^\dagger &= \frac{1}{2}(1+\cos(D_{jk}t))\sigma_z^j \otimes \mathbb{1}^k + \frac{1}{2}(1-\cos(D_{jk}t))\mathbb{1}^j \otimes \sigma_z^k \\ &+ \sin(D_{jk}t)(\sigma_x^j \otimes \sigma_y^k - \sigma_y^j \otimes \sigma_x^k).\end{aligned} \tag{4.3}$$

As a result the revival of the initial density matrix after the second evolution period becomes incomplete. The decay of correlation amplitudes in the MCSD experiment are used to probe the sensitivity of the environment to the mixing.

Figure 4.2 presents the pulse program for implementating of the MCSD experiment. The mixing of quantum information in the environment happens in a window after the evolution step, during which the homonuclear dipolar interaction is turned on by a break in the application of the MREV-8 sequence. The heteronuclear dipolar interaction, on the other hand, is refocused with the use of the Hahn echo sequence, $(\frac{\pi}{2})_x - (\pi)_x - (\frac{\pi}{2})_{\bar{x}}$ on the central spin. This pulse sequence cancels the zeroth order average Hamiltonian term of

Figure 4.2: Pulse sequence designed for the detection of Multi-spin Correlation after mixing of quantum information, the MCSD experiment

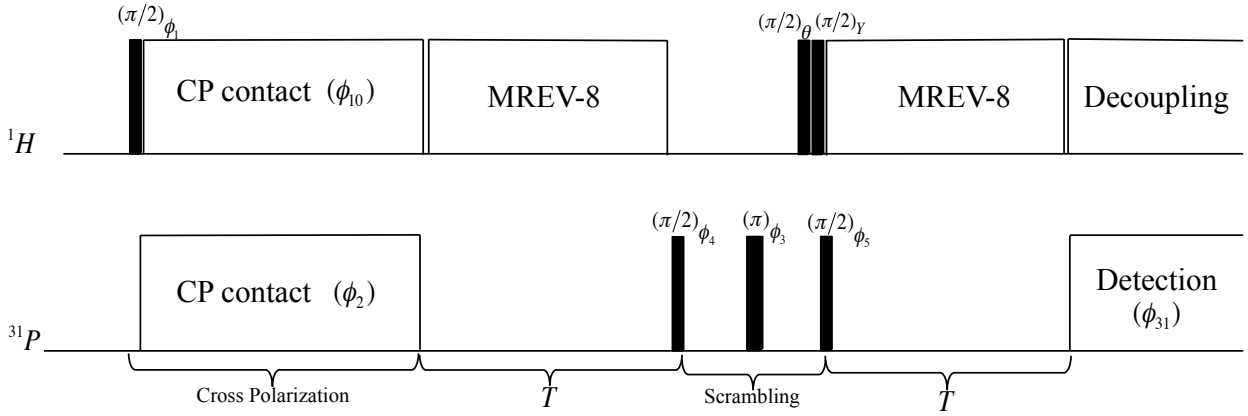

Table 4.1: Phase table shows phase cycling implementation of Cyclopes, Exorcycle and spin temperature alteration phase shifts.

ϕ_1	ϕ_{10}	ϕ_2	^{31}P phase	ϕ_4	ϕ_3	ϕ_5	Receiver
Y	X	X	X	X	X	$\bar{X}$	X
$\bar{Y}$	X	X	$\bar{X}$	$\bar{X}$	X	X	$\bar{X}$
Y	X	Y	Y	Y	X	Y	$\bar{Y}$
$\bar{Y}$	X	Y	$\bar{Y}$	$\bar{Y}$	X	$\bar{Y}$	Y
Y	X	X	X	X	Y	X	$\bar{X}$
$\bar{Y}$	X	X	$\bar{X}$	$\bar{X}$	Y	$\bar{X}$	X
Y	X	Y	Y	Y	Y	$\bar{Y}$	Y
$\bar{Y}$	X	Y	$\bar{Y}$	$\bar{Y}$	Y	Y	$\bar{Y}$
Y	X	X	X	X	$\bar{X}$	$\bar{X}$	X
$\bar{Y}$	X	X	$\bar{X}$	$\bar{X}$	$\bar{X}$	X	$\bar{X}$
Y	X	Y	Y	Y	$\bar{X}$	Y	$\bar{Y}$
$\bar{Y}$	X	Y	$\bar{Y}$	$\bar{Y}$	$\bar{X}$	$\bar{Y}$	Y
Y	X	X	X	X	$\bar{Y}$	X	$\bar{X}$
$\bar{Y}$	X	X	$\bar{X}$	$\bar{X}$	$\bar{Y}$	$\bar{X}$	X
Y	X	Y	Y	Y	$\bar{Y}$	Y	Y
$\bar{Y}$	X	Y	$\bar{Y}$	$\bar{Y}$	$\bar{Y}$	$\bar{Y}$	$\bar{Y}$

$\mathcal{H}_{SE}$ during the mixing window and overall plays the role of a $(\pi)_{\mathrm{x}}$ pulse to invert the sign of the $\mathcal{H}_{SE}$ for the second evolution interval. The Exorcycle phase cycle is used to remove the errors caused by imperfections in the application of the RF pulses in the Hahn echo sequence. The duration of the mixing window is increased in steps of $2\mu s$ to capture the dynamics of correlations in the environment. The encoding pulse is applied at the end of this window. During the second evolution interval, the spin operators that were produced during the first evolution step will refocus and will contribute to the observable signal. All the other spin terms, caused by the mixing between the environment spins can not be refocused and as a result the echo amplitude will decay.

4.2 MCSD results:

The MCSD experiments were performed with seven different evolution times:

$$T = 76, 152, 228, 304, 380, 456, 532\mu s$$

corresponding to $l = 2, 4, 6, 8, 10, 12, 14$ cycles of MREV-8 sequences in the evolution interval. For each evolution time the duration of mixing windows were varied from 0 to 30 μs in steps of $2\mu s$. The step size and maximum length of the window were chosen to cover the complete dynamics of multi-spin correlations in the environment with an appropriate resolution, figure 4.3 and 4.4. These plots present the decay of correlation amplitudes for fixed evolution times. The horizontal axis indicates the length of the mixing window τ and a longer mixing (or equivalently a stronger perturbation in the environment) results in a greater loss of echo amplitude.

At $\tau = 0$ the amplitude of correlation orders reflects the results of the MCD experiment and they show a decay same as the MCD data set.

The MCSD experimental results demonstrate that as the size of correlations between the central spin and the environment increase with the evolution time, the decay of correlation amplitudes happens faster as well. These decay rates and the influence of environment size on them are different for various correlation orders. To get more insight in the decay dynamics we fit the decay of each correlation amplitude to a Gaussian function, figure 4.5.

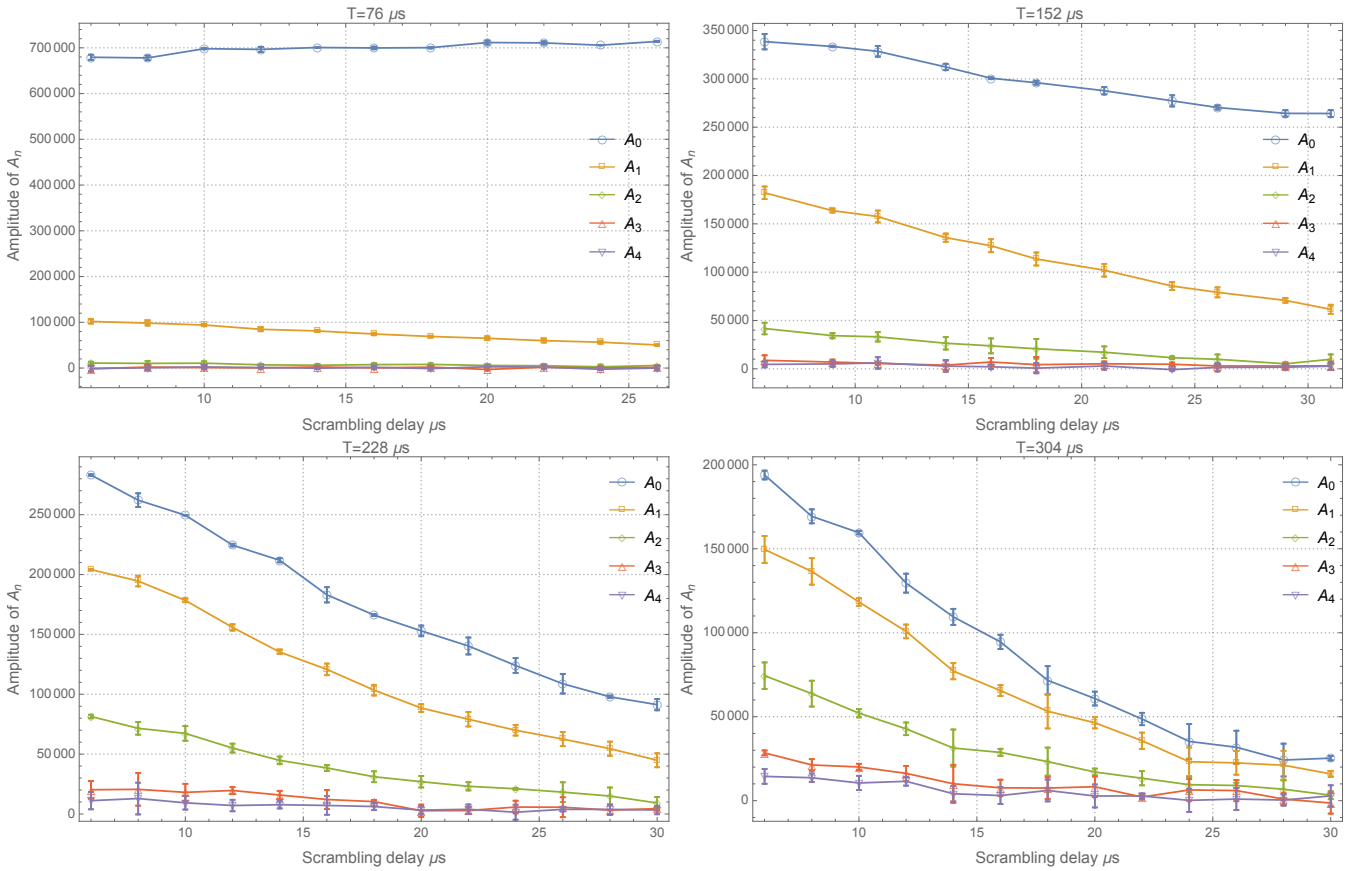

Figure 4.3: MCSD experimental results indicate the decay of amplitude of multi-spin correlation terms $A_n(T)$ for 2,4,6,8 MREV-8 cycles. The error bars are evaluated from the signal-to-noise ratio of correlation amplitudes.

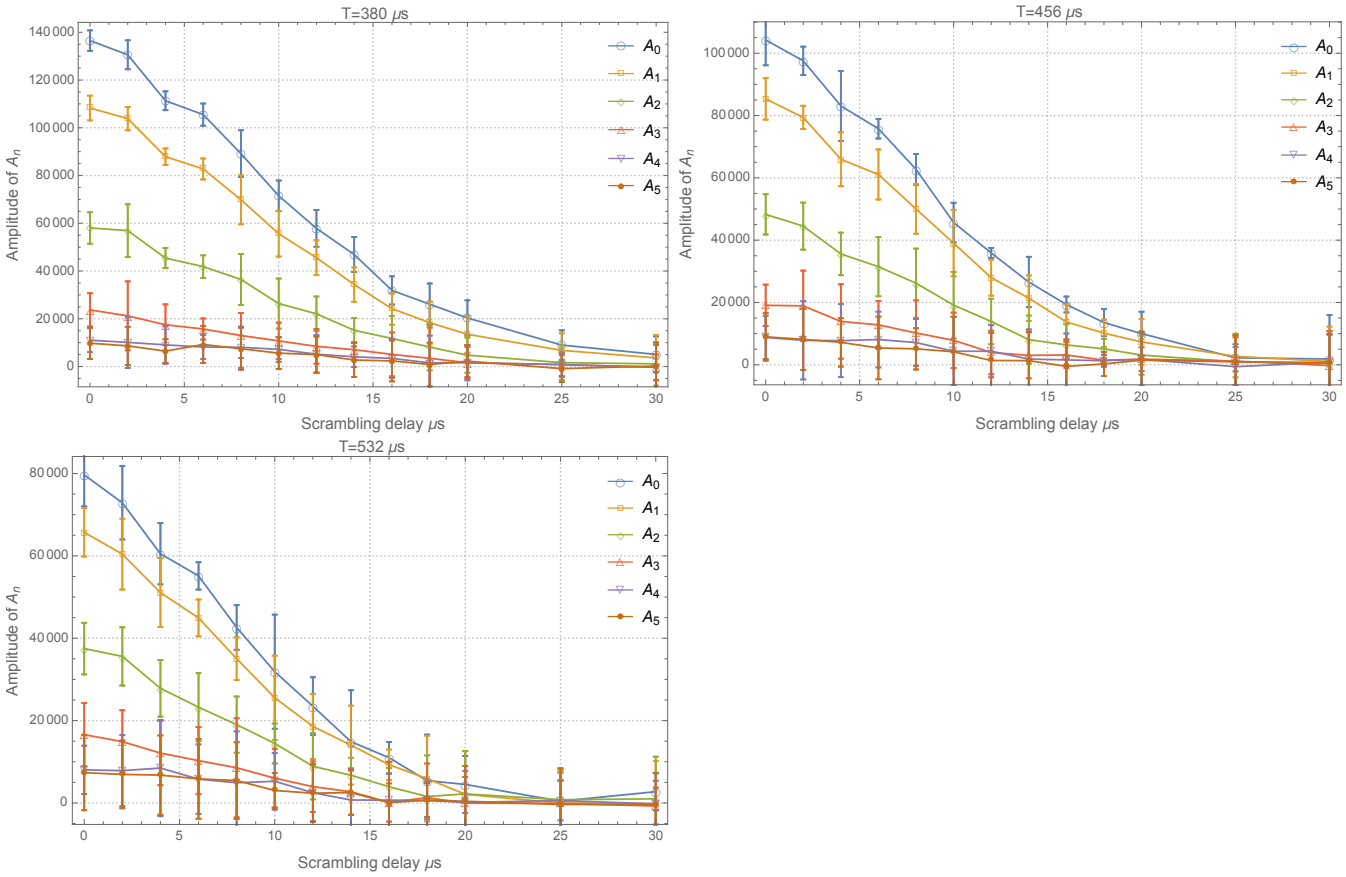

Figure 4.4: MCSD experimental results indicate the decay of amplitude of multi-spin correlation terms $A_n(T)$ for 10,12,14 MREV-8 cycles.

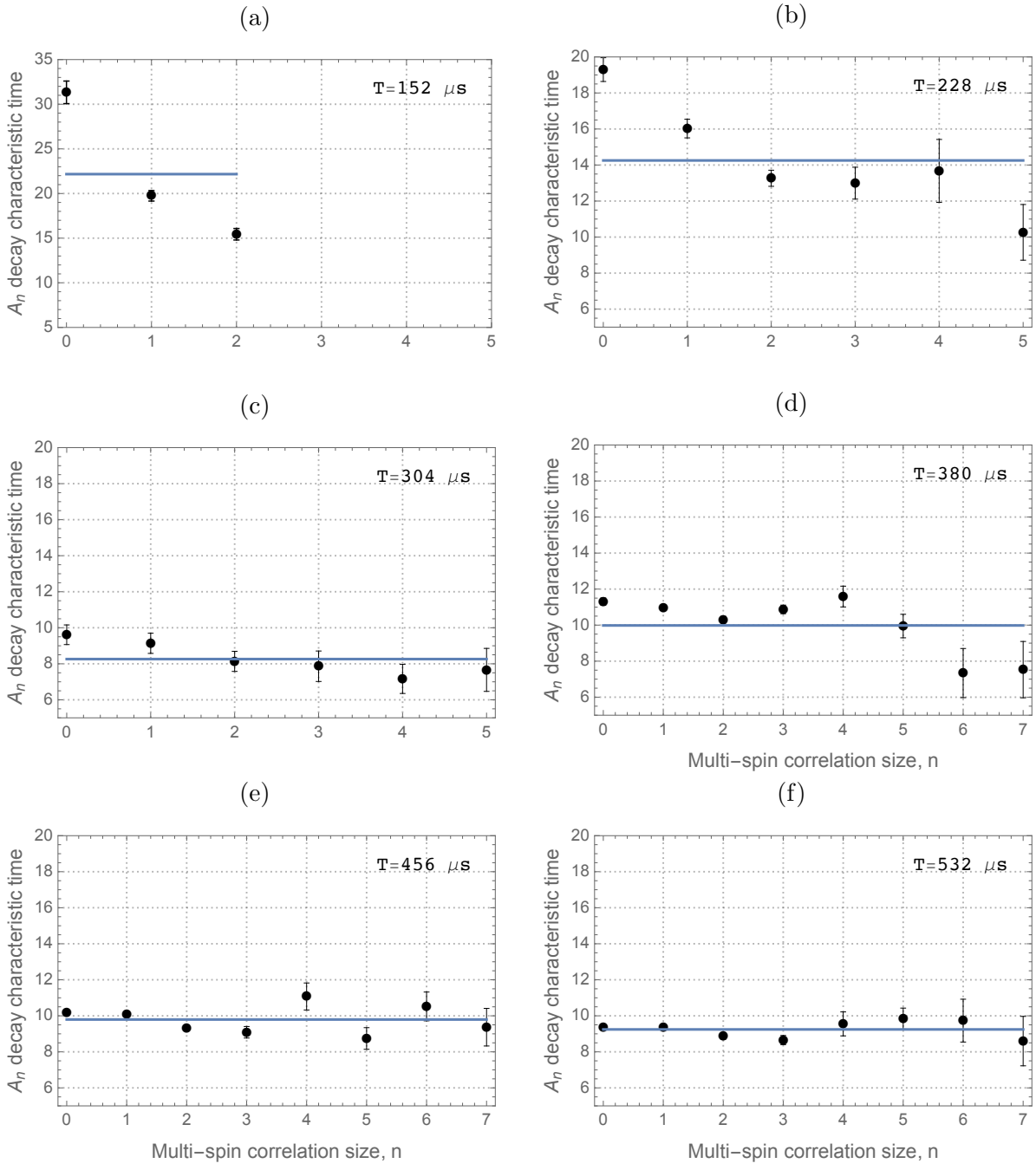

Figure 4.5: The changes in the decay characteristic times for correlation amplitudes for fixed evolution times, fitted to Gaussian functions. Continuous line indicates the mean of all decay characteristic times.

Notice that in the first two plots, $T = 152\mu s$ and $228\mu s$, the decay rate increases with correlation order. This is expected as there are more spins involved in larger correlations and therefore the probability of swap increases with the number of spins involved. Now the question is why the difference between decay rates of various correlation orders becomes smaller as the evolution time increases? This is due to the fact that the decay rate strongly depends on the number of spins involved in a correlation operator. When the average size of the correlations between the central spin and the environment is small, the number of spins in correlation terms are close to the order of correlation. As an example for $T = 152\mu s$ the majority of $n = 1$ correlation terms are produced by $(\sigma_{\mathrm{X}}^{cs} \otimes \sigma_{\mathrm{Z}})$ operators since the amplitude of $n = 3$ and larger correlation orders are very small. By comparison for long evolution times where the average size of correlation is large, operators with a higher number of spins such as $(\sigma_{\mathrm{X}}^{cs} \otimes \sigma_{\mathrm{Z}} \otimes \sigma_{\mathrm{Z}} \otimes \sigma_{\mathrm{Z}})$ and $(\sigma_{\mathrm{X}}^{cs} \otimes \sigma_{\mathrm{Z}} \otimes \sigma_{\mathrm{Z}} \otimes \sigma_{\mathrm{Z}} \otimes \sigma_{\mathrm{Z}} \otimes \sigma_{\mathrm{Z}})$ also contribute to the $n = 1$ term. Since the number of spins in these operator is large, they are susceptible to higher probability of spin swaps. As a result decay rate of correlation orders does not greatly change when the average correlation size of the environment is large.

4.3 Coin game

In the MCD and MCSD experiments we study the dynamics of multi-spin correlations between the central spin and the spin environment. We can measure the distribution of multi-spin correlations for different evolution times and look at the effect of the size of correlations between the central spin and the environment on the decay of correlation amplitudes. In this section we are going to use a classical simulation to motivate the concept of information content effect on the mixing dynamics.

We have designed a classical game to imitate the dynamics of spin swap in the central spin problem. Suppose that there are N coins all set to heads, representing N spins in the environment. In the spin environment, complete revival of the echo signal happens when all the interactions between the central spin and the environment are refocused. After the evolution under the $\mathcal{H}_{SE}$ for time T spins in the environment become correlated to the central spin and the average number of spins involved in these correlations can be measured with the MCD experiment. Let us assume that for a particular evolution time T_k, on average k spins are correlated with the central spin. After the evolution interval,

if there is no mixing window, evolution under the inverse of $\mathcal{H}_{SE}$ will evolve the k spins back to the initial uncorrelated state and we get a complete revival of observable signal at time $2T_k$. In our coin game this correlation to the central spin is simulated with flipping k random coins from heads to tails, where each coin may be flipped only once. The evolution under the inverse Hamiltonian is simulated with flipping the same coins again, which brings the final state of all the coins to heads and results in a complete revival of the initial state of the coins. The flip-flop interaction in the spin system results in the swaps between correlated spins and results in the decay of the observable signal amplitude. Random swap actions between coins can be used to simulate this interaction in the environment, with the restriction that each swap action can only happen once. In this section k random coins are flipped at first round of coin flipping, then we swap two random coins. If they are both Heads or Tails no change in the order of coins is made and after the second round of coin flips the coin state will be all Heads. Now consider a swap between two opposite coins (the first coin is Heads and the second one is Tails or vise versa). In this case after the second round of coin flips, $\frac{2}{N}$ of the initial order is lost. For $k < N/2$ increasing k will increase the probability of swapping opposite coins, which we will call a successful coin swap. For N total coins, with k random coin flips, if we swap two coins the probability of having a successful swap is:

$$\begin{aligned} P_{sswap} &= P_{TH} + P_{HT} \\ &= \frac{k}{N}\frac{N-k}{N-1} + \frac{N-k}{N}\frac{k}{N-1} \\ &= 2\frac{kN-k^2}{N^2-N}. \end{aligned} \tag{4.4}$$

$\frac{2}{N}P_{sswap}$ gives the distance of the final state of the coins from their initial state. In this classical way of thinking about the central spin we are relating the state of coins to the local field observed by the central spin and the changes caused by fluctuating spins in the environment. If all the coins are on heads after the second round of coin flips, the initial local field is revived. Any changes in the state of coins causes a disturbance in the local field observed by the central spin which leads to imperfections in the revival, or a loss of signal. Consequently, the changes in the local field caused by each swap action may be written as $\frac{2}{N}P_{sswap}$. For this simple example we are ignoring cases in which the same two spins are swapped twice and that means that after each swap the probability of having a

successful swap, remains unchanged. Therefore the probability of success for m coin swaps is considered to be m times the probability of success for one coin swap.

To test the capability of our classical game we can evaluate the changes in the local field arising from spin flips in accordance with equation 4.4 and compare the results with the decay of echo amplitudes from last section. Recall that the echo signal amplitudes are the square of weights of density matrix terms, equation 3.14, and any change in the local field will show up as a squared quantity in the final signal amplitude. Let us introduce an echo amplitude based on the probability of doing successful coin swaps. We call this Coin Echo Amplitude (CEA):

$$\begin{aligned} CEA_{(m,k,N)} &:= (1 - \frac{2m}{N} P_{sswap})^2 \\ &= (1 - \frac{4m}{N} \frac{kN - k^2}{N^2 - N})^2 \end{aligned} \tag{4.5}$$

with m representing the number of swap actions, k describing the number of flipped coins for a group of N total coins. Figure 4.6 presents a comparison between the CEA prediction and the experimental data from the scrambling decay of the echo amplitude for different average cluster sizes in the environment. For the evaluation of the CEA we used the number of spins in the environment $N = 15$, k was set according to the average size of correlations in corresponding evolution time T while m is varied from 1 to 15.

Although this classical game falls short in accounting for the details of interactions between spins and is not designed to show complexities in the dynamics of multi-spin correlations, it can motivate our model for the spin environment and its mixing dynamics. Most importantly it shows the effect of average correlation size in the environment on the rate of decay due to spin swaps. This result once again points at the importance of understanding the distribution of multi-spin correlations between the central spin and the environment for describing the evolution of the central spin and making predictions about signal decay rates.

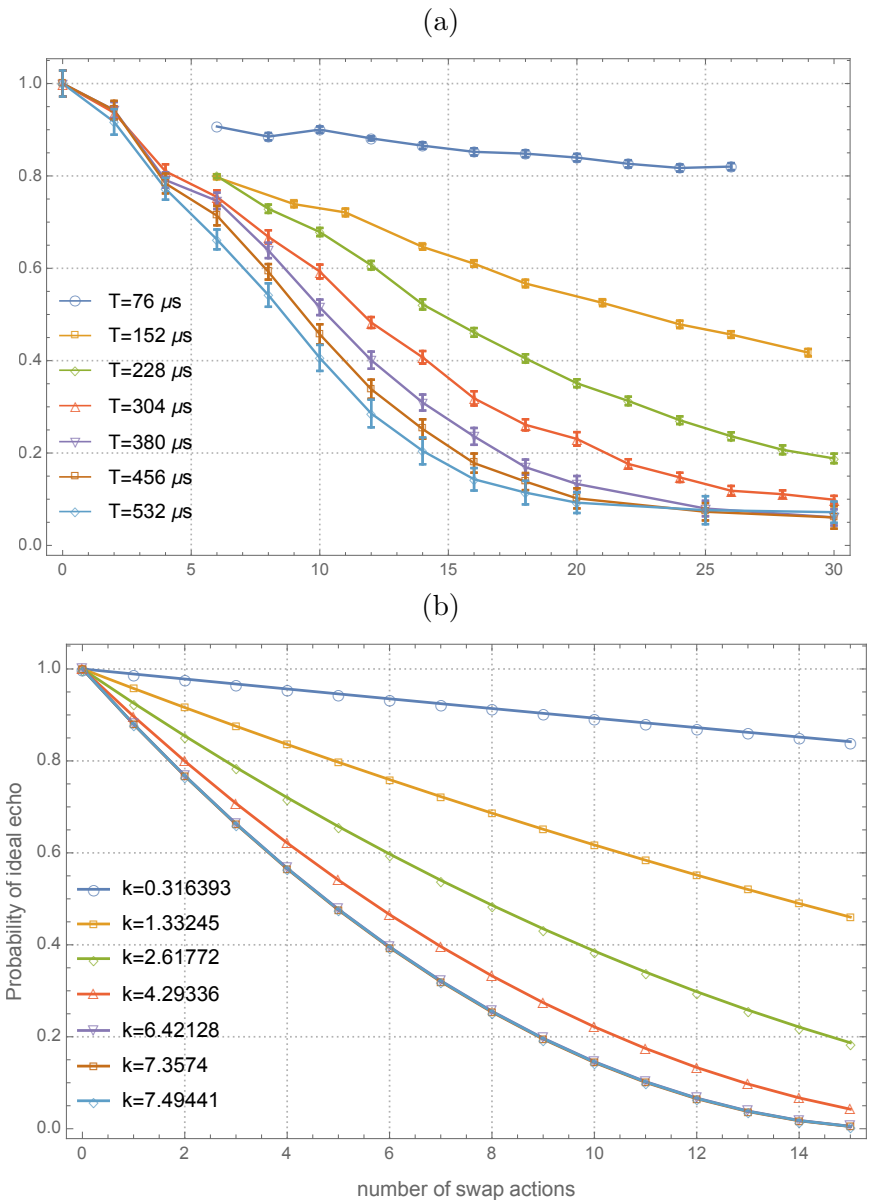

Figure 4.6: CEA for seven different k values compared with decay of the total signal of seven evolution times.

Chapter 5

The sensitivity of quantum information to environment perturbations

Sensitivity to small perturbation is a key property when describing either classical or quantum dynamics. For the central spin problem the perturbation is normally taken to be the dipolar coupling in the environment which results in a mixing of the environment spins through the flip-flop term. The correlations that the perturbation is effecting are those established via the heteronuclear coupling of the central spin with the environment spins.

We are interested in characterizing the expected increase in sensitivity to perturbations as the extent of correlations between the central spin and the environment increases.

5.1 Environment sensitivity to perturbation

In order to have a clear picture of the central spin dynamics, we have separated in time the processes that normally occur simultaneously: the growth of correlations between the central spin and the environment, and the mixing of the environment spins. This separation makes it straight forward to quantify the extent of each process and connects well to out-of-time-order correlation functions.

Before exploring the experimental design, it is important to look more carefully at the connectivity of the central spin to the environment. The ^{31}P central spin is coupled to the ^{1}H environment spins via a through space heteronuclear dipolar interaction. During the build up of the correlations between the central spin and the environment, the homonuclear dipolar interaction, ^{1}H to ^{1}H, is suppressed. Therefore, the effective Hamiltonian for the interaction between the central spin and the N spins in the environment is:

$$\sum_{k=1}^{N} \omega_k (3\cos^2\theta_k - 1)\sigma_{\mathrm{z}}^{cs} \otimes (\sigma_{\mathrm{x}}^{k} + \sigma_{\mathrm{z}}^{k}). \tag{5.1}$$

The $(\sigma_{\mathrm{x}}^{k} + \sigma_{\mathrm{z}}^{k})$ environment dependence arises from the average Hamiltonian of the environment spins under the MREV-8 multiple pulse sequence. This is described completely in chapter 2. Here we are interested in the angular dependence of the heteronuclear dipolar coupling. The radial dependence is captured in ω_k.

The dipolar Hamiltonian is a second rank spherical tensor with the spatial dependency of $(3\cos\theta - 1)^2$ to the angle between the vector connecting two spins and the static field. Therefore, there is a cone defined by the magic angle $\theta_m = \arctan\sqrt{2} = 54.7$ degrees, along which spins have no interaction with each other. Figure 5.1 presents an orientation of the PPh_3 molecule in which two of the spins in the environment are on the magic angle cone and have no heteronuclear dipolar interaction to the central spin despite having homonuclear dipolar interaction with other spins in the environment. These spins will not participate in any correlations to the central spin during the evolution but they may swap with other environmental spins during the mixing window, and become correlated to the central spin indirectly. This correlation can not be revived back to the initial state during the second evolution interval and ultimately results in the loss of quantum information in the environment. As a result, spins in the environment can be divided in two groups of "connected" and "not-connected" spin baths.

Considering the distribution of the heteronuclear dipolar coupling we can look at the average number of strongly correlated spins to estimate the size of each bath.Figure 5.1 also shows that for each frequency, how many spins have larger heteronuclear dipolar frequencies on average, in a simulation of 2500 random orientations of the PPh_3 molecule. In the time scale of our longest experiment with $T = 532\mu s$ on average 5.9 spins in the environment have a dipolar coupling stronger than 940 Hz to the central spin, and can strongly couple to it. The rest of spins in the environment are part of not-coupled spin bath.

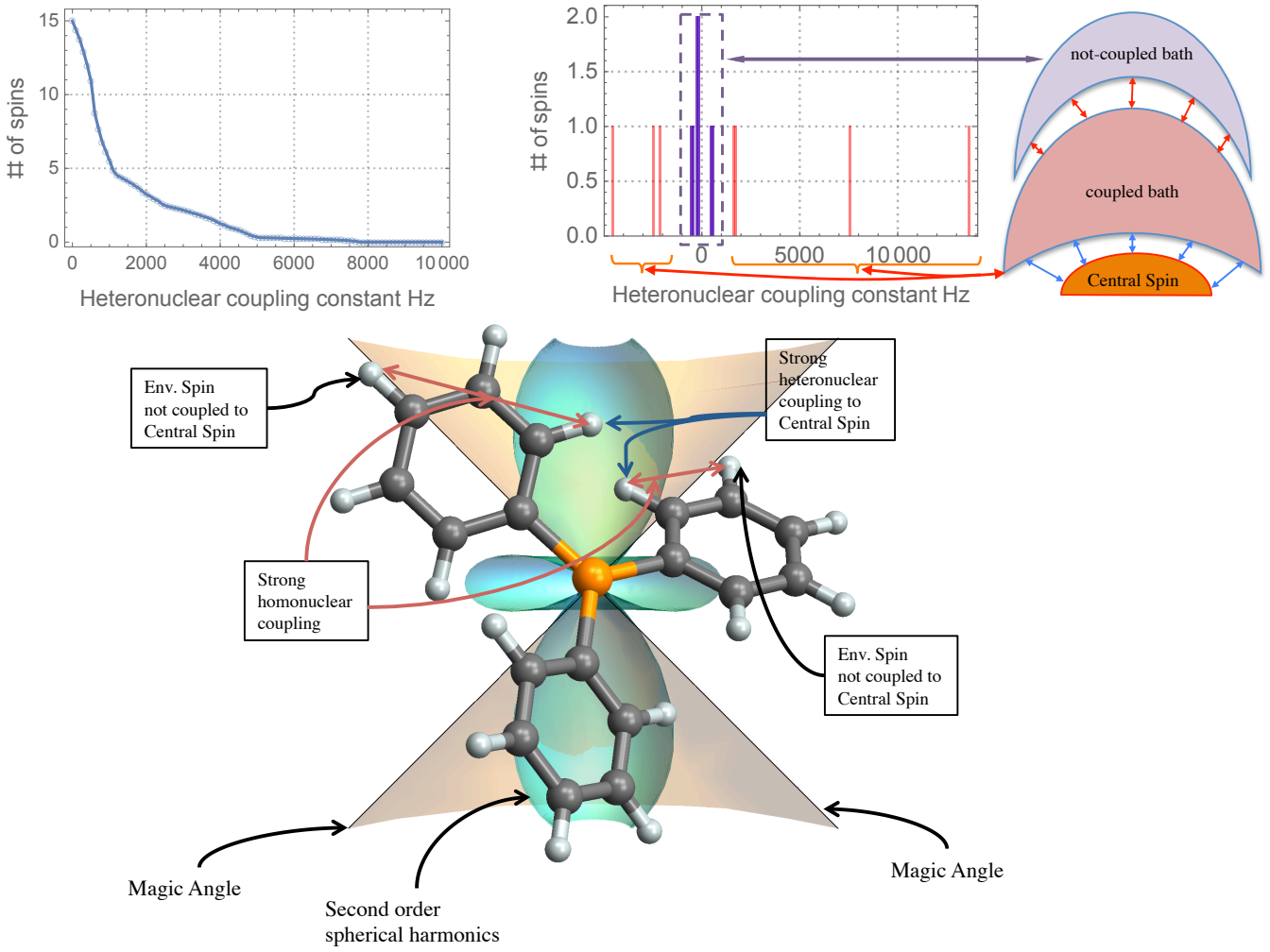

Figure 5.1: The angular dependence of the central spin coupling to the environment spins results in the environment having two distinct pools of coupled and not-coupled spins. The not-coupled bath consists of those environmental spins that are only weakly coupled to the central spin. They sit near two cones oriented at the magic angle to the external magnetic field. Top right: The coupled(Red) and not-coupled(Blue) spin baths. Eight spins with heteronuclear dipolar interactions smaller than 1000 Hz belong to not-coupled bath. Top left: Distribution of heteronuclear dipolar coupling between the central spin and environment spins. The vertical axis depicts the average number of spins with frequencies larger than heteronuclear dipolar frequencies in the horizontal axis. This simulation is done by averaging over 2500 random orientation of PPh_3.

There are two consequences:

- The correlations that are developed to the central spin never include all of the environment spins
- Since the environment is fully coupled by the perturbation, we will never observe a fully correlated state that is insensitive to the perturbation

Consider a simplified version of the MCSD experiment in which no encoding pulse is applied and the amplitude of the echo signal is observed at the end of experiment. The experiment starts with the initial state $\rho_0 = \rho^{CS} \otimes \frac{\mathbb{1}}{2}^{\otimes N}$ and after evolution time T and a mixing window of length τ the resulting signal is determined by the overlap between the initial and the final density matrix.

$$S_{(2T,\tau)} = \mathrm{Tr}[\rho_{(2T+\tau)}\rho_0]. \tag{5.2}$$

First let's take a look at this experiment when no mixing is applied $\tau = 0$. The evolution under the heteronuclear dipolar interaction between the central spin and spins in the environment is described by a unitary U_{evo}:

$$\begin{aligned} U_{evo}(T) &= \mathrm{e}^{-i\mathcal{H}_{evo}T} && (5.3)\\ \mathcal{H}_{evo} &= \alpha \sum_{j=1}^{N} d_j(\sigma_{\mathrm{z}}^{cs} \otimes \sigma_{\mathrm{z}}^{j} + \sigma_{\mathrm{z}}^{cs} \otimes \sigma_{\mathrm{x}}^{j}) && (5.4)\\ d_j &= \frac{\gamma_H \gamma_P \hbar^2}{r_j^3}(1 - 3\cos\theta_j^2) && (5.5) \end{aligned}$$

First notice that if no mixing is applied, the evolution of the density matrix in this experiment results in the complete revival of the initial state:

$$\begin{aligned} \rho_0 &\xrightarrow[\text{evolution}]{\mathcal{H}_{evo},T} U_{evo}(T).\rho_0.U_{evo}^{\dagger}(T)\\ \rho_{(T)} &\xrightarrow[\text{evolution}]{-\mathcal{H}_{evo},T} U_{evo}^{\dagger}(T).U_{evo}(T).\rho_0.U_{evo}^{\dagger}(T)(\tau).U_{evo}(T)\\ \rho_{(2T)} &= \rho_0 && (5.6)\\ \Rightarrow \quad & S_{(2T)} = \mathrm{Tr}[\rho_{(2T)}\rho_0] = 1. && (5.7) \end{aligned}$$

Now when the mixing window is introduced, spins in the environment evolve under the homonuclear dipolar interaction:

$$\begin{aligned} U_{mix}(\tau) &= \mathrm{e}^{-i\mathcal{H}_{mix}\tau} && (5.8)\\ \mathcal{H}_{mix} &= \mathbb{1}^{\mathrm{cs}}\otimes\sum_{j<k}^{\mathrm{env}} D_{jk}(\sigma^j_{\mathrm{z}}\sigma^k_{\mathrm{z}} - \frac{1}{4}(\sigma^j_+\sigma^k_- + \sigma^j_-\sigma^k_+)) && (5.9)\\ D_{jk} &= \frac{\gamma_H^2\hbar^2}{r^3_{jk}}(1-3\cos\theta^2_{jk}). \end{aligned}$$

Evolution of the density matrix and the observable signal can then be described as:

$$\begin{aligned} \rho_0 &\xrightarrow[\text{evolution}]{\mathcal{H}_{evo},T} U_{evo}(T).\rho_0.U^\dagger_{evo}(T)\\ \rho_{(T)} &\xrightarrow[\text{mixing}]{\mathcal{H}_{mix},\tau} U_{mix}(\tau).U_{evo}(T).\rho_0.U^\dagger_{evo}(T).U^\dagger_{mix}(\tau)\\ \rho_{(T+\tau)} &\xrightarrow[\text{evolution}]{-\mathcal{H}_{evo},T} U^\dagger_{evo}(T).U_{mix}(\tau).U_{evo}(T).\rho_0.U^\dagger_{evo}(T).U^\dagger_{mix}(\tau).U_{evo}(T) && (5.10)\\ \Rightarrow\quad & S_{(2T+\tau)} = \mathrm{Tr}[\rho_{(2T+\tau)}\rho_0]\\ =\quad & \mathrm{Tr}[U^\dagger_{evo}(T).U_{mix}(\tau).U_{evo}(T).\rho_0.U^\dagger_{evo}(T).U^\dagger_{mix}(\tau).U_{evo}(T).\rho_0] && (5.11) \end{aligned}$$

The echo signal amplitude is reduced by the perturbation when it interferes with the refocusing of the heteronuclear dipolar coupling. The sensitivity of the central spin/environment correlations to the mixing is determined by the commutation relation between the mixing Hamiltonian and the unitary evolution and the extent of environmental correlations affect this. In section 5.2, the data set for this experiment is presented and discussed. In the next section a correlation function is introduced which has the same form as this experiment.

5.1.1 Out of Time Order Correlations

Out of Time Order Correlations (OTOC) are useful for describing the mixing of quantum information in a strongly interacting quantum system. They are measured via an echo experiment generally by time-reversing a multi-body Hamiltonian. In the MCSD experiment, correlations of the central spin to environment spins become partially mixed by the homonuclear interaction between the environment spins. As a result, they are perfectly suited for analysis with OTOC correlation functions.

Previous studies of mixing of quantum information in black holes and condensed matter systems use OTOC functions to provide a measure for loss of quantum information in them [96, 32, 31, 97]. As a measure for the time scale of quantum information mixing, OTOC may be used to characterize the thermalization of the density matrix in a closed system [32, 31, 98, 99, 100, 101]. The mixing time in thermalization context is defined as the time needed for the evolution of the spin system to reach a state were spins are indistinguishable from each other i.e. the entropy of spin system reaches to a significant ratio of the fully mixed state.

The OTOC metric is defined as

$$\mathcal{F}_{(T)} = \left\langle W_T^\dagger V^\dagger W_T V \right\rangle \tag{5.12}$$

where V and W are two initially commuting unitary operators and $W_T = U_{(-T)} \cdot W \cdot U_{(T)}$ in the Heisenberg picture. $U_{(T)} = \exp[-i\mathcal{H}T]$ is the unitary for the evolution of the spins under the interaction Hamiltonian for time T. In a many-body system with non-trivial interactions, this metric quantifies the spread of quantum information or the rate in which two initially commuting operators V and W lose their commutivity [31].

$$\left\langle |[W_T, V]|^2 \right\rangle = 2(1 - \mathrm{Re}[\mathcal{F}_{(T)}]) \tag{5.13}$$

To connect the signal from our echo experiment in equation 5.10 with the OTOC metric we define:

$$W_\tau = U_{mix}(\tau). \tag{5.14}$$

The OTOC experiment is normally proposed as an echo measurement with a fixed mixing window used as the perturbation. The results lead to a map of reduced refocusing under the evolution. It is necessary that the mixing Hamiltonian commute with the initial state.

The normal arguments are in the Heisenberg frame, so the mixing operator evolved in time is used.

$$W_\tau(T) = U_{evo}^\dagger(T).W_\tau.U_{evo}(T). \tag{5.15}$$

So the evolved state can be written as

$$\rho_{(2T,\tau)} = W_\tau^\dagger(T).\rho_0.W_\tau(T) \tag{5.16}$$

and the overlap with the initial state is

$$S_{(2T,\tau)} = \mathrm{Tr}[W_\tau^\dagger(T).\rho_0.W_\tau(T).\rho_0] \quad (5.17)$$
$$= \mathcal{F}_\tau(T). \quad (5.18)$$

In the last equation we have assumed that $V = \rho_0^{cs} = \frac{1}{2}\sigma_{\mathrm{x}}$.

The observable signal of the MCSD experiment for fixed mixing window lengths is an example of an OTOC metric. These results are presented in the next section. The decay of the OTOC metric is predicted to be exponential for multi-body systems.

5.2 Sensitivity to fixed perturbations

We implement the experiment as an OTOC measure. Figure 5.2 shows the echo amplitude decaying as a function of evolution time for five different mixing windows (perturbations). An increase in the evolution time results in more correlations between the central spin and the environment. These data indicate that with the same perturbation, the amplitude of the echo becomes smaller for longer evolution times. In other words, the correlations between the central spin and the environment become more sensitive to the perturbation at longer evolution times.

The decay of the echo signal for $\tau = 0$, arises from the decoherence in our system and not the mixing inside the environment and it was studied in the context of the MCD experiment in chapter 3. We normalized these plots with respect to the $\tau = 0$ data and the data is shown in figure 5.3. This gives a clearer picture of the dynamics of correlations between the central spin and the environment, due to the mixing of spins in the environment.

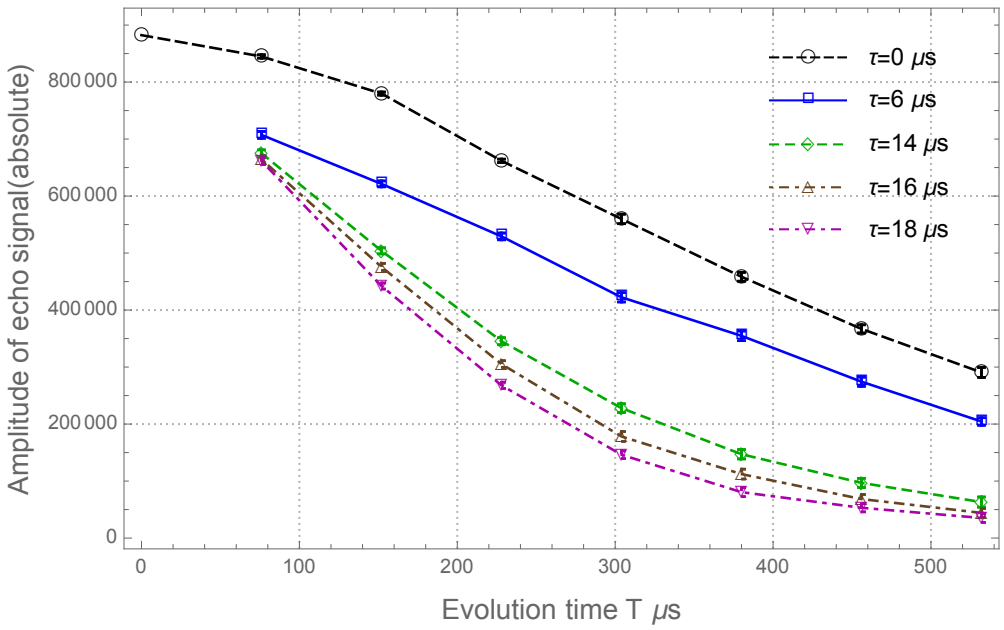

Figure 5.2: The decay of echo signal (no encoding) as a function of evolution time T, for five fixed mixing windows, τ. During the evolution time the MREV-8 sequence is used to refocus the homonuclear dipolar interaction in the environment. The length of our MREV-8 cycle is 38 μs and we chose to add two MREV-8 sequences in each step of the evolution time. Consequently, data points are recorded every 76 μs.

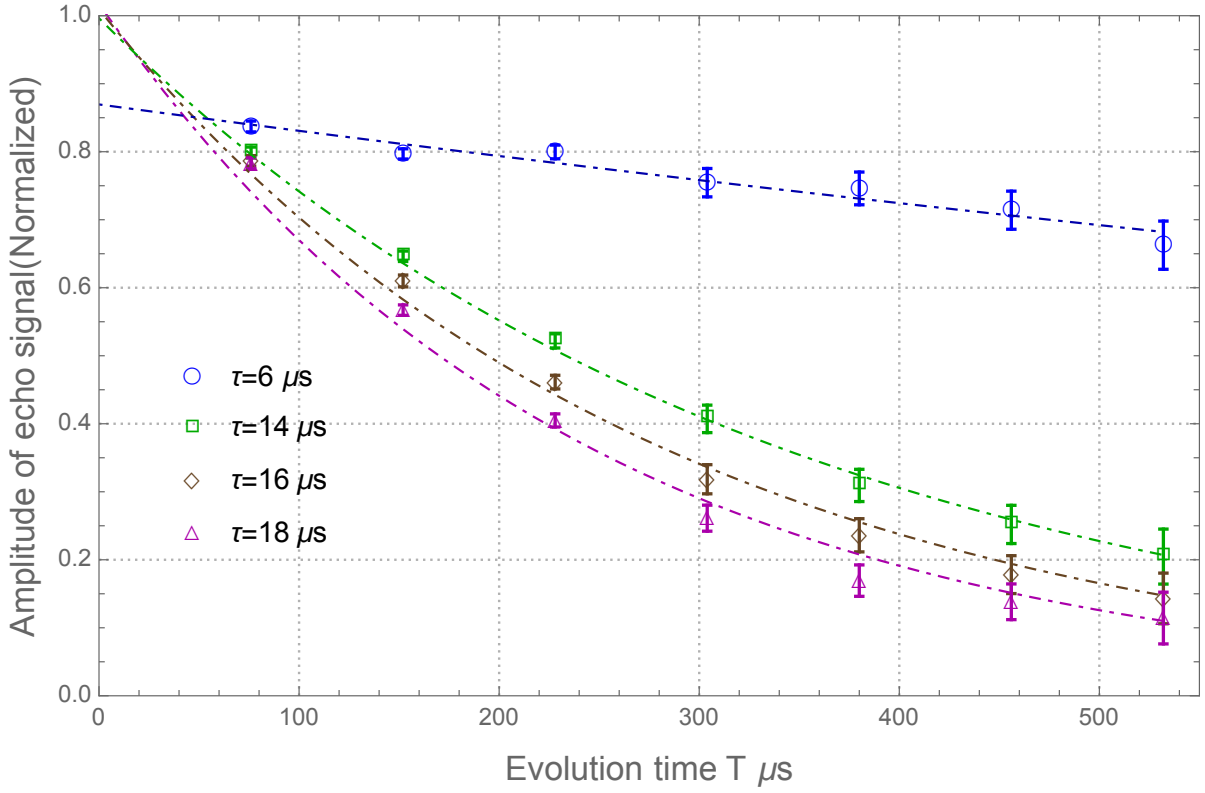

Figure 5.3: Sensitivity of the central spin/environment correlations to fixed perturbations. Data is normalized with respect to $\tau = 0$ data set. The error bars are evaluated via the signal to noise ratio of each data set in combination with $\tau = 0$ errors. The dashed lines are Lorentzian fits with characteristic decay times of $2200 \pm 300, 338 \pm 7, 280 \pm 10, 240 \pm 10 \mu s$ for $\tau = 6, 14, 16, 18 \mu s$ respectively.

The sample is a powder and the homonuclear dipolar coupling varies with molecular orientation. Figure 5.4 shows a plot of distribution of the largest dipolar frequencies over a powder average. The largest frequency of 19,750 Hz corresponds to two nearest neighbor spins on a single phenyl ring being oriented along the external magnetic field direction.

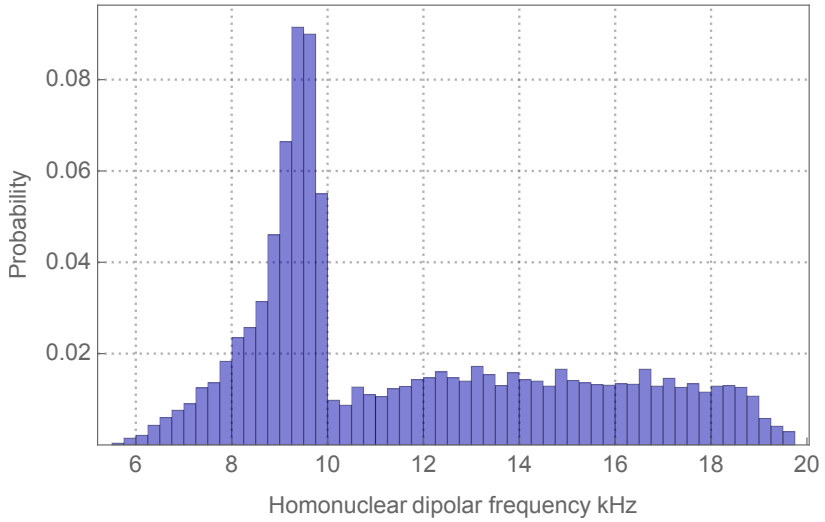

Figure 5.4: Absolute value of the largest dipolar frequency for proton spins in a phenyl ring. Probabilities are reported on average over all molecular orientations.

The sensitivity to perturbation plots in Figure 5.3 show two distinct behaviors. When the perturbation is very short (the $6\mu s$ curve) then most of the sample does not see this. So regardless of the evolution time, the central spin for most molecules is refocused and the decay should have a form

$$\begin{aligned} S(t) &= \alpha + \beta \exp[-at] \\ \alpha + \beta &= 1 \end{aligned} \tag{5.19}$$

For the longer perturbation times the data shows that all of the sample participates and the expected exponential decays are observed.

An important limitation of Fig 5.3 is that the effect of the perturbation is not actually a function of the evolution time, it is a function of the number and strengths of correlations

between the central spin and the environment spins. Recall that in the coin game the probability of going back to the initial order, was heavily influenced by the number of initial coin flips. Fortunately, we already demonstrated that we can measure the extent of correlation through the MCD experiment, discussed in chapter 3. The relevant data is reproduced in figure 5.5.

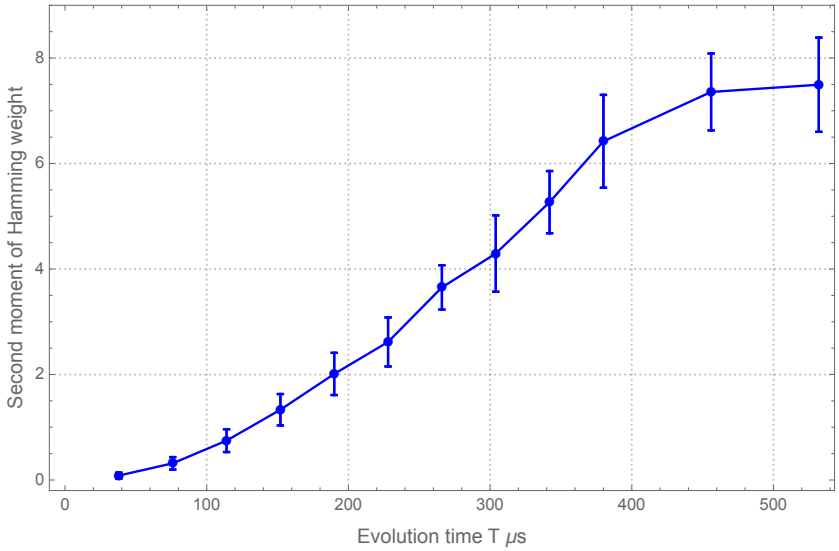

Figure 5.5: The growth of the second moment of the Hamming Weight for the central spin/environment correlations, as a function of evolution time.

Notice that the correlations build slowly at first and then with longer evolution times grow quickly before saturating. As expected the saturation happens at much less than the 15 spins in the environment since the angular dependence of the dipolar coupling means that some environment spins are only very weakly coupled to the central spin.

In figure 5.6 we show the data plotted versus the growth of central spin-to-environment correlations. Now the data have an easily recognizable form. The $\tau = 6\mu s$ data decays only slowly since most spins do not contribute. As the extent of the perturbation in the environment grows the decays become faster. The horizontal axis reports on the second moment of Hamming weight for central spin/environment correlations. Notice that both the early and late time points are compressed due to the slow initial growth and the late saturation of the central spin/environment correlations.

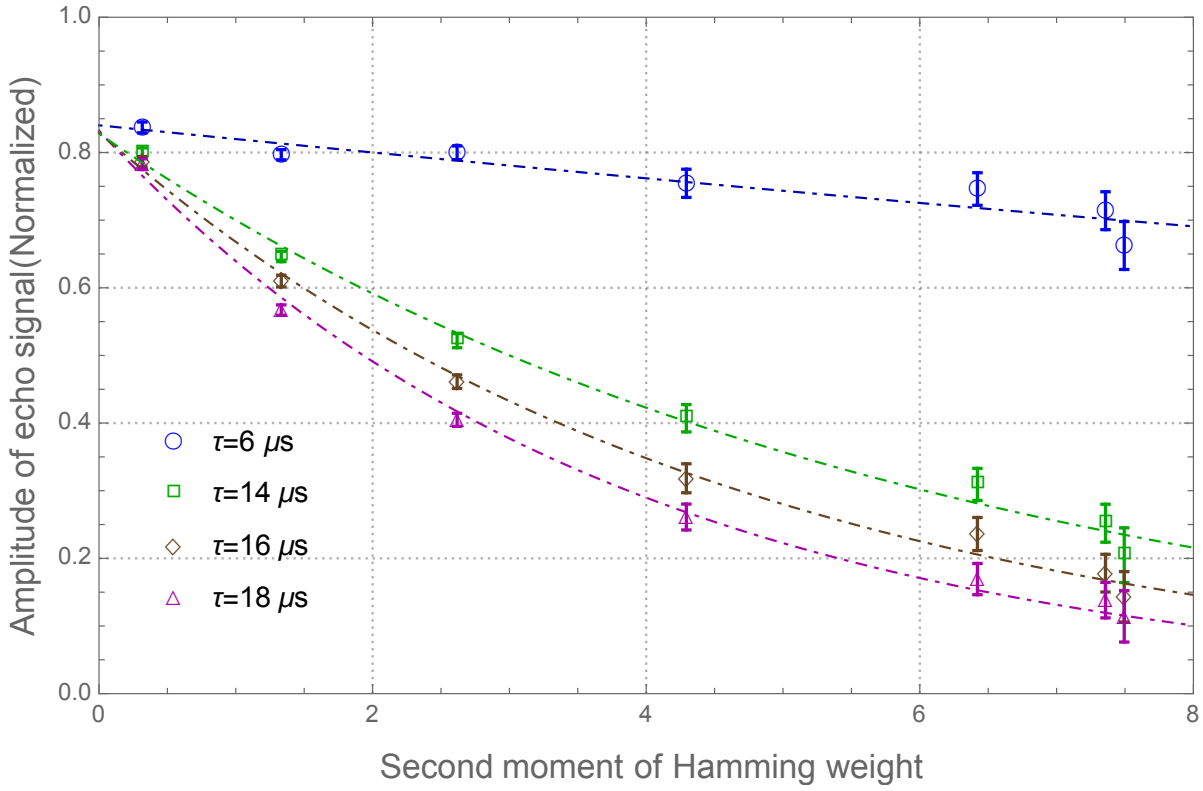

Figure 5.6: The decay of echo amplitude as a function of the second moment of Hamming weight for the central spin/environment correlations. The dashed lines are Lorentzian fits with characteristic decay size of $41 \pm 7, 5.9 \pm 0.3, 4.6 \pm 0.2, 3.8 \pm 0.2$ for $\tau = 6, 14, 16, 18 \mu s$ respectively.

The characteristic correlation size extracted from the fits describes the extent of central spin/environment correlations necessary for the given perturbation to be effective at destroying them. For the $\tau = 6\mu s$ perturbation there is no such size since the perturbation leaves the environment for most molecules unchanged. We see this also from the fit which returns an unreasonably large value. The three larger perturbations can lead to a full mixing of the environment. The characteristic correlation sizes decrease with increasing perturbation.

This work suggests a necessary rethinking of the way the Out-of-Time-Ordered-Correlation function is used to characterize sensitivity to perturbations. Instead of thinking of the evolution step as just a unitary process, mapping it based on the information flow to the environment, gives a more clear picture of the spin dynamics. In this case the second moment of the Hamming weight is the natural measure for the quantum information flow, in other cases it may be a shared entropy.

Chapter 6

Conclusion and Outlook

6.1 Conclusion

The idea behind this work was to design NMR experiments for the study of quantum information evolution in the central spin problem. The study of dephasing in the central spin setup indicates that, in order to describe the quantum evolution of the central spin, multi-spin correlations between the central spin and environment spins should be understood and analyzed. This analysis of multi-spin correlations reveals the extent of correlations between the central spin and the environment, and the rate of information flow from the central spin to the environment.

In order to experimentally access multi-spin correlations between the central spin and the environment, NMR spectrometer was modified with fast electronics. A set of tuning algorithms were used to minimize the effects of non-ideal RF pulses in our experiment. The NMR sample is chosen to resemble the central spin structure and it is characterized precisely. A para-magnetic relaxation agent were added to the sample to decrease the T_1 relaxation time.

The multi-spin Correlation Detection or MCD experiment utilizes rotational symmetry of multi-spin correlations, as a distinguishing property for different orders of correlated spins. Multi-spin correlations between the central spin and the environment are directly observed using the MCD experiment. A set of experimental results with different evolu-

tion times, reveal the flow dynamics of quantum information from the central spin to the environment. The average cluster size of correlated spins in the environment is used as a measure for information content of the environment, which grows with the evolution time of the MCD experiment.

We have introduced a set of operators $\hat{P}_n$ that can project different parts of the density matrix on the multi-spin operators. The results of these projections give the weights of each multi-spin correlated operator $C_n(T)$, which are identical to the square root of amplitudes of multi-spin correlated operators evaluated by the MCD method. This confirms that the MCD experiment is correctly probing the evolution of multi-spin correlations.

Multi-spin Correlation Scrambling Detection (MCSD) experiment quantifies the sensitivity of the central spin/environment correlations to the mixing interaction in environment. The results of MCSD experiment plotted for fixed evolution times show that the decay of correlation amplitudes during the mixing window, depends on their correlation order as well as the average cluster size of the central spin/environment correlations.

A classical coin game is used to motivate our proposed model for dynamics of quantum information scrambling. If we extract the average size of correlations from the MCD experiment and use it as an input, the classical coin model predicts the scrambling rates with the same trend as the experimental data for the decay of echo amplitudes.

The results of the MCSD experiment plotted for fixed mixing windows, indicate the sensitivity of the central spin/environment correlations to perturbations in the environment. These results can be described in the form of an Out-of-Time-Order Correlation metric. We find that mapping the OTOC metric to the second moment of the Hamming weight instead of the evolution time, gives a superior picture for the dynamics of information in our system.

6.2 Future direction

- There is a need for more data points at short evolution times specially at $T = 0$. We have an improved design for performing experiments with a constant length for mixing interval(using magic echo pulse sequence), that can be used to collect $T = 0$ data points

- In order to grow the size of correlations between the central spin and the environment, we are designing an experiment with Magic Angle Spinning (MAS) to remove the spatial dependency of the heteronuclear coupling. This experiment can bring the environment close to the saturation limit

- We are designing bench marking experiments in order to characterize the environmental noise. These experiments can be used to distinguish between Markovian and non-Markovian dynamics in the environment

- We are planning to study central spin systems with more than one spin in them. The idea is to investigate effects of initial entanglement on the flow of quantum information from the central spin to the environment

- We are designing experiments to observe the quantum information transfer between two uncoupled qubits when they share the same spin environment. The difference in the selection rules for growth of correlations via homonuclear and heteronuclear dipolar interactions is going to be used in this experiment

- Although we have access to dynamics of various correlation orders, only results of the MCSD experiment for the echo amplitudes were used in evaluation of the OTOC metric. We are interested in expanding the theory to use the rest of our results

- A new experiment is being designed to directly observe the flow of quantum information from the environment to the central spin.

- With utilizing a spectrometer with a larger magnetic field, we are planning to run the MCSD experiment for a sample with environment size of 27.

References

[1] D. G Cory, J. B Miller, and A. N Garroway. Time-suspension multiple-pulse sequences: applications to solid-state imaging. *Journal of Magnetic Resonance (1969)*, 90(1):205–213, 1990.

[2] H. Cho, T. D. Ladd, J. Baugh, D. G. Cory, and C. Ramanathan. Multispin dynamics of the solid-state nmr free induction decay. *Phys. Rev. B*, 72:054427, Aug 2005.

[3] P. W. Anderson. Spectral diffusion, phonons, and paramagnetic spin-lattice relaxation. *Phys. Rev.*, 114:1002–1005, May 1959.

[4] J. R. Klauder and P. W. Anderson. Spectral diffusion decay in spin resonance experiments. *Phys. Rev.*, 125:912–932, Feb 1962.

[5] B. Herzog and E. L. Hahn. Transient nuclear induction and double nuclear resonance in solids. *Phys. Rev.*, 103:148–166, Jul 1956.

[6] E. Joos, H.D. Zeh, C. Kiefer, D.J.W. Giulini, J. Kupsch, and I.O. Stamatescu. *Decoherence and the Appearance of a Classical World in Quantum Theory*. Springer Berlin Heidelberg, 2013.

[7] Rolf Landauer. The physical nature of information. *Physics Letters A*, 217(4):188–193, 1996.

[8] W. G. Unruh. Maintaining coherence in quantum computers. *Phys. Rev. A*, 51:992–997, Feb 1995.

[9] D. Bacon. Decoherence, Control, and Symmetry in Quantum Computers. *eprint arXiv:quant-ph/0305025*, May 2003.

[10] D. P. Divincenzo. The Physical Implementation of Quantum Computation. *Fortschritte der Physik*, 48:771–783, 2000.

[11] Fei Yan, Simon Gustavsson, Jonas Bylander, Xiaoyue Jin, Fumiki Yoshihara, David G. Cory, Yasunobu Nakamura, Terry P. Orlando, and William D. Oliver. Rotating-frame relaxation as a noise spectrum analyser of a superconducting qubit undergoing driven evolution. 4:2337 EP –, 08 2013.

[12] David D. Awschalom, Lee C. Bassett, Andrew S. Dzurak, Evelyn L. Hu, and Jason R. Petta. Quantum spintronics: Engineering and manipulating atom-like spins in semiconductors. *Science*, 339(6124):1174–1179, 2013.

[13] P. Gumann, O. Patange, C. Ramanathan, H. Haas, O. Moussa, M. L. W. Thewalt, H. Riemann, N. V. Abrosimov, P. Becker, H.-J. Pohl, K. M. Itoh, and D. G. Cory. Inductive measurement of optically hyperpolarized phosphorous donor nuclei in an isotopically enriched silicon-28 crystal. *Phys. Rev. Lett.*, 113:267604, Dec 2014.

[14] J. R. Maze, J. M. Taylor, and M. D. Lukin. Electron spin decoherence of single nitrogen-vacancy defects in diamond. *Phys. Rev. B*, 78:094303, Sep 2008.

[15] M. Brune, E. Hagley, J. Dreyer, X. Maître, A. Maali, C. Wunderlich, J. M. Raimond, and S. Haroche. Observing the progressive decoherence of the "meter" in a quantum measurement. *Phys. Rev. Lett.*, 77:4887–4890, Dec 1996.

[16] C. J. Myatt, B. E. King, Q. A. Turchette, C. A. Sackett, D. Kielpinski, W. M. Itano, C. Monroe, and D. J. Wineland. Decoherence of quantum superpositions through coupling to engineered reservoirs. *Nature*, 403(6767):269–273, 01 2000.

[17] Klaus Hornberger, Stefan Uttenthaler, Björn Brezger, Lucia Hackermüller, Markus Arndt, and Anton Zeilinger. Collisional decoherence observed in matter wave interferometry. *Phys. Rev. Lett.*, 90:160401, Apr 2003.

[18] E. L. Hahn. Spin echoes. *Phys. Rev.*, 80:580–594, Nov 1950.

[19] H. Y. Carr and E. M. Purcell. Interaction between nuclear spins in hd gas. *Phys. Rev.*, 88:415–416, Oct 1952.

[20] S. R. Hartmann and E. L. Hahn. Nuclear double resonance in the rotating frame. *Phys. Rev.*, 128:2042–2053, Dec 1962.

[21] W-K. Rhim, A. Pines, and J. S. Waugh. Time-reversal experiments in dipolar-coupled spin systems. *Physical Review B*, 3(3):684–696, 02 1971.

[22] J S Waugh. Uncoupling of local field spectra in nuclear magnetic resonance: determination of atomic positions in solids. *Proceedings of the National Academy of Sciences*, 73(5):1394–1397, 1976.

[23] J. S. Waugh, L. M. Huber, and U. Haeberlen. Approach to high-resolution nmr in solids. *Phys. Rev. Lett.*, 20:180–182, Jan 1968.

[24] P. Caravatti, L. Braunschweiler, and R. R. Ernst. Heteronuclear correlation spectroscopy in rotating solids. *Chemical Physics Letters*, 100(4):305–310, 1983.

[25] G. S. Boutis, P. Cappellaro, H. Cho, C. Ramanathan, and D. G. Cory. Pulse error compensating symmetric magic-echo trains. *Journal of Magnetic Resonance*, 161(2):132–137, 4 2003.

[26] B. Cowan. *Nuclear Magnetic Resonance and Relaxation*. Cambridge University Press, 2005.

[27] A. Abragam. *The Principles of Nuclear Magnetism*. Oxford University Press, 1961.

[28] I. A. Merkulov, Al. L. Efros, and M. Rosen. Electron spin relaxation by nuclei in semiconductor quantum dots. *Phys. Rev. B*, 65:205309, Apr 2002.

[29] Neil Shenvi, Rogerio de Sousa, and K. Birgitta Whaley. Universal scaling of hyperfine-induced electron spin echo decay. *Phys. Rev. B*, 71:224411, Jun 2005.

[30] W. H. Zurek, F. M. Cucchietti, and J. P. Paz. Gaussian Decoherence and Gaussian Echo from Spin Environments. *Acta Physica Polonica B*, 38:1685, May 2007.

[31] Brian Swingle, Gregory Bentsen, Monika Schleier-Smith, and Patrick Hayden. Measuring the scrambling of quantum information. *Physical Review A*, 94(4):040302–, 10 2016.

[32] Nima Lashkari, Douglas Stanford, Matthew Hastings, Tobias Osborne, and Patrick Hayden. Towards the fast scrambling conjecture. *Journal of High Energy Physics*, 2013(4):22, 2013.

[33] N. Bloembergen, E. M. Purcell, and R. V. Pound. Relaxation effects in nuclear magnetic resonance absorption. *Phys. Rev.*, 73:679–712, Apr 1948.

[34] Wojciech Hubert Zurek. Decoherence, einselection, and the quantum origins of the classical. *Rev. Mod. Phys.*, 75:715–775, May 2003.

[35] V. V. Dobrovitski, A. E. Feiguin, D. D. Awschalom, and R. Hanson. Decoherence dynamics of a single spin versus spin ensemble. *Phys. Rev. B*, 77:245212, Jun 2008.

[36] F. M. Cucchietti, D. A. R. Dalvit, J. P. Paz, and W. H. Zurek. Decoherence and the loschmidt echo. *Physical Review Letters*, 91(21):210403–, 11 2003.

[37] F. M. Cucchietti, J. P. Paz, and W. H. Zurek. Decoherence from spin environments. *Physical Review A*, 72(5):052113–, 11 2005.

[38] Rodolfo A. Jalabert and Horacio M. Pastawski. Environment-independent decoherence rate in classically chaotic systems. *Physical Review Letters*, 86(12):2490–2493, 03 2001.

[39] Dmitry A. Abanin and Eugene Demler. Measuring entanglement entropy of a generic many-body system with a quantum switch. *Physical Review Letters*, 109(2):020504–, 07 2012.

[40] Jan Fischer and Heinz-Peter Breuer. Correlated projection operator approach to non-markovian dynamics in spin baths. *Physical Review A*, 76(5):052119–, 11 2007.

[41] Edwin Barnes, Łukasz Cywiński, and S. Das Sarma. Master equation approach to the central spin decoherence problem: Uniform coupling model and role of projection operators. *Physical Review B*, 84(15):155315–, 10 2011.

[42] Wayne M. Witzel, Malcolm S. Carroll, Łukasz Cywiński, and S. Das Sarma. Quantum decoherence of the central spin in a sparse system of dipolar coupled spins. *Phys. Rev. B*, 86:035452, Jul 2012.

[43] Rogerio de Sousa and S. Das Sarma. Theory of nuclear-induced spectral diffusion: Spin decoherence of phosphorus donors in si and gaas quantum dots. *Phys. Rev. B*, 68:115322, Sep 2003.

[44] Wang Yao, Ren-Bao Liu, and L. J. Sham. Theory of electron spin decoherence by interacting nuclear spins in a quantum dot. *Phys. Rev. B*, 74:195301, Nov 2006.

[45] Ren-Bao Liu, Wang Yao, and L J Sham. Control of electron spin decoherence caused by electron–nuclear spin dynamics in a quantum dot. *New Journal of Physics*, 9(7):226, 2007.

[46] S. K. Saikin, Wang Yao, and L. J. Sham. Single-electron spin decoherence by nuclear spin bath: Linked-cluster expansion approach. *Physical Review B*, 75(12):125314–, 03 2007.

[47] Wen Yang and Ren-Bao Liu. Quantum many-body theory of qubit decoherence in a finite-size spin bath. *Physical Review B*, 78(8):085315–, 08 2008.

[48] Wen Yang and Ren-Bao Liu. Quantum many-body theory of qubit decoherence in a finite-size spin bath. ii. ensemble dynamics. *Physical Review B*, 79(11):115320–, 03 2009.

[49] Wen-Long Ma, Gary Wolfowicz, Nan Zhao, Shu-Shen Li, John JL Morton, and Ren-Bao Liu. Uncovering many-body correlations in nanoscale nuclear spin baths by central spin decoherence. *Nature Communications*, 5:4822, 09 2014.

[50] W.S. Warren, D.P. Weitekamp, and A. Pines. Theory of selective excitation of multiplequantum transitions. *The Journal of Chemical Physics*, 73(5):2084–2099, 2017/02/06 1980.

[51] J. Baum, M. Munowitz, A. N. Garroway, and A. Pines. Multiple-quantum dynamics in solid state nmr. *The Journal of Chemical Physics*, 83(5):2015–2025, 1985.

[52] Michael Munowitz, Alexander Pines, and Michael Mehring. Multiple-quantum dynamics in nmr: A directed walk through liouville space. *The Journal of Chemical Physics*, 86(6):3172–3182, 1987.

[53] Michael Munowitz and Alexander Pines. Principles and applications of multiple-quantum nmr. *Advances in Chemical Physics*, 66, 2007.

[54] Michael Munowitz. *Coherence and NMR*. JOHN WILEY & SONS, 1988.

[55] Serge Lacelle, Son-Jong Hwang, and Bernard C. Gerstein. Multiple quantum nuclear magnetic resonance of solids: A cautionary note for data analysis and interpretation. *The Journal of Chemical Physics*, 99(11):8407–8413, 2017/02/06 1993.

[56] Gonzalo A. Álvarez and Dieter Suter. Localization effects induced by decoherence in superpositions of many-spin quantum states. *Phys. Rev. A*, 84:012320, Jul 2011.

[57] Marko Lovrić, Hans Georg Krojanski, and Dieter Suter. Decoherence in large quantum registers under variable interaction with the environment. *Phys. Rev. A*, 75:042305, Apr 2007.

[58] S. I. Doronin, E. B. Fel'dman, and A. I. Zenchuk. Numerical analysis of relaxation times of multiple quantum coherences in the system with a large number of spins. *The Journal of Chemical Physics*, 134(3):034102, 2011.

[59] U. Haeberlen and J. S. Waugh. Coherent averaging effects in magnetic resonance. *Phys. Rev.*, 175:453–467, Nov 1968.

[60] ULRICH Haeberlen. *High Resolution NMR in Solids Selective Averaging*, pages 1–190. Academic Press, 1976.

[61] C. Ramanathan, H. Cho, P. Cappellaro, G. S. Boutis, and D. G. Cory. Encoding multiple quantum coherences in non-commuting bases. *Chemical Physics Letters*, 369(3–4):311–317, 2 2003.

[62] K. X. Wei, C. Ramanathan, and P. Cappellaro. Exploring Localization in Nuclear Spin Chains. *ArXiv e-prints*, December 2016.

[63] D. H. Levy and K. K. Gleason. Multiple quantum nuclear magnetic resonance as a probe for the dimensionality of hydrogen in polycrystalline powders and diamond films. *Journal of physical chemistry*, 96(20):8125–8131, 1992.

[64] J. Emerson. *Open Quantum System Course Note*. University of Waterloo, 2009.

[65] H.P. Breuer and F. Petruccione. *The Theory of Open Quantum Systems*. OUP Oxford, 2007.

[66] KARL Kraus, A. Bohm, J.D. Dollard, and W. H. Wooters. *States, Effects, and Operations Fundamental Notions of Quantum Theory*. Lecture Notes in Physics. Springer Berlin Heidelberg, 1983.

[67] W. Forrest Stinespring. Positive functions on c*-algebras. *Proceedings of the American Mathematical Society*, 6(2):211–216, 1955.

[68] Heinz-Peter Breuer, Elsi-Mari Laine, and Jyrki Piilo. Measure for the degree of non-markovian behavior of quantum processes in open systems. *Phys. Rev. Lett.*, 103:210401, Nov 2009.

[69] F. O. Zelaya, S. Crozier, S. Dodd, R. Mckenna, and D. M. Doddrell. Measurement and compensation of field inhomogeneities caused by differences in magnetic susceptibility. *Journal of Magnetic Resonance, Series A*, 115(1):131–136, 1995.

[70] N. Soffe, J. Boyd, and M. Leonard. The construction of a high-resolution 750 mhz probehead. *Journal of Magnetic Resonance, Series A*, 116(1):117–121, 1995.

[71] Serge Stroobandt. Single-layer helical round wire coil inductor calculator. http://hamwaves.com/antennas/inductance.html.

[72] S Idziak and U Haeberlen. Design and construction of a high homogeneity rf coil for solid-state multiple-pulse nmr. *Journal of Magnetic Resonance (1969)*, 50(2):281 – 288, 1982.

[73] Elena Vinogradov, P. K. Madhu, and Shimon Vega. *Strategies for High-Resolution Proton Spectroscopy in Solid-State NMR*. Springer Berlin Heidelberg, Berlin, Heidelberg 2005.

[74] Michael Mehring. *High Resolution NMR in Solids*. Springer-Verlag, second edition, 1982.

[75] WK. Rhim, D. D. Elleman, and R. W. Vaughan. Analysis of multiple pulse nmr in solids. *The Journal of Chemical Physics*, 59(7):3740–3749, 1973.

[76] E. Fukushima and S.B.W. *Experimental Pulse NMR: A Nuts and Bolts Approach*. Avalon Publishing, 1993.

[77] M. D Schnall, V Harihara Subramanian, and J. S Leigh. The application of overcoupled tank circuits to nmr probe design. *Journal of Magnetic Resonance (1969)*, 67(1):129–134, 1986.

[78] G. C Chingas. Overcoupling nmr probes to improve transient response. *Journal of Magnetic Resonance (1969)*, 54(1):153–157, 1983.

[79] J. B. Miller, B. H. Suits, A. N. Garroway, and M. A. Hepp. Interplay among recovery time, signal, and noise: Series- and parallel-tuned circuits are not always the same. *Concepts in Magnetic Resonance*, 12(3):125–136, 2000.

[80] W.K. Rhim, D. D. Elleman, L. B. Schreiber, and R. W. Vaughan. Analysis of multiple pulse nmr in solids. ii. *The Journal of Chemical Physics*, 60(11):4595–4604, 1974.

[81] B. C. Gerstein and C. R. Dybowski. *Transient techniques in NMR of solids*. ACADEMIC PRESS, INC., 1985.

[82] Gerald A. Pearson. *Shimming an NMR magnet*. Chemistry Department, University of Iowa, Iowa City, IA 52252, 1993.

[83] K. Schmidt-Rohr and H. W. Spiess. *Multidimensional Solid-State NMR and Polymers*. Academic Press, San Diego, 1994.

[84] D. G Cory. A new multiple-pulse cycle for homonuclear dipolar decoupling. *Journal of Magnetic Resonance (1969)*, 94(3):526–534, 1991.

[85] D. P Burum, M Under, and R. R Ernst. A new "tune-up"nmr pulse cycle for minimizing and characterizing phase transients. *Journal of Magnetic Resonance (1969)*, 43(3):463–471, 1981.

[86] WK. Rhim, D. D. Elleman, and R. W. Vaughan. Enhanced resolution for solid state nmr. *The Journal of Chemical Physics*, 58(4):1772–1773, 1973.

[87] T Michael Doncan. *A Compilation of Chemical Shift Anisotropies*. The Farragut Press, Chicago, 1990.

[88] D. P Burum and A Bielecki. An improved experiment for heteronuclear-correlation 2d nmr in solids. *Journal of Magnetic Resonance (1969)*, 94(3):645–652, 1991.

[89] R. K. Hester, J. L. Ackerman, B. L. Neff, and J. S. Waugh. Separated local field spectra in nmr: Determination of structure of solids. *Phys. Rev. Lett.*, 36:1081–1083, May 1976.

[90] C. P. Slichter. *Principles of Magnetic Resonance*. Springer, 1989.

[91] DG Cory and WM Ritchey. Inversion recovery cross-polarization nmr in solid semicrystalline polymers. *Macromolecules*, 22(4):1611–1615

[92] R. L. Strombotne and E. L. Hahn. Longitudinal nuclear spin-spin relaxation. *Phys. Rev.*, 133:A1616–A1629, Mar 1964.

[93] Jacco D. van Beek, Marina Carravetta, Gian Carlo Antonioli, and Malcolm H. Levitt. Spherical tensor analysis of nuclear magnetic resonance signals. *The Journal of Chemical Physics*, 122(24):244510, 2005.

[94] Hans Georg Krojanski and Dieter Suter. Scaling of decoherence in wide nmr quantum registers. *Phys. Rev. Lett.*, 93:090501, Aug 2004.

[95] Karen K. Gleason. *Multiple Quantum NMR in Solids*. John Wiley & Sons, Ltd, 2007.

[96] M. Gärttner, J. G. Bohnet, A. Safavi-Naini, M. L. Wall, J. J. Bollinger, and A. M. Rey. Measuring out-of-time-order correlations and multiple quantum spectra in a trapped ion quantum magnet. *ArXiv e-prints*, August 2016.

[97] J. Li, R. Fan, H. Wang, B. Ye, B. Zeng, H. Zhai, X. Peng, and J. Du. Measuring out-of-time-order correlators on a nuclear magnetic resonance quantum simulator. *ArXiv e-prints*, September 2016.

[98] M. Rigol, V. Dunjko, and M. Olshanii. Thermalization and its mechanism for generic isolated quantum systems. *Nature*, 452:854–858, April 2008.

[99] Rahul Nandkishore and David A. Huse. Many-body localization and thermalization in quantum statistical mechanics. *Annual Review of Condensed Matter Physics*, 6(1):15–38, 2015.

[100] J. S. Waugh. Thermodynamic equilibrium in isolated spin systems. *Applied Magnetic Resonance*, 27(1

[101] Asher Peres. Stability of quantum motion in chaotic and regular systems. *Phys. Rev. A*, 30:1610–1615, Oct 1984.

APPENDICES

Appendix A

Codes and Pulse Programs

A.1 Pulse program: the MCD experiment

In the following the pulse program for detection of multi-spin correlations in the spin environment is presented. This is a 2D NMR experiment on proton and ^{31}P channels . F1 is set to pulse and to receive the spin signal at the phosphorous frequency and F2 is set to pulse and to decouple the environment spins, ^{1}H. This Pulse program is executable in Bruker TopSpin.

```
define delay small      ;small window in MREV_8, about 3us with duplexer
"small=d3-p2"
define delay large                              ;large window in MREV_8
"large=d3+d3-p2"
```

```
1 ze                              ;acquire into a cleared memory
10u reset:f1 reset:f2    ;synchronise RF pulse and detection F1:31P F2:1H
10u pl2:f2 pl1:f1                        ;set power level for each channel
```

```
2 d11 do:f2                                          ;turn OFF the decoupling
d11 pl2:f2                                  ;cross polarization power for 1H
d1 pl1:f1                     ;Relaxation delay, cross polarization power 1H

p2:f2 ph1                ;Initialization pulse for cross polarization
0.3u
(p15 ph2):f1 (p15:spf0 pl22 ph10):f2           ;Cross Polarization contact


0.5u  pl2:f2                               ;31P power level set to High power

4 p2:f2 ph20^                                 ;Evolution starts, MREV-8 on 1H
small
p2:f2 ph20^
large
p2:f2 ph20^
small
p2:f2 ph20^
large
p2:f2 ph20^
small
p2:f2 ph20^
large
p2:f2 ph20^
small
p2:f2 ph20^
large pl3:f1
lo to 4 times l1                             ;Evolution ends after l1 loops


(center                                                              ;sync.
```

```
(p2 ph4 2u p2 ph5):f2                                    ;Rx)\phi on 1H
(p1*2 ph3):f1                                ;central \pi pulse on 31P
)


5 p2:f2 ph20^                    ;inverted evolution starts, MREV-8 on 1H
small
p2:f2 ph20^
large
p2:f2 ph20^
small
p2:f2 ph20^
large
p2:f2 ph20^
small
p2:f2 ph20^
large
p2:f2 ph20^
small
p2:f2 ph20^
large
lo to 5 times l1                   ;Inverted evolution ends after l1 loops


go=2 ph31 cpds2:f2             ;Detection on 31P channel, CW on 1H channel
d11 do:f2 wr #0 if #0                            ;data record on memory

1m ip1                                    ;phase incrementation for Rx)\phi
1m ip10
1m ip4

lo to 2 times td1                            ;Loop over for various phases
```

```
HaltAcqu, 1m
7 exit


;phase program:

ph1=  (32)8 24
ph2=  0 0 1 1
ph3=  0 0 0 0 1 1 1 1 2 2 2 2 3 3 3 3
ph4=  (32) 8 24
ph5=  3 1
ph10= (32)0
ph20=0 1 3 2 2 1 3 0
ph30=(360)115
ph31= 0 2 3 1 2 0 1 3


;parameters:

;small : small delay in MREV_8 sequence, typically 2.5-4.5 usec
;large : large delay in MREV_8 sequence
;L1    ; loop counter for evolution period, number of MREV_8 cycles
;TD1   : number of steps in \phi
;d11   : 30ms
;d1    : T1 relaxation delay
;d3    : delay to set small and large window
;PL1   : power level for 1H, High power
;PL2   : power level for 31P contact
;PL3   : power level for 31P, High power
;PL22  : Power level for Hartman_Hahn condition 31P
;P1    : 31P Hard 90 pulse
;P2    : 1H Hard 90 pulse
;P15   : 31P contact pulse in Cross Polarization
```

```
;SPF0  : 1H contact shaped pulse in Cross Polarization
;CPDS2 : 1H CW decoupling during data acquisition
;PH1   : Initialization pulse phase, spin temperature alteration phase cycling
;PH2   : 31P pulse phase during the contact
;PH3   : 31P \pi pulse phase, Exorcycle
;PH4   : 1H phase, encoding
;PH5   : 1H phase, encoding
;PH10  : 1H pulse phase during contact
;PH20  : 1H MREV_8 Phase
;PH31  : Receiver phase
```

A.2 Construction of P_n multi-spin operators for one ring:

Definitions:

$$\begin{aligned} X &:= \sigma_X \\ Y &:= \sigma_Y \\ Z &:= \sigma_Z \\ PXp &:= \sigma_Y + i\sigma_Z \\ PXm &:= \sigma_Y - i\sigma_Z \\ nH1 &= 5 \end{aligned}$$

```
Pn5 = N[Sqrt[2/2^5]] KroneckerProduct[Subscript[\[DoubleStruckOne],
2], PXp, PXp, PXp, PXp, PXp];
```

```
Pn4[[1]] =
N[Sqrt[2/2^4]] Table[
Subscript[\[DoubleStruckOne],
2]\[CircleTimes]KroneckerProduct[
Permutations[{a, a, a, a, id}][[i, 1]],
Permutations[{a, a, a, a, id}][[i, 2]],
Permutations[{a, a, a, a, id}][[i, 3]],
Permutations[{a, a, a, a, id}][[i, 4]],
Permutations[{a, a, a, a, id}][[i, 5]]], {i,
Length[Permutations[{a, a, a, a, id}]]}] /. {a -> PXp,
id -> Subscript[\[DoubleStruckOne], 2]};
Pn4[[2]] =
N[Sqrt[2/2^4]] Table[
Subscript[\[DoubleStruckOne],
2]\[CircleTimes]KroneckerProduct[
Permutations[{a, a, a, a, id}][[i, 1]],
Permutations[{a, a, a, a, id}][[i, 2]],
Permutations[{a, a, a, a, id}][[i, 3]],
Permutations[{a, a, a, a, id}][[i, 4]],
Permutations[{a, a, a, a, id}][[i, 5]]], {i,
Length[Permutations[{a, a, a, a, id}]]}] /. {a -> PXp, id -> X};

Pn3[[1]] =
N[Sqrt[2/2^3]] Table[
Subscript[\[DoubleStruckOne],
2]\[CircleTimes]KroneckerProduct[
Permutations[{a, a, a, id, id}][[i, 1]],
Permutations[{a, a, a, id, id}][[i, 2]],
Permutations[{a, a, a, id, id}][[i, 3]],
Permutations[{a, a, a, id, id}][[i, 4]],
Permutations[{a, a, a, id, id}][[i, 5]]], {i,
Length[Permutations[{a, a, a, id, id}]]}] /. {a -> PXp,
id -> Subscript[\[DoubleStruckOne], 2]};
```

```
Pn3[[2]] =
N[Sqrt[2/2^3]] Table[
Subscript[\[DoubleStruckOne],
2]\[CircleTimes]KroneckerProduct[
Permutations[{a, a, a, id, id}][[i, 1]],
Permutations[{a, a, a, id, id}][[i, 2]],
Permutations[{a, a, a, id, id}][[i, 3]],
Permutations[{a, a, a, id, id}][[i, 4]],
Permutations[{a, a, a, id, id}][[i, 5]]], {i,
Length[Permutations[{a, a, a, id, id}]]}] /. {a -> PXp, id -> X};
Pn3[[3]] =
N[Sqrt[2/2^3]] Table[
Subscript[\[DoubleStruckOne],
2]\[CircleTimes]KroneckerProduct[
Permutations[{a, a, a, b, id}][[i, 1]],
Permutations[{a, a, a, b, id}][[i, 2]],
Permutations[{a, a, a, b, id}][[i, 3]],
Permutations[{a, a, a, b, id}][[i, 4]],
Permutations[{a, a, a, b, id}][[i, 5]]], {i,
Length[Permutations[{a, a, a, b, id}]]}] /. {a -> PXp, b -> X,
id -> Subscript[\[DoubleStruckOne], 2]};
Pn3[[4]] =
N[Sqrt[2/2^5]] Table[
Subscript[\[DoubleStruckOne],
2]\[CircleTimes]KroneckerProduct[
Permutations[{a, a, a, a, b}][[i, 1]],
Permutations[{a, a, a, a, b}][[i, 2]],
Permutations[{a, a, a, a, b}][[i, 3]],
Permutations[{a, a, a, a, b}][[i, 4]],
Permutations[{a, a, a, a, b}][[i, 5]]], {i,
Length[Permutations[{a, a, a, a, b}]]}] /. {a -> PXp, b -> PXm};

Pn2[[1]] =
```

```
N[Sqrt[2/2^2]] Table[
Subscript[\[DoubleStruckOne],
2]\[CircleTimes]KroneckerProduct[
Permutations[{a, a, id, id, id}][[i, 1]],
Permutations[{a, a, id, id, id}][[i, 2]],
Permutations[{a, a, id, id, id}][[i, 3]],
Permutations[{a, a, id, id, id}][[i, 4]],
Permutations[{a, a, id, id, id}][[i, 5]]], {i,
Length[Permutations[{a, a, id, id, id}]]}] /. {a -> PXp,
id -> Subscript[\[DoubleStruckOne], 2]};
Pn2[[2]] =
N[Sqrt[2/2^2]] Table[
Subscript[\[DoubleStruckOne],
2]\[CircleTimes]KroneckerProduct[
Permutations[{a, a, id, id, id}][[i, 1]],
Permutations[{a, a, id, id, id}][[i, 2]],
Permutations[{a, a, id, id, id}][[i, 3]],
Permutations[{a, a, id, id, id}][[i, 4]],
Permutations[{a, a, id, id, id}][[i, 5]]], {i,
Length[Permutations[{a, a, id, id, id}]]}] /. {a -> PXp,
id -> X};
Pn2[[3]] =
N[Sqrt[2/2^2]] Table[
Subscript[\[DoubleStruckOne],
2]\[CircleTimes]KroneckerProduct[
Permutations[{a, a, b, b, id}][[i, 1]],
Permutations[{a, a, b, b, id}][[i, 2]],
Permutations[{a, a, b, b, id}][[i, 3]],
Permutations[{a, a, b, b, id}][[i, 4]],
Permutations[{a, a, b, b, id}][[i, 5]]], {i,
Length[Permutations[{a, a, b, b, id}]]}] /. {a -> PXp, b -> X,
id -> Subscript[\[DoubleStruckOne], 2]};
Pn2[[4]] =
```

```
N[Sqrt[2/2^2]] Table[
Subscript[\[DoubleStruckOne],
2]\[CircleTimes]KroneckerProduct[
Permutations[{a, a, b, id, id}][[i, 1]],
Permutations[{a, a, b, id, id}][[i, 2]],
Permutations[{a, a, b, id, id}][[i, 3]],
Permutations[{a, a, b, id, id}][[i, 4]],
Permutations[{a, a, b, id, id}][[i, 5]]], {i,
Length[Permutations[{a, a, b, id, id}]]}] /. {a -> PXp, b -> X,
id -> Subscript[\[DoubleStruckOne], 2]};
Pn2[[5]] =
N[Sqrt[2/2^4]] Table[
Subscript[\[DoubleStruckOne],
2]\[CircleTimes]KroneckerProduct[
Permutations[{a, a, a, b, id}][[i, 1]],
Permutations[{a, a, a, b, id}][[i, 2]],
Permutations[{a, a, a, b, id}][[i, 3]],
Permutations[{a, a, a, b, id}][[i, 4]],
Permutations[{a, a, a, b, id}][[i, 5]]], {i,
Length[Permutations[{a, a, a, b, id}]]}] /. {a -> PXp, b -> PXm,
id -> Subscript[\[DoubleStruckOne], 2]};
Pn2[[6]] =
N[Sqrt[2/2^4]] Table[
Subscript[\[DoubleStruckOne],
2]\[CircleTimes]KroneckerProduct[
Permutations[{a, a, a, b, id}][[i, 1]],
Permutations[{a, a, a, b, id}][[i, 2]],
Permutations[{a, a, a, b, id}][[i, 3]],
Permutations[{a, a, a, b, id}][[i, 4]],
Permutations[{a, a, a, b, id}][[i, 5]]], {i,
Length[Permutations[{a, a, a, b, id}]]}] /. {a -> PXp, b -> PXm,
id -> X};
```

```
Pn1[[1]] =
N[Sqrt[2/2^1]] Table[
Subscript[\[DoubleStruckOne],
2]\[CircleTimes]KroneckerProduct[
Permutations[{a, id, id, id, id}][[i, 1]],
Permutations[{a, id, id, id, id}][[i, 2]],
Permutations[{a, id, id, id, id}][[i, 3]],
Permutations[{a, id, id, id, id}][[i, 4]],
Permutations[{a, id, id, id, id}][[i, 5]]], {i,
Length[Permutations[{a, id, id, id, id}]]}] /. {a -> PXp,
id -> Subscript[\[DoubleStruckOne], 2]};
Pn1[[2]] =
N[Sqrt[2/2^1]] Table[
Subscript[\[DoubleStruckOne],
2]\[CircleTimes]KroneckerProduct[
Permutations[{a, id, id, id, id}][[i, 1]],
Permutations[{a, id, id, id, id}][[i, 2]],
Permutations[{a, id, id, id, id}][[i, 3]],
Permutations[{a, id, id, id, id}][[i, 4]],
Permutations[{a, id, id, id, id}][[i, 5]]], {i,
Length[Permutations[{a, id, id, id, id}]]}] /. {a -> PXp,
id -> X};
Pn1[[3]] =
N[Sqrt[2/2^1]] Table[
Subscript[\[DoubleStruckOne],
2]\[CircleTimes]KroneckerProduct[
Permutations[{a, b, b, b, id}][[i, 1]],
Permutations[{a, b, b, b, id}][[i, 2]],
Permutations[{a, b, b, b, id}][[i, 3]],
Permutations[{a, b, b, b, id}][[i, 4]],
Permutations[{a, b, b, b, id}][[i, 5]]], {i,
Length[Permutations[{a, b, b, b, id}]]}] /. {a -> PXp, b -> X,
```

```
id -> Subscript[\[DoubleStruckOne], 2]};
Pn1[[4]] =
N[Sqrt[2/2^1]] Table[
Subscript[\[DoubleStruckOne],
2]\[CircleTimes]KroneckerProduct[
Permutations[{a, b, b, b, id}][[i, 1]],
Permutations[{a, b, b, b, id}][[i, 2]],
Permutations[{a, b, b, b, id}][[i, 3]],
Permutations[{a, b, b, b, id}][[i, 4]],
Permutations[{a, b, b, b, id}][[i, 5]]], {i,
Length[Permutations[{a, b, b, b, id}]]}] /. {a -> PXp,
b -> Subscript[\[DoubleStruckOne], 2], id -> X};
Pn1[[5]] =
N[Sqrt[2/2^1]] Table[
Subscript[\[DoubleStruckOne],
2]\[CircleTimes]KroneckerProduct[
Permutations[{a, b, b, id, id}][[i, 1]],
Permutations[{a, b, b, id, id}][[i, 2]],
Permutations[{a, b, b, id, id}][[i, 3]],
Permutations[{a, b, b, id, id}][[i, 4]],
Permutations[{a, b, b, id, id}][[i, 5]]], {i,
Length[Permutations[{a, b, b, id, id}]]}] /. {a -> PXp, b -> X,
id -> Subscript[\[DoubleStruckOne], 2]};
Pn1[[6]] =
N[Sqrt[2/2^3]] Table[
Subscript[\[DoubleStruckOne],
2]\[CircleTimes]KroneckerProduct[
Permutations[{a, b, b, id, id}][[i, 1]],
Permutations[{a, b, b, id, id}][[i, 2]],
Permutations[{a, b, b, id, id}][[i, 3]],
Permutations[{a, b, b, id, id}][[i, 4]],
Permutations[{a, b, b, id, id}][[i, 5]]], {i,
Length[Permutations[{a, b, b, id, id}]]}] /. {a -> PXm,
```

```
b -> PXp, id -> Subscript[\[DoubleStruckOne], 2]};
Pn1[[7]] =
N[Sqrt[2/2^3]] Table[
Subscript[\[DoubleStruckOne],
2]\[CircleTimes]KroneckerProduct[
Permutations[{a, b, b, id, id}][[i, 1]],
Permutations[{a, b, b, id, id}][[i, 2]],
Permutations[{a, b, b, id, id}][[i, 3]],
Permutations[{a, b, b, id, id}][[i, 4]],
Permutations[{a, b, b, id, id}][[i, 5]]], {i,
Length[Permutations[{a, b, b, id, id}]]}] /. {a -> PXm,
b -> PXp, id -> X};
Pn1[[8]] =
N[Sqrt[2/2^3]] Table[
Subscript[\[DoubleStruckOne],
2]\[CircleTimes]KroneckerProduct[
Permutations[{a, b, b, c, id}][[i, 1]],
Permutations[{a, b, b, c, id}][[i, 2]],
Permutations[{a, b, b, c, id}][[i, 3]],
Permutations[{a, b, b, c, id}][[i, 4]],
Permutations[{a, b, b, c, id}][[i, 5]]], {i,
Length[Permutations[{a, b, b, c, id}]]}] /. {a -> PXm, b -> PXp,
c -> X, id -> Subscript[\[DoubleStruckOne], 2]};
Pn1[[9]] =
N[Sqrt[2/2^5]] Table[
Subscript[\[DoubleStruckOne],
2]\[CircleTimes]KroneckerProduct[
Permutations[{a, a, a, b, b}][[i, 1]],
Permutations[{a, a, a, b, b}][[i, 2]],
Permutations[{a, a, a, b, b}][[i, 3]],
Permutations[{a, a, a, b, b}][[i, 4]],
Permutations[{a, a, a, b, b}][[i, 5]]], {i,
Length[Permutations[{a, a, a, b, b}]]}] /. {a -> PXp, b -> PXm};
```

```
Pn0[[1]] =
N[Sqrt[2]] {KroneckerProduct[Subscript[\[DoubleStruckOne], 2],
Subscript[\[DoubleStruckOne], 2], Subscript[\[DoubleStruckOne],
2], Subscript[\[DoubleStruckOne], 2],
Subscript[\[DoubleStruckOne], 2], Subscript[\[DoubleStruckOne],
2]], KroneckerProduct[Subscript[\[DoubleStruckOne], 2], X, X, X,
X, X]};
Pn0[[2]] =
N[Sqrt[2]] Table[
Subscript[\[DoubleStruckOne],
2]\[CircleTimes]KroneckerProduct[
Permutations[{a, id, id, id, id}][[i, 1]],
Permutations[{a, id, id, id, id}][[i, 2]],
Permutations[{a, id, id, id, id}][[i, 3]],
Permutations[{a, id, id, id, id}][[i, 4]],
Permutations[{a, id, id, id, id}][[i, 5]]], {i,
Length[Permutations[{a, id, id, id, id}]]}] /. {a -> X,
id -> Subscript[\[DoubleStruckOne], 2]};
Pn0[[3]] =
N[Sqrt[2]] Table[
Subscript[\[DoubleStruckOne],
2]\[CircleTimes]KroneckerProduct[
Permutations[{a, a, a, a, id}][[i, 1]],
Permutations[{a, a, a, a, id}][[i, 2]],
Permutations[{a, a, a, a, id}][[i, 3]],
Permutations[{a, a, a, a, id}][[i, 4]],
Permutations[{a, a, a, a, id}][[i, 5]]], {i,
Length[Permutations[{a, a, a, a, id}]]}] /. {a -> X,
id -> Subscript[\[DoubleStruckOne], 2]};
Pn0[[4]] =
N[Sqrt[2]] Table[
```

```
Subscript[\[DoubleStruckOne],
2]\[CircleTimes]KroneckerProduct[
Permutations[{a, a, id, id, id}][[i, 1]],
Permutations[{a, a, id, id, id}][[i, 2]],
Permutations[{a, a, id, id, id}][[i, 3]],
Permutations[{a, a, id, id, id}][[i, 4]],
Permutations[{a, a, id, id, id}][[i, 5]]], {i,
Length[Permutations[{a, a, id, id, id}]]}] /. {a -> X,
id -> Subscript[\[DoubleStruckOne], 2]};
Pn0[[5]] =
N[Sqrt[2]] Table[
Subscript[\[DoubleStruckOne],
2]\[CircleTimes]KroneckerProduct[
Permutations[{a, a, a, id, id}][[i, 1]],
Permutations[{a, a, a, id, id}][[i, 2]],
Permutations[{a, a, a, id, id}][[i, 3]],
Permutations[{a, a, a, id, id}][[i, 4]],
Permutations[{a, a, a, id, id}][[i, 5]]], {i,
Length[Permutations[{a, a, a, id, id}]]}] /. {a -> X,
id -> Subscript[\[DoubleStruckOne], 2]};
Pn0[[6]] =
N[Sqrt[2/2^2]] Table[
Subscript[\[DoubleStruckOne],
2]\[CircleTimes]KroneckerProduct[
Permutations[{a, b, id, id, id}][[i, 1]],
Permutations[{a, b, id, id, id}][[i, 2]],
Permutations[{a, b, id, id, id}][[i, 3]],
Permutations[{a, b, id, id, id}][[i, 4]],
Permutations[{a, b, id, id, id}][[i, 5]]], {i,
Length[Permutations[{a, b, id, id, id}]]}] /. {a -> PXp,
b -> PXm, id -> Subscript[\[DoubleStruckOne], 2]};
Pn0[[7]] =
N[Sqrt[2/2^2]] Table[
```

```
Subscript[\[DoubleStruckOne],
2]\[CircleTimes]KroneckerProduct[
Permutations[{a, b, id, id, id}][[i, 1]],
Permutations[{a, b, id, id, id}][[i, 2]],
Permutations[{a, b, id, id, id}][[i, 3]],
Permutations[{a, b, id, id, id}][[i, 4]],
Permutations[{a, b, id, id, id}][[i, 5]]], {i,
Length[Permutations[{a, b, id, id, id}]]}] /. {a -> PXp,
b -> PXm, id -> X};
Pn0[[8]] =
N[Sqrt[2/2^4]] Table[
Subscript[\[DoubleStruckOne],
2]\[CircleTimes]KroneckerProduct[
Permutations[{a, a, b, b, id}][[i, 1]],
Permutations[{a, a, b, b, id}][[i, 2]],
Permutations[{a, a, b, b, id}][[i, 3]],
Permutations[{a, a, b, b, id}][[i, 4]],
Permutations[{a, a, b, b, id}][[i, 5]]], {i,
Length[Permutations[{a, a, b, b, id}]]}] /. {a -> PXp, b -> PXm,
id -> Subscript[\[DoubleStruckOne], 2]};
Pn0[[9]] =
N[Sqrt[2/2^4]] Table[
Subscript[\[DoubleStruckOne],
2]\[CircleTimes]KroneckerProduct[
Permutations[{a, a, b, b, id}][[i, 1]],
Permutations[{a, a, b, b, id}][[i, 2]],
Permutations[{a, a, b, b, id}][[i, 3]],
Permutations[{a, a, b, b, id}][[i, 4]],
Permutations[{a, a, b, b, id}][[i, 5]]], {i,
Length[Permutations[{a, a, b, b, id}]]}] /. {a -> PXp, b -> PXm,
id -> X};
Pn0[[10]] =
N[Sqrt[2/2^2]] Table[
```

```
Subscript[\[DoubleStruckOne],
2]\[CircleTimes]KroneckerProduct[
Permutations[{a, b, c, id, id}][[i, 1]],
Permutations[{a, b, c, id, id}][[i, 2]],
Permutations[{a, b, c, id, id}][[i, 3]],
Permutations[{a, b, c, id, id}][[i, 4]],
Permutations[{a, b, c, id, id}][[i, 5]]], {i,
Length[Permutations[{a, b, c, id, id}]]}] /. {a -> PXp,
b -> PXm, c -> X, id -> Subscript[\[DoubleStruckOne], 2]};
Pn0[[11]] =
N[Sqrt[2/2^2]] Table[
Subscript[\[DoubleStruckOne],
2]\[CircleTimes]KroneckerProduct[
Permutations[{a, b, c, c, id}][[i, 1]],
Permutations[{a, b, c, c, id}][[i, 2]],
Permutations[{a, b, c, c, id}][[i, 3]],
Permutations[{a, b, c, c, id}][[i, 4]],
Permutations[{a, b, c, c, id}][[i, 5]]], {i,
Length[Permutations[{a, b, c, c, id}]]}] /. {a -> PXp, b -> PXm,
c -> X, id -> Subscript[\[DoubleStruckOne], 2]};
```

With u being the unitary for evolution of spin system for $1\mu s$, we evolve density matrix for $250\mu s$:

```
rho0 = SparseArray[
1/2^(nH1 + 1)
KroneckerProduct[Subscript[\[DoubleStruckOne], 2] + X,
Subscript[\[DoubleStruckOne], 2^nH1]]];

ut = Table[N[MatrixPower[u, i]], {i, 250}];

rhot = N[NestList[ut .#.ut\[ConjugateTranspose] &, rho0, 250]];
```

We use $\hat{P}_n$ operators to calculate the weights for correlation orders $|C_n|$ in the $\rho(t)$:

```
A[[5]] =
Table[Abs[Purity[PartialTr[rhot[[i]].Pn5, {2, 2^nH1}, {2}]]], {i,
250}];

A[[4]] =
Table[Sum[
Abs[Sum[Purity[
PartialTr[rhot[[i]][[i]].Pn4[[k, j]], {2, 2^nH1}, {2}]], {j,
Length[Pn4[[k]]]}]], {k, Length[Pn4]}], {i, 250}];

A[[3]] =
Table[Sum[
Abs[Sum[Purity[
PartialTr[rhot[[i]]Pn3[[k, j]], {2, 2^nH1}, {2}]], {j,
Length[Pn3[[k]]]}]], {k, Length[Pn3]}], {i, 250}];

A[[2]] =
Table[Sum[
Abs[Sum[Purity[
PartialTr[rhot[[i]].Pn2[[k, j]], {2, 2^nH1}, {2}]], {j,
Length[Pn2[[k]]]}]], {k, Length[Pn2]}], {i, 250}];

A[[1]] =
Table[Sum[
Abs[Sum[Purity[
PartialTr[rhot[[i]].Pn1[[k, j]], {2, 2^nH1}, {2}]], {j,
Length[Pn1[[k]]]}]], {k, Length[Pn1]}], {i, 250}];

A[[0]] =
Table[Sum[
```

```
Abs[Sum[Purity[
PartialTr[rhot[[i]].Pn0[[k, j]], {2, 2^nH1}, {2}]], {j,
Length[Pn0[[k]]]}]], {k, Length[Pn0]}] - 1, {i, 250}];
```

A.3 Pulse program: the MCSD experiment

Following is the pulse program designed for detection of multi-spin correlations in the spin environment after information scrambling.

```
define delay small      ;small window in MREV_8, about 3us with duplexer
"small=d3-p2"
define delay large         ;large window in MREV_8
"large=d3+d3-p2"



1 ze                              ;acquire into a cleared memory
10u reset:f1 reset:f2      ;synchronise RF pulse and detection F1:31P F2:1H
10u pl2:f2 pl1:f1                          ;set power level for each channel


2 d11 do:f2                                        ;turn OFF the decoupling
d11 pl2:f2                                  ;cross polarization power for 1H
d1 pl1:f1                     ;Relaxation delay, cross polarization power 1H

p2:f2 ph1                ;Initialization pulse for cross polarization
0.3u
```

```
(p15 ph2):f1 (p15:spf0 pl22 ph10):f2           ;Cross Polarization contact


0.5u  pl2:f2                                ;31P power level set to High power

4 p2:f2 ph20^                                  ;Evolution starts, MREV-8 on 1H
small
p2:f2 ph20^
large
p2:f2 ph20^
small
p2:f2 ph20^
large
p2:f2 ph20^
small
p2:f2 ph20^
large
p2:f2 ph20^
small
p2:f2 ph20^
large pl3:f1
lo to 4 times l1                               ;Evolution ends after l1 loops


(ralign                                           ;sync. encoding after delay
(p2 ph4 2u p2 ph5):f2                                              ;Rx)\phi on 1H
(p1 ph3 d2 p1*2 ph6 d2 p1 ph7):f1          ;central \pi during delay  on 31P
)


5 p2:f2 ph20^                         ;inverted evolution starts, MREV-8 on 1H
small
p2:f2 ph20^
```

```
large
p2:f2 ph20^
small
p2:f2 ph20^
large
p2:f2 ph20^
small
p2:f2 ph20^
large
p2:f2 ph20^
small
p2:f2 ph20^
large
lo to 5 times l1                    ;Inverted evolution ends after l1 loops


go=2 ph31 cpds2:f2             ;Detection on 31P channel, CW on 1H channel
d11 do:f2 wr #0 if #0                              ;data record on memory

1m ip1                                      ;phase incrementation for Rx)\phi
1m ip10
1m ip4

lo to 2 times td1                              ;Loop over for various phases

HaltAcqu, 1m
7 exit


;phase program:

ph1=  (32)8 24
ph2=  0 0 1 1
```

```
ph3=  0 2 1 3
ph4=  (32) 8 24
ph5=  3 1
ph6=  0 0 0 0 1 1 1 1 2 2 2 2 3 3 3 3
ph7=  2 0 1 3 0 2 3 1
ph10= (32)0
ph20=0 1 3 2 2 1 3 0
ph30=(360)115
ph31= 0 2 3 1 2 0 1 3


;parameters:

;small : small delay in MREV_8 sequence, typically 2.5-4.5 usec
;large : large delay in MREV_8 sequence
;L1    ; loop counter for evolution period, number of MREV_8 cycles
;TD1   : number of steps in \phi
;d11   : 30ms
;d1    : T1 relaxation delay
;d2    : 1/2 scrambling delay
;d3    : delay to set small and large window
;PL1   : power level for 1H, High power
;PL2   : power level for 31P contact
;PL3   : power level for 31P, High power
;PL22  : Power level for Hartman_Hahn condition 31P
;P1    : 31P Hard 90 pulse
;P2    : 1H Hard 90 pulse
;P15   : 31P contact pulse in Cross Polarization
;SPF0  : 1H contact shaped pulse in Cross Polarization
;CPDS2 : 1H CW decoupling during data acquisition
;PH1   : Initialization pulse phase, spin temperature alteration phase cycling
;PH2   : 31P pulse phase during the contact
;PH3   : 31P 90 pulse phase, Exorcycle
```

```
;PH4   : 1H phase, encoding
;PH5   : 1H phase, encoding
;PH6   : 31P \pi pulse phase, Exorcycle
;PH7   : 31P 90 pulse phase, Exorcycle
;PH10  : 1H pulse phase during contact
;PH20  : 1H MREV_8 Phase
;PH31  : Receiver phase
```